DYNAMIC MODELING FOR CONTROL OF THE DRILLING PROCESS USING ACOUSTIC EMISSION

By

YUNSHUN CHIOU

Bachelor of Science

National Central University

Chung-Li, Taiwan, R.O.C.

1983

Submitted to the Faculty of the
Graduate College of the
Oklahoma State University
in partial fulfillment of
the requirements for
the Degree of
MASTER OF SCIENCE
December, 1989

Thesis
1989
C539d
cop.2

Oklahoma State Univ. Library

DYNAMIC MODELING FOR CONTROL OF

THE DRILLING PROCESS USING

ACOUSTIC EMISSION

Thesis Approved:

Thesis Adviser

Dean of the Graduate College

ACKNOWLEDGEMENTS

I would like to take this opportunity to acknowledge and express my sincere appreciation to my adviser, Dr. S. Y. Liang, for his insight, guidance, and limitless patience. His influence on the outcome of this endeavor was invaluable. I also thank him for helping me in writing this thesis despite his demanding schedule.

I would also take this opportunity to thank my committee members, Dr. G. E. Young and Dr. P. M. Moretti, for their advisement in the course of this work.

Many thanks to my wife, SHUJEN YANG, for making me feel it was all worthwhile; and my parents for giving me the opportunities they never had.

TABLE OF CONTENTS

LIST OF TABLES

Table | page

LIST OF FIGURES

Figure | Page

Figure Page

CHAPTER I

INTRODUCTION

The objective of this thesis work is to develop a dynamic model for the control of drilling processes using acoustic emission (AE). This objective is accomplished through the experimental quantification of AE signal rate as a dynamic function of the machining parameters and work material properties in drilling.

Research over the last several years has established the effectiveness of acoustic emission (AE) based on sensing methodologies for machine tool condition monitoring and process analysis. The sensitivity of the AE signal to the various contact areas and deformation regions in the cutting and chip formation process has led to the evaluation of the analysis of AE signals as a basic tool for analysis of the cutting process. However, there still remains much unknown about the basic properties of the AE signals generated in the drilling process, such as chip workpiece friction energy rate, the basic cutting work rate of AE signal as the simple dependency on machining parameters and the energy dissipated associated with chip breaking formation in drilling.

In recent decades, there has been a steady increase in the number of computer numerically controlled (CNC) machine tools. The CNC systems have generated a lot of interest because of their accuracy, repeatability, and productivity. However, a common drawback of these systems is that the cutting conditions, such as cutting speed and feedrate, are determined by the part programmer. Consequently, the values selected depends upon the programmer's experience and knowledge of the machining process. An improper choice of such values can cause tool breakage or even more serious results. To prevent such accidents, part programmers tend to select conservative values for the cutting condition. Unfortunately, this reduces the production rate. To avoid the problem, a number of attempts have been made to develop more flexible controllers for the metal cutting processes.

Drilling is one of the basic processes of the hole generating process which is among the most important operations in manufacturing. Because of their importance in nearly all production operations, twist drilling have been the subject of numerous investigation for decades by many researchers.

In 1955, Oxford [1] published the basic mechanics of the drilling process which introduced a fundamental investigation on drilling. Many mathematical models to describe the characteristics of the drilling machining process were also published by relating some control parameters to input and output. There are several input parameters in the drilling process, such as spindle speed, feedrate, tool and workpiece material properties, and cutting fluid. The output parameters include the cutting temperature, chip thickness, thrust, torque, surface finish, power consumption, vibration amplitude, acoustic emission, and tool wear [2] [3] [4] [5] [6] [7] [8] [35].

In 1957, Oxford and Shaw [2] published formulas for computing the torque and thrust required by a twist drill when drilling most steels having Brinell hardness of less than 250. The equations relate the torque and thrust as a function of feed, drill diameter, length of chisel edge, and material work hardness.

There was a considerable amount of continuing fundamental research on drilling. Some research of the drilling machining system aimed not only at the substantial improvement in tool life but also at more accurate prediction of tool performance related to cutting force in drilling operation.

In 1982, Fabris and Podder [11] published their report which dealt with optimization of the drilling process. Their paper showed that the end of drill tool life can be accurately determined by monitoring the rate of change of thrust or torque.

In 1987, Conrad and Mcclamroch [9] published a stochastic drilling model for tool wear, called a diffusion-threshold model which allows the drilling machining economics problem to be formulated as a stochastic optimal control problem incorporating measurement feedback of tool wear. This model is compared to a Taylor tool life formula. Conditions are given so that the two models agree in the mean sense. Two types of control policies are described. The first is a traditional machining economics policy type called age replacement. In age replacement policies, the tool replacement decision is based on part counts (age), and the machining parameters are fixed. The second type of policy is called a (one step) feedback policy. In feedback policies, drill wear measurements may be available at discrete times. This model utilizes tool wear feedback and allows on-line decision making.

In 1988, Thangaraj and Wright [10] developed a real time control system for the drilling process to monitor the performance of the twist drills based on the prediction of the incipient failure of the drill and retraction before significant damage occurs. They found that the gradient of the drilling thrust force, calculated using a digital filter with the necessary frequency specifications, exhibits a sharp increase several seconds before any serious failure. The feedback control system is developed by monitoring drill wear until failure prediction is detected and then the feed has to be stopped.

In 1988, Li and Wu [11] also published a report which introduced an approach for on-line monitoring of drill wear states by using a fuzzy C-means algorithm. They represented drill wear condition by four fuzzy grades that are initial, small, normal and severe. The grade "severe" is proposed to be used as the prediction of tool replacement.

In the interest of maximizing the metal removal rate and preventing tool breakage in the drilling process, the adaptive control systems are widely applied in industry to maximize machining parameters (e.g., feed rate or cutting speed) subject to process and system whthin the limit of allowable torque or thrust.

In 1980, Mathias and Welch [13] proposed the use of watts-transducer type of torque sensor for adaptive drilling control. The watts-transducer consists of current and voltage transformers connected to voltage signals which are proportional to the motor current and voltage. These signals are multiplied by an integrated-circuit multiplier to produce a signal proportional to horsepower consumed. The horsepower losses of the spindle drive are automatically subtracted out when the cutter is free of the work. The horsepower signal developed during cutting is divided by a signal representing rpm to produce the true cutting-torque signal. The control is commonly called torque-controlled drilling. The sensor torque signal is compared with a voltage representing the torque limit for the drill to produce a feedrate-override command.

To obtain the net cutting torque acting on the cutting tool, the system establishes a tare torque and subtracts it from the caclulated total torque. The tare torque is required to cut air and includes the torque needed to overcome friction and windage in the spindle drive. Experimental data obtained under various cutting conditions are used to determine the threshold levels. This is a drawback of this system. Also, as the measurement based on the inertia of the system, the response may not always be fast enough to avoid tool failure [10].

The Z-axis thrust force is also used as a control parameter for the adaptive control drilling process [14]. The adaptive control drilling system is designed to sense the hardness of different material and automatically adjust cutting speeds accordingly. By altering drill advancement (or penetration) rates, the time required to cut a single hole in a three-material sandwhich or "stackup" of graphite, titanium and aluminum on the B-2 will be reduced. It is currently applied in the fabrication of B-2 bombers. When drilling a hole, the new tool uses "thrust"- the longitudinal constant pressure required to help a bit cutting into the material at a constant rate. As the drill initially moves toward a surface of any layer, it is commanded to advance quickly until the bit contacts the next material by sensing the reaction pressure.

In 1983, Mathias [20] proposed that the key to opening up adaptive control technology to more manufacturers lies in the development of improved sensors with associated consideration on resolution reliability and cost effectiveness. The wide range of tool diameters required on flexible manufacturing systems needs sensors with resolutions in the ±5 lb (22N) range. In addition, the higher frequence response for sensors in the 1-10 kHz range is necessary.

In most of the previous approaches of the drilling process for control, the torque and the thrust are considered as the primary control parameters for the drilling process. However, the literature on modeling of the drilling process for control is very limited even though the adaptive control of drilling has been applied widely in industry.

The use of vibration analysis technique has also been applied for on-line monitoring of the tool wear condition in drilling process in industry. Drill-up [35] is an instrument designed to provide on-line monitoring of vibration generated in the drilling process. It prevents breakage of small diameter drills used on automatic feed drilling machines with spindle retract ability and provides the signal to the machine tool controller indicating that the driller is no longer normal.

The intent of this research is to investigate the possibility and effectiveness to model the drilling process for control by monitoring the acoustic emission (AE) generated during drilling. Acoustic emission sensor is characterized by its higher frequency response in the 30k-1Mhz range than that of force sensor in the 500-1500hz range.

The study on the relationship between acoustic emission and the cutting process was first developed by Dornfeld and Kannatey-Asibu [28] by establishing a comprehensive analytical relationship between acoustic emission and the orthogonal cutting process. Some aspects for acoustic emission modeling correlated to work material properties, cutting conditions, and tool geometry were also discussed [25] [26] [27]. Aside from the detecting of these cutting processes by monitoring input and output parameters, there is added need for modeling of the drilling process by using acoustic emission.

There are several advantages of acoustic emission for on-line detection of cutting process.

1) the signal frequency range is far above that of machine tool vibrations and other sources of noises. Therefore, undesirable noise components can easily be removed from the signal using a high-pass filter.
2) the AE transducer can be mounted easily on the tool, tool holder or workpiece and does not interfere with the cutting process.

One of the most significant methods to analyze AE is the measurement of the energy content of the AE signals. The rate with which the energy is transmitted by the signal can be directly correlated with the rate of energy generated by the original AE source. Unlike the measurement of torque or Z-axis thrust during drilling, the measurement of acoustic emission provides complete information of energy content.

Of almost the same importance is the control and measurement of the experimental parameters characterizing the detected AE. A wide varity of AE measurements can be carried out according to the type of AE signal, the experimental intrumentation used, and the personal preferences of the individual research workers.

In drilling process, cutting parameters will change the acoustic emission content independently, since the acoustic power released is proportional to the strain rate in the cutting process. In this research, both static and dynamics analysis are used to characterize the acoustic emission TMS (true mean square) signal with an autogressive model. The model parameter are constantly updated according to the acoustic TMS signal dynamics which are dependent on acoustic emission source mechanism. As a result, these time varying parameters are expected to contain information about the cutting process. It is necessary to perform off-line parameter calibration and identification under any cutting condition to map out the allowable parameters. The parameters are affected by the change of feedrate and spindle speed. This research will present the static equation and dynamic model for the drilling process by sensing acoustic emission during drilling. Feedrate is chosen as the controlling input since the tool wear is less affected by feedrate than by spindle speed.

The PID control algorithm proposed in this thesis is to achieve feedback control of the discrete time model of acoustic emission TMS signal generated during drilling and to minimize tool wear. The model tracks only the dynamic properties but not mean energy level of the acoustic emission signal.

CHAPTER II

DRILLING PROCESS CHARACTERISTICS

2.1 Drilling process

The hole making processes are among the most important operations in manufacturing. The drilling is one of the basic processes of the hole generating process.

The drilling process is a complex three dimensional cutting process. An ordinary, standard twist drill shown in figure 1 is characterized by a geometry in which the normal rake angle and the velocity of the cutting edge are a function of their distance from the center of the drill.

The conical point twist drill is characterized by its radius Rd, web thickness 2t, point angle 2ρ, chisel edge angle ψ, and helix angle β. It has two cutting edges: a chisel edge, and main cutting edge. The main cutting edge can be estimated from the formulas of Oxford [1] and Galloway [36]:

$$\sin[i(r)] = \frac{-t\sin\rho}{r} \qquad (2.1)$$

$$\tan[\alpha(r)] = \frac{(r^2 - t^2 \sin^2 \rho)\tan\beta}{Rd\,(r^2 - t^2)^{1/2}} - \frac{t\cos\rho}{(r^2 - t^2)^{1/2}} \qquad (2.2)$$

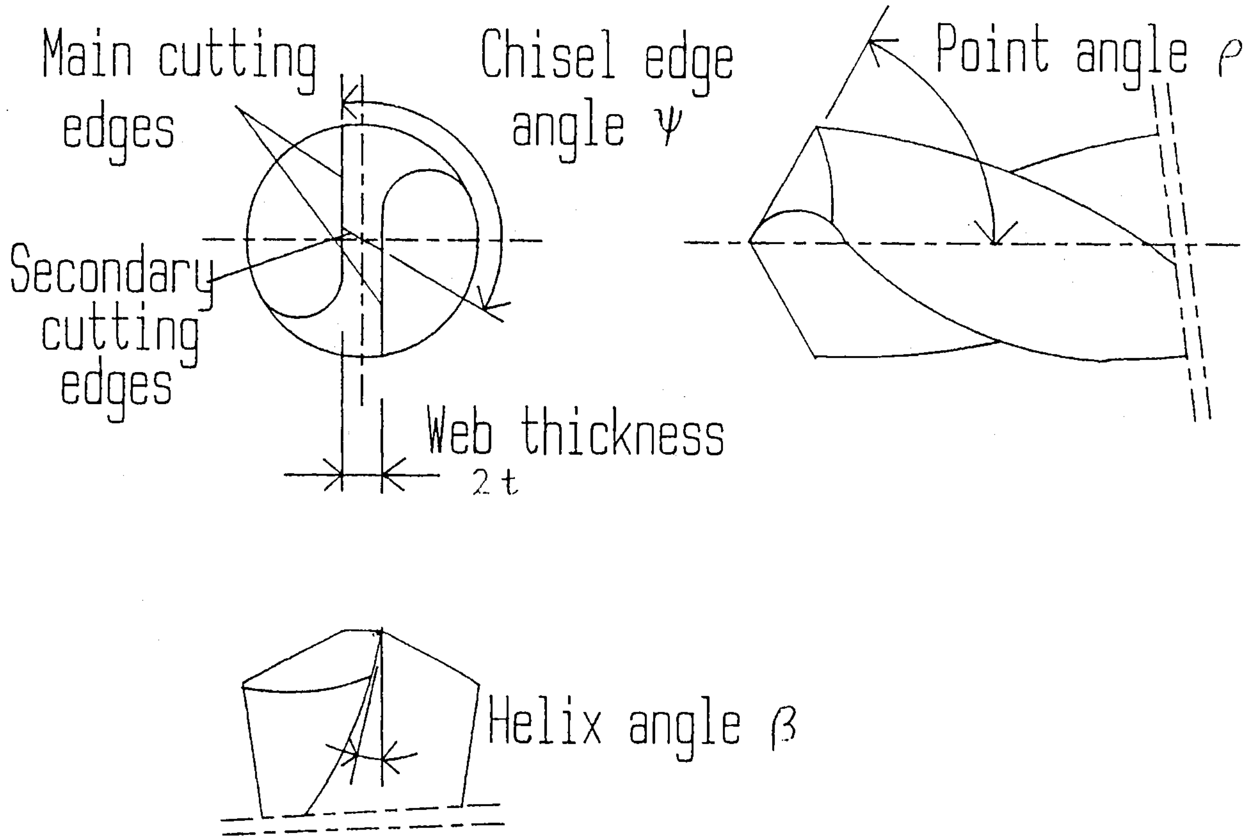

Figure 1. Drill Geometry and Variables

where r is the radial distance from the drill axis.

The drilling process involves the cutting operation at the cutting edges and chisel edge and the extrusion operation at the chisel edge of the drill as shown in figure 2. In a basic analysis only the main cutting edge need to be considered since it produces the only substantial chip and accounts for most (more than 85 percent) of the power consumption [3][6].

The drilling process in which the cutting edges can be divided into oblique cutting elements of the type shown in figure 3 is similar to most turning and milling operations. The cutting edge of a cross section of figure 3 in a plane act in a manner similar to the two dimensional tool of figure 4. The geometry of the cutting process at a point is defined by the cutting speed U, rake angle α, shear angle ϕ, uncut chip thickness t1, chip thickness t2, and the clearance angle φ.

2.2 Sources of AE During drilling

Acoustic emission (AE) refers to the elastic stress waves generated as a result of the rapid release of strain energy within a material due to a rearrangement of its internal structure. The stress waves generated by the structural rearrangement can produce displacements on the surface of the material which are detected by converting them into electrical signal using piezoelectric transducer. An appropriate method for analyzing the AE signals is one

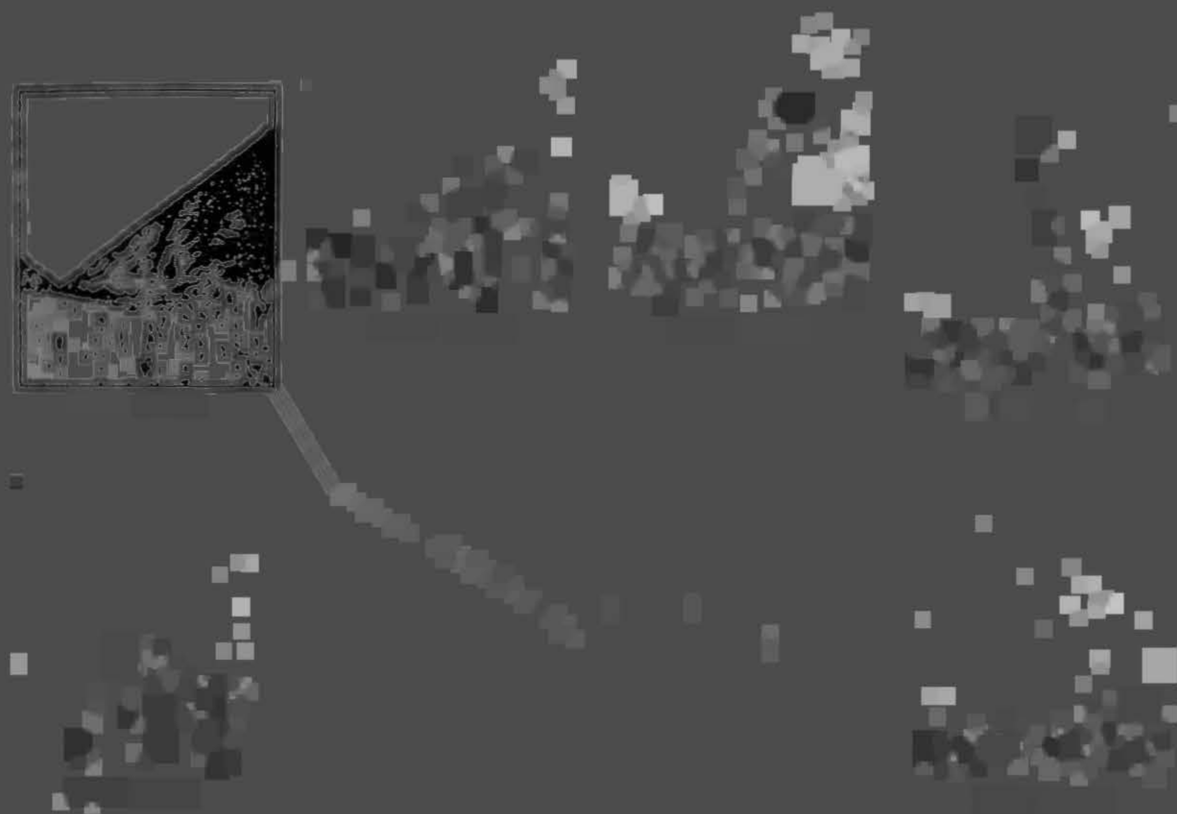

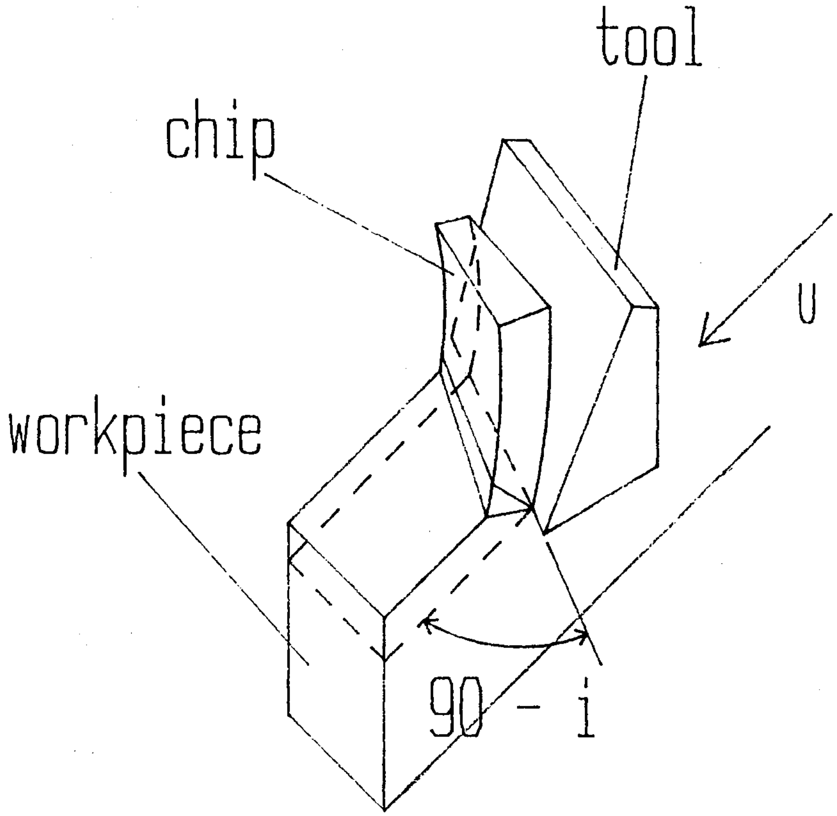

Figure 3. A Divided Oblique Cutting Element in the Cutting Edges in Drilling

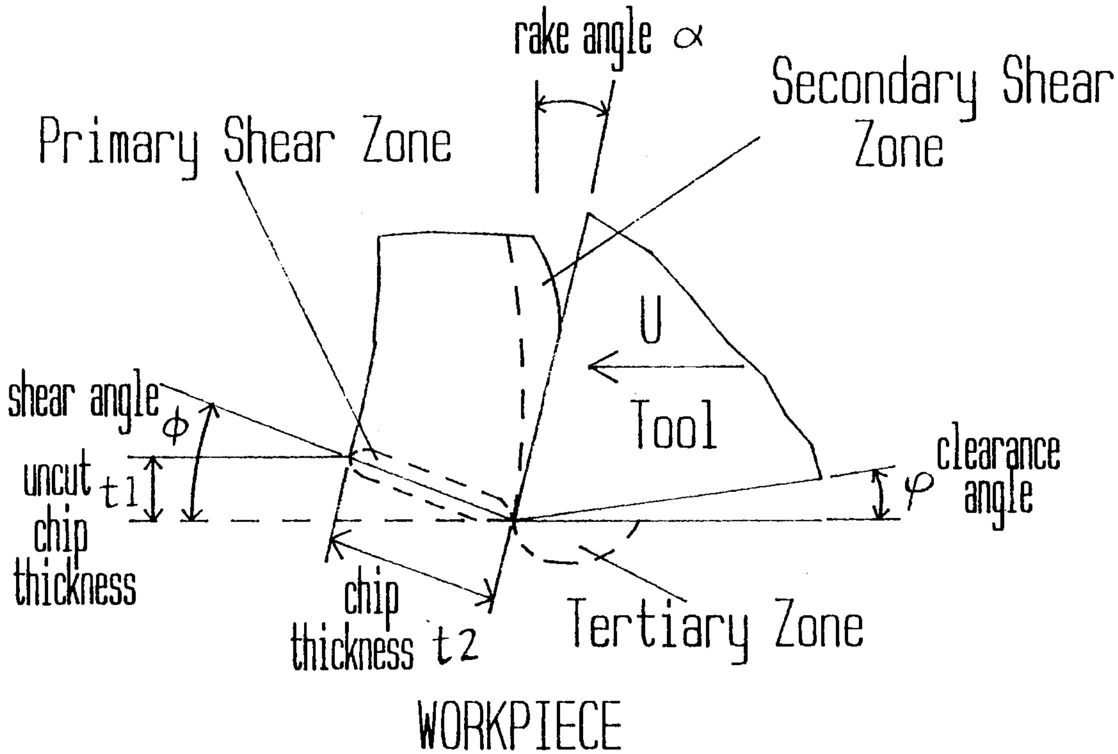

Figure 4. Cross Section of the Cutting Process with a Tool in a Plane Normal to the Cutting Edge

that gives a measure of the energy content of the signal. The energy rate of the signal could then be related directly to the work rate of the AE source. A convenient measure of this energy content is the RMS or TMS value of the signal.

For an element of volume dv subjected to stresses σ_{ij} which results in plastic strain increments $d\epsilon_{ij}$, the increment of work can be expressed as:

$$dWt = \sigma_{ij}\, d\epsilon_{ij}\, dv \tag{2.3}$$

Considering the bulk of the material, the work rate $\dot{W}t$ is then given by:

$$\dot{W}t = \int_{v} \sigma_{ij}\, \epsilon_{ij}\, dv \tag{2.4}$$

If the material is subjected to a constant stress σ and strain rate $\dot{\epsilon}$, then the work rate becomes:

$$\dot{W}t = \sigma\, \dot{\epsilon}\, v \tag{2.5}$$

where v is the volume of material being deformed.

$\dot{W}t$ is the energy source for AE that is generated from plastic deformation. Equation (2.5) shows that the energy rate of an emission signal is dependent on the rate of deformation (strain rate), the applied stress, and volume of material involved in the deformation process.

A common and simple way to measure such energy is the evaluation of the root mean square (RMS) voltage of the signal. The RMS value of an a-c signal is that the value of the signal could then be related directly to the work rate which, if passed through the same circuit for the same period time, would produce the same expenditure of energy as the a-c signal and expressed quantitatively as:

$$RMS = \left[\frac{1}{\Delta T}\int_{0}^{\Delta T} V(t)^{2}\, dt\right]^{1/2} \qquad (2.6)$$

where

V(t) = the signal function; and

ΔT = averaging time period.

Thus the energy rate of a signal is expressed as:

$$\frac{dE}{dt} \propto (RMS)^{2} \qquad (2.7)$$

Also, TMS is the square of RMS; that is,

$$TMS = \frac{1}{\Delta T}\int_{0}^{\Delta T} V(t)^{2}\, dt = RMS^{2} \qquad (2.8)$$

For a system with a significant amount of background noise, the TMS value of the actual signal can be calculated using the relationship:

$$TMS = RMS^{2} + RMS_{N}^{2} \qquad (2.9)$$

where RMS_N = the RMS value of the background noise.

This shows that TMS of background noise can be subtracted directly from TMS of total to give the TMS of the total signal only.

The TMS is representative of power derived from equation (2.8).

$$energy \propto \int_{o}^{\Delta T} V(t)^2 dt = \Delta T \; TMS \qquad (2.10)$$

In fact, the area under a TMS v.s. time curve will be proportional to AE energy.

With respect to the generation of AE, there are three three areas of interest in the orthogonal cutting process:

1. the primary deformation zone (shere zone);
2. the secondary deformation zone (chip-tool interface);
3. the tertiary zone (tool flank-workpiece interface). In addition to these, there is a fourth source of AE during metal cutting;

The development of the model was based on defining the contribution to AE generation based on calculation of work rate in the primary zone and secondary zone. These calculations were based on the simplified Ernst and Merchant model of the orthogonal machining process [37]. The work rate in the primary zone, $\dot{W}s$, is:

$$\dot{W}s = d \; t1 \; \tau k \frac{\cos\alpha}{\sin\phi \cos(\phi - \alpha)} U \qquad (2.11)$$

where

d = depth of cut (width of chip);

$t1$ = uncut chip thickness;

τk = average material shear strength;

ϕ = shear angle;

α = rake angle; and

U = cutting velocity;

The work rate in the sliding and sticking region of the secondary shear zone, $\dot{W}_{c1}$ and $\dot{W}_{c2}$, are given as:

$$\dot{W}_{c1} = \frac{1}{3} \tau k \, d \, (l - l_1) \, U_{ch} \qquad (2.12)$$

$$\dot{W}_{c2} = \tau k \, d \, l_1 \, U_{ch} \qquad (2.13)$$

where

l = contact length between the chip and the tool rake face;

l_1 = length from the tool edge to the end of the sliding zone on the rake face;

U_{ch} = chip velocity = $\sin\phi/\cos(\phi-\alpha)$.

Conbining equation (2.11), (2.12), and (2.13) gives a relationship between the acoustic emission signal and the cutting parameters based on the Ernst and Merchant model:

$$RMS = C_1 \{ \tau k \, d \, U \, [\frac{\cos\alpha}{\sin\phi \, \cos(\phi-\alpha)} f] + [\frac{1}{3} (l+l_1) \frac{\sin\phi}{\cos(\phi-\alpha)}] \}^{1/2} \qquad (2.14)$$

where C_1 is a constant influenced by tool geometry, instrumentation gain, etc.

The coefficient set at 0.5 in equation (2.14) was consistent with the results of the diamond turning processes carried out in [38]. A refinement of the model in [28] was proposed by [38]. This work added a term, $\tau k d U w$ (where w is the average length of the tool flank-workpiece interface), to equation (2.14). The equation (2.14) is rewritten as:

$$RMS = C_1 \{\tau k\ d\ U\ [C_2 \frac{\cos\alpha}{\sin\phi \cos(\phi-\alpha)} f] + [C_3 \frac{1}{3} (l+2l_1) \frac{\sin\phi}{\cos(\phi-\alpha)}] + C_4 w\}^m \quad (2.15)$$

where

C_2, C_3, C_4 are the factors of signal attenuation, and

m is material-depedent.

In spite of the theoretical model developed to predict AE energy from the orthogonal cutting process, many pratical considerations have limited the accuracy of the model under actual cutting conditions. These considerations include the microscopic variations of other materials used in machining experiments [39] as well as variations in instrumentation and signal transmission path with the experimental setup [29]. The three dimensional machining process has additional sources of signal variation due to chip formation and flow over the tool and to tool geometry effects.

As the cutting process becomes more idealized (no build up edge, no friction, sharp edges, etc.), the sensitivity of the AE signal to process variables (feedrate, depth of cut, cutting speed) increases. This was seen in the study [29] of using diamond tools to turn two aluminum alloys and free cutting brass. This was a continuous chip-forming material for the machining condition which is close to "ideal". A similar result was found by [40] for turning carbon steel (S45C according to JIS) with a P20 carbide tool. However, the model coefficients in the diamond machining tests of [29] did not verify the quantitative model in equation (2.15). With very few exceptions, the model for the power function is given as:

$$RMS = K_t U^a f^b d^c + D_v \tag{2.16}$$

where

K_t = constant;

a, b, c = coefficients;

U = cutting speed;

f = feed;

d = depth of cut; and

D_v = offset value;

In drilling, the cutting process as shown in figure 5 is continuous with varying chip load, relative tool/workpiece velocity, the potential for chip conjection and friction generated in the drilled hole. The chips in drilling are formed at the bottom of the hole and consequently deformed by the contact with the hole wall and drill flute; the rubbing action between the chip and workpiece due to this effect generates a significant amount of high amplitude AE signals, thus additional TMS_f energy rate signals are generated during drilling due to friction between the chip and the wall of the drilled hole. Based on

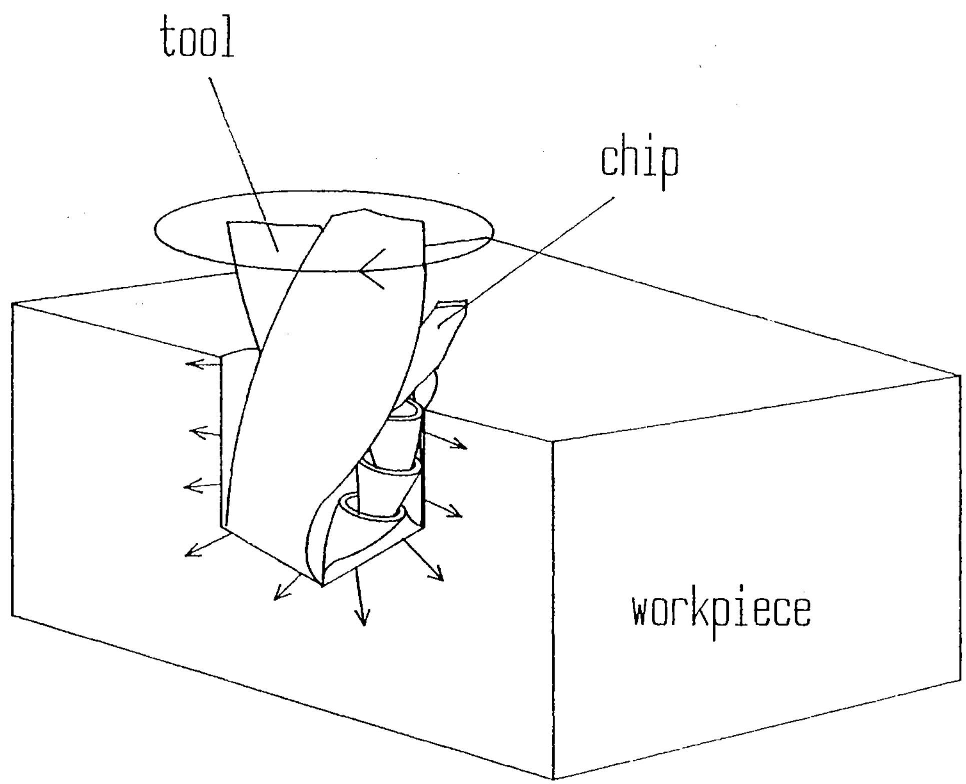

Figure 5. Typical Interaction Between the Tool, Chip and Workpiece During Drilling

well established equations for friction in these systems, and adding an approximation for the energy dissipation in the frictional process and generation of acoustic emission, an expression linking the energy of AE to the sliding/friction is defined as [25]:

$$RMS = (K_r\ n\ \tau_s\ A_a\ V)^{m/2} \qquad (2.17)$$

where

K_r and m = constants depends on the AE measurement system;

n = coefficient relating real area of contact to apparent area of contact, function of surface roughness and elastic properties of the material;

τ_s = interfacial shear strength of the material;

Aa = apparent area of contact;

V = sliding velocity.

Equation (2.17) can also be written as:

$$TMSf = (K\ n\ \tau_s\ Aa\ V)^{m} \qquad (2.18)$$

For a time period Δt, the contact area between the chip and wall of the drilled hole is proportional to Fr Δt, i.e.

$$Aa = Ka\ Fr\ \Delta t \qquad (2.19)$$

where

Fr = feedrate (inch/min);

Ka = coefficient related to actual contact area;

Also, V = w D/2, where w is spindle speed. and D is the diameter of tool. Equation (2.18) can be given as:

$$TMSf = (K_r\ n\ \tau_s\ Ka\ Fr\ \Delta t\ w\ D\ /\ 2)^m$$

$$= Kf\ w^m\ H^m \qquad (2.20)$$

where

$Kf = (K\ Kan\ \tau_s\ D/2)^m$; and

$H = Fr\ \Delta t$ (inch);

As the chips flow over the flutes, the energy rate, $\dot{W}f$, generates the corresponding accoustic emission, TMSf. Therefore,

$$\dot{W}f = TMSf \qquad (2.21)$$

However TMSf generated during drilling is also related to the geometry of the tool and the chip form. Therefore the exponential coefficient for H and w need to be verified by experiments. Equation (2.20) may be written as:

$$TMSf = Kf\ W^r\ H^s \qquad (2.22)$$

This will be indentified in chapter 3.

2.3 Analytical model of Drilling process

Cutting parameters in the drilling process will change the acoustic content independently because the acoustic power released is proportional to the strain rate in the cutting process.

To get a basic idea of the fundamental properties of acoustic emission generated during drilling, a rather primitive model is assumed. Investigation presented in this report is based upon the analysis of acoustic emission sources contributing to the total measurement of AE.

As mentioned before, there are several sources of acoustic emission during drilling. To analyze the drilling process conducted in this thesis, it would be effective and simple to assume that energy rate of acoustic emission generated in the drilling process includes only two main sources: cutting work rate, TMSc as indicated in equation (2.16), and frictional energy rate, TMSf, as indicated in equation (2.22).

The resultant work rate of acoustic emission, TMS, generated in the workpiece during drilling would be the sum of the cutting work rate and the frictional work rate. Since there is no parameter of depth of cut in the drilling process, the first component, TMSc, is measured based upon the relationship between the instantaneous feedrate and spindle speed with a proportional gain, ie..

$$TMSc = Kc\, W^{p}\, Fr^{q} \qquad (2.23)$$

where

Kc = proportional constant;

W = spindle speed;and

Fr = feedrate;

The second component, TMSf, is measured based upon the relationship between the instantaneous depth of the drilled hole and spindle speed with a proportional constant, Kf, as indicated in equation (2.22). Therefore from equations

(2.7) and (2.10), the total energy rate, TMS, during drilling is the sum of both cutting TMSc, and frictional TMSf, i.e.

$$TMS = \dot{W}c + \dot{W}f = TMSc + TMSf \qquad (2.24)$$

Acoustic emission generated during drilling due to chip breaking can be filtered out by using module set at a slow response. The tool wear effect can be minimized by sharpening the drill bit or by replacing it with a new tool to achieve the ideal cutting condition as mentioned previously.

To verify these values of exponents p, q, r, and s, a large number of tests were made. Detailed experiments will be shown in Chapter III.

CHAPTER III

DRILLING PROCESS DYNAMICS

The objective of this work presented here is to develop a model which adequately relates the AE signal to changes in the drilling process parameters. General equations are derived for drilling TMS and found to be in good agreement with experimental data obtained by use of an AE sensor mounted on the surface of the workpiece. The dynamics from feedrate command to the actual feedrate does not have a strong dependence on cutting condition.

3.1 System of the Drilling Process

In the following section, a discrete time model for the drilling process will be derived. Acoustic emission generated during drilling is directly measured by the AE sensor attached to the workpiece. The command feedrate from the controller is taken as the input. In developing a discrete time model for the drilling process with the feedrate command as input and the measured TMS as an output, it is convenient to consider the process as composed of four basic elements (figure 6).

1) the CNC feed motor dynamics from the command feedrate to actual tool movement (Gm).

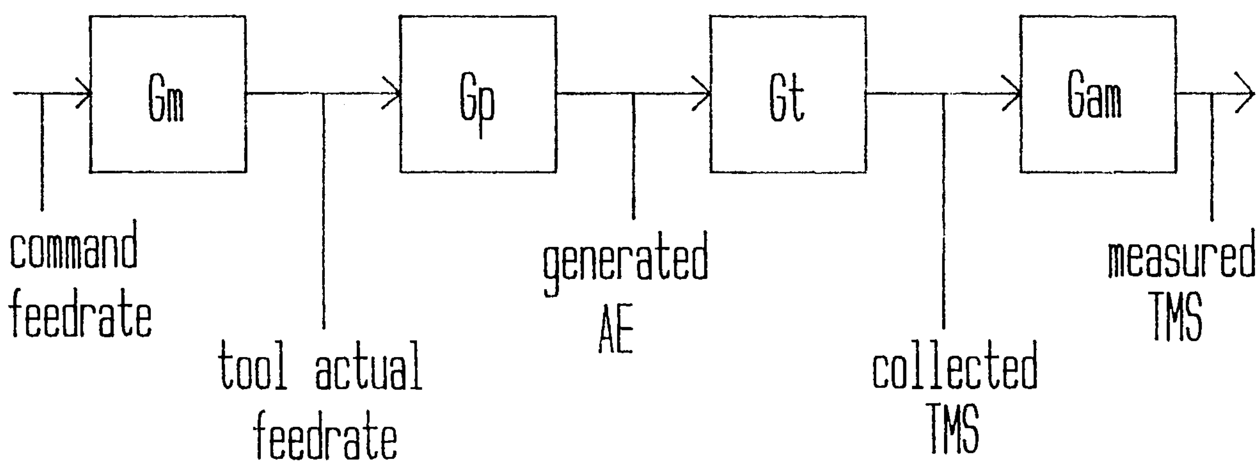

Figure 6. Drilling Process Representation

2) metal cutting dynamics from tool movement to acoustic emission (*Gp*).

3) transducer dynamics (*Gt*).

4) amplifier and filtering module dynamics (*Gam*).

The complexity of the system depends on the complexity of each element. The CNC feed servomotor dynamics, *Gm*(z), can be proposed as a second order system which will be discussed in the following sections.

In addition, since the AE transduder usually has a very large band width (30k ~ 1MHz), one can ignore the AE transducer dynamics.

3.2 Experimental Set-up

A series of experiments were conducted to test the performance of the basic elements of the drilling process as mentioned in the previous section.

Drilling exprériments were carried out on a Bridgeport interact 412 series milling machine, equipped with X, Y, Z feed motors of the permanent magnet type driven by a "pulse width modulated" servo drive unit situated in the electrical cabinet. A 125 line/revolution encoder is built into the Z motor and provides the axis position. The Z traverse movement is accomplished by means of a hardened and preloaded 5 pitch ball screw with recirculating ball nuts. The Z axis ballscrew is fixed to the head casting D.C. motors to turn the screw through a tooth belt drive.

The control unit has facilities for automatic cycling of the machine from the stored program and for interlocking of the power feed controls. It is a close loop feedback system. The specification of positioning speed for Z axis are shown in Table I, and the specification of spindle are shown in Table II.

The drill tools used in drilling experiments were high speed steel, ϕd = 23/64", point angle 118°, and helix angle 30°.

The workpiece used for the experiments was SAE1018 steel.

The AE sensor is a Dunegan Model WD-667 which has a bandwidth of 1MHz. It is acoustically coupled to the surface of the workpiece so that the dynamic surface motion propagates into the AE sensor. The dynamic strain in the workpiece produces a voltage-time signal as the sensor output.

The preamplifier is a Dunegan Model 1801-50H, high-pass at 50kHz, 40 dB. The AE sensor sensitivity reduces if it is directly connected to an amplifier through a long coaxial cable, therefore the preamplifier with fixed gain is connected between the AE sensor and the amplifier and located close to the AE sensor to improve the AE sensor sensitivity.

The amplifier is a Dunegan Model 302A Dual conditioner equipped with a two channel amplifier and threshold detector. Each channel provides 0 to 60 dB of voltage amplification adjustable in 1 dB increments.

TABLE I

SPECIFICATION OF POSITIONING SPEED FOR Z AXIS

Specification	Value
Axis Travel	
Spindle (Z axis)	300 mm
Positioning Speed	
Auto (Z)	7.5 m/min
Manual (Z)	0 - 4.5 m/min
Feedrate Range	1 to 12 m/min
Control	
Axis drive	Bosch P.W.M.
Control	Heidenhain TNC 151P
Input Range	0.001 - 29999.999 mm

TABLE II

SPECIFICATION OF SPINDLE

Specification	Value
Spindle	
Spindle Drive 30 min. rotating	5.5 Kw
Spindle Drive Continuous	3.7 Kw
Spindle Speed ranger (Standard)	40 - 4000 r.p.m
Spindle Speed Control	Direct Command
Spindle Diameter	65 mm
Spindle Working Area (Distance from nose to Table Top)	
Minimum	90 mm
Maximum	500 mm
Control	
Spindle motor	Fanuc a.c. variable frequency

The modulator is also a Dunegan Model 404 Dual RMS/TMS module which provides a DC voltage proportional to either the RMS (root-mean-square) of the input signal or the TMS (true-mean-square) of the input signal. Each channel can provide -20, 0, 20 dB of gain. The response time can be selected to be fast, medium, or slow, corresponding to time constants of 10 ms, 60 ms, 240 ms, respectively. Frequency response is from 1 kHz to 1 MHz. A slow response means that some short duration bursts will have little or no affect on the output. If short term changes are important, then a faster response may be necessary.

The linear velocity transducer is an AST/SERVO SYSTEM P/N895001-2D type with a sensitivity of 45 mv/in/sec and 3.4 inch stroke. It is used to measure the voltage signal of the actual feedrate.

An IBM personal AT computer was used in conjuction with Metral-byte Labtech software, Das-8, and Das-16 for measurement purposes.

3.3 Experimental Condition

The set-up described in section 3.2 was used to perform the drilling experiments. A series of drilling tests were conducted on SAE1018 hot rolled steel with ϕd = 23/64" drill bits as shown in figure 7. All tests were run dry without coolant.

The range of spindle speed varies from 200 rpm to 1200 rpm, and the range of feedrate varies from 0.5 ipm to 5 ipm.

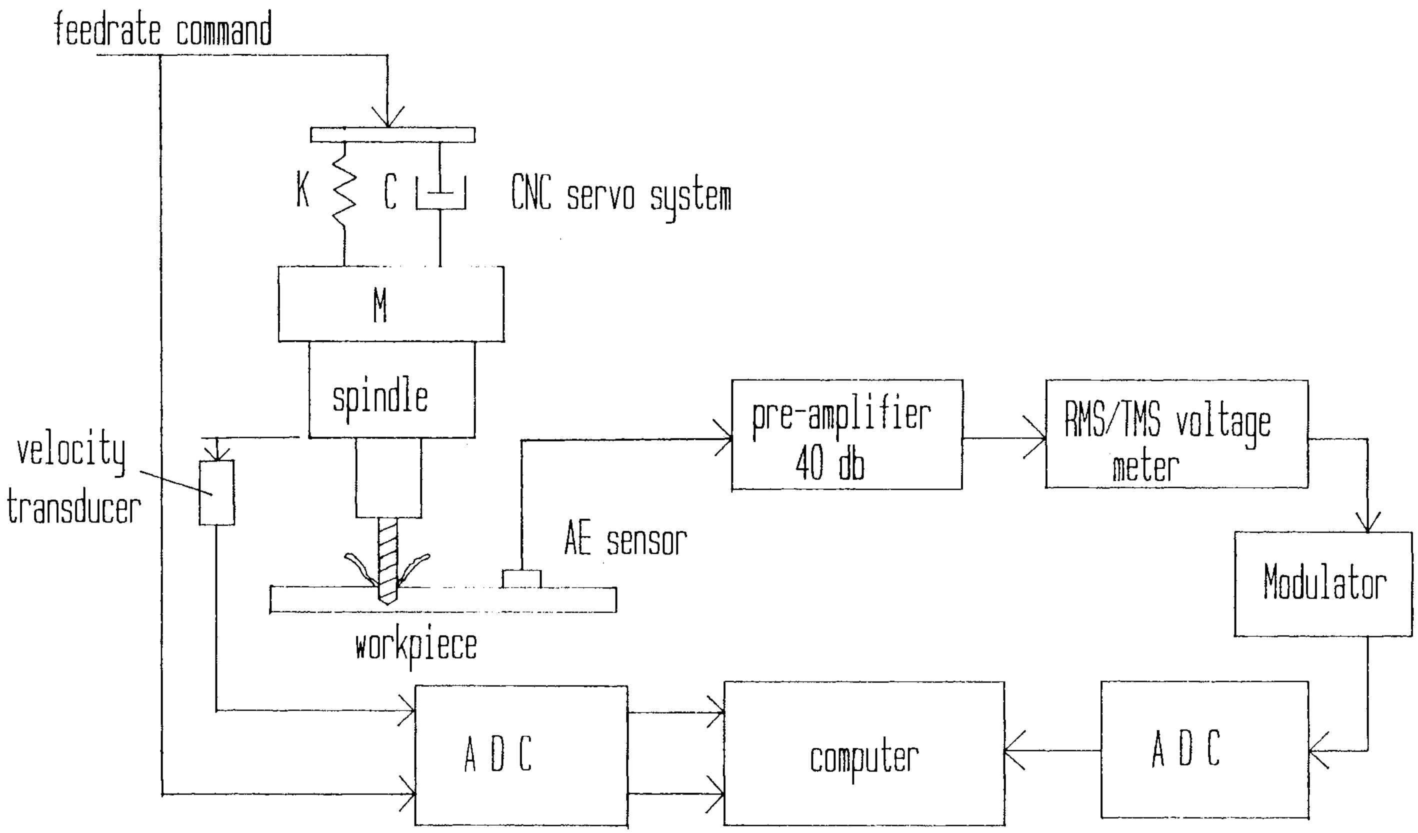

Figure 7. Experimental Set-Up and Signal Processing Flow Diagram

The drill tool would have rapid tool wear and serious chip conjestion if feed is too large, therefore in the the experiments, the feeds were set at less than 0.01 ipr. After each test was finished, the drill tool would be examined and cleaned to ensure that there was no build up edge, chip curls, or tool wear on the drill tool. The drill bit was sharpened after every 20 tests. Only 3 inches of the drill bit was used to prevent the difference of dynamic response due to the torque effect during drilling.

The AE sensor was mounted on the surface of the workpiece.

The linear velocity transducer was mounted in the CNC milling machine, and the rod of linear velocity transducer was connected with the spindle to measure the actual feedrate. The signal generated by the linear velocity transducer is proportional to the actual feedrate of the spindle.

The programmed feedrate override took place in the analog circuit that generates DC voltage to the servo DC motor.

The signals generated through the AE sensor, the feedrate override circuit and the LVT were measured and collected simultaneously in the DAS-16 screw terminal.

The experimental procedures used were the following:

1) Use a center drill to drill a small hole for centering.
2) Replace the center drill with a ϕd 23/64" drill

tool by a tool change command in the CNC milling machine.

3) Drill into the workpiece to specified depth.
4) Stop the operation. Check the condition of drill tool.
5) Change the reference point, spindle speed, and feed rate in the program.
6) Go back to step 1 and repeat the procedures.

3.4 Parameter Estimation

Since the servo system is simply constructed of a motor and an inertial load of the feed screw, the CNC feed servo motor dynamics, *Gm*, can be proposed as a second order system as shown in figure 7. The parameters M, K, and C are a lumped represention of all mass, stiffness, and damping effects in the drilling system which led to discrepancies between the actual velocity of the tool, *U*a, and the command input, *U*c. As mentioned before, closed loop d.c. drives are used for positioning. The sampled-data proportional control law is implemented in software on each of the axis controller. Reference-pulse interpolation is used, the pulses being generated by a separate feedrate control. The servoamplifier used on *Z* axis, in conjuction with permanent magnet d.c. servomotor, results in zero steady state error with constant force disturbance. Tachometer feedback is also used to increase the bandwidth of the position loop. The pulse transfer function between command feedrate and actual feedrate can be reprensented as:

$$\frac{Ua(z)}{Uc(z)} = \frac{b0\ z + b1}{z^{2} + a1\ z + a2} \qquad (3.1)$$

where $a1$, $a2$, $b0$, $b1$ are the parameters of transfer function.

Several tests were done by measuring the voltage of the command feedrate from the override in the CNC milling machine and the voltage of actual feedrate from the linear velocity transducer to estimate a model of CNC servo system.

The estimation algorithm used in this work was based on the least square algorithm with exponential data weighting [44],

$$\theta(K) = \theta(K-1) + \frac{P(K-1)\phi(K-1)[Y(K) - \theta^{T}(K-1)\ \phi(K-1)]}{\lambda + \phi^{T}(K-1)\ P(K-1)\ \phi(K-1)} \qquad (3.2)$$

and

$$P(K) = \frac{1}{\lambda} P(K-1) - \frac{P(K-1)\phi(K-1)\phi^{T}(K-1)P(K-1)}{\lambda + \phi^{T}(K-1)P(K-1)\phi(K-1)} \qquad (3.3)$$

The vector $\theta(K)$ contains the estimates of the process prameters, and the vector $\phi(K)$ is the measurement vector for the process in equation (3.1), $\theta^{T}(K) = [\ \hat{a1}(K), \hat{a2}(K), \hat{b0}(K), \hat{b1}(K)]$. The forgetting factor, λ, has the interpretation that if $\lambda = 1$, the algorithm reduces to the least square algorithm and as λ gets smaller, the algorithm "forgets" the old data faster.

The algorithm performs quite well. However, the algorithm has two drawbacks. First, the input signals need to be sufficiently rich (persistently exciting) so that the estimated parameters can converge very well. The second drawback to this algorithm is that a value for the forgetting factor must be chosen. It can be shown [41] that for stability,

$$0 < \lambda \leq 1.0 \tag{3.4}$$

Typically, a value of about 0.95 to 0.99 is suggested [44]. If the parameters change slowly and the primary concern is the final values, then the choice of λ is not important, because the estimator will finally converge to the correct values. However, if the performance during parameter convergence is significant, the choice of λ is more important. When λ is close to 1.0 the estimator reacts more slowly than when λ is small.

The test input signal, which for convenience is usually refered to as white noise [42], although not physically realizable and hence in practice is replaced by an approximation to white noise, is added to the normal system input, and a cross correlation is carried out between the system output and the test signal input. Usually, pseudo random binary sequences (PRBS) are very useful approximations to periodic white noise and are the forcing function most widely used for identification to achieve the richness.

Due to the limitation of experimental set-up, the PRBS was not available to be sent into override circuit in CNC milling machine. However, several tests were done by adjusting the handwheel randomly to generate random signal in the override circuit. The power spectrum of the input signal is shown in figure 8. The parameters of the transfer function (*Gm*) were identified roughly but still satisfactory.

3.5 Experimental Results and Discussion

In order to verify Equations (2.22) and (2.23), a series of experiments were made by drilling SAE 1018 carbon steel (hardness of 190 BHN). A view of the experimental set-up and condition has been disscussed in previous sections.

It was found during drilling that TMS increases as a ramp output. The typical experimental data of TMS generated during drilling for a step input of command feedrate is shown in figure 9. In order to investigate a variety of metal drilling problems, it is convenient and effective to separate the TMS into two parts, cutting workrate, TMSc, and frictional workrate, TMSf, as shown in figure 10.i.e.,

$$TMS = TMSc + TMSf \qquad (3.5)$$

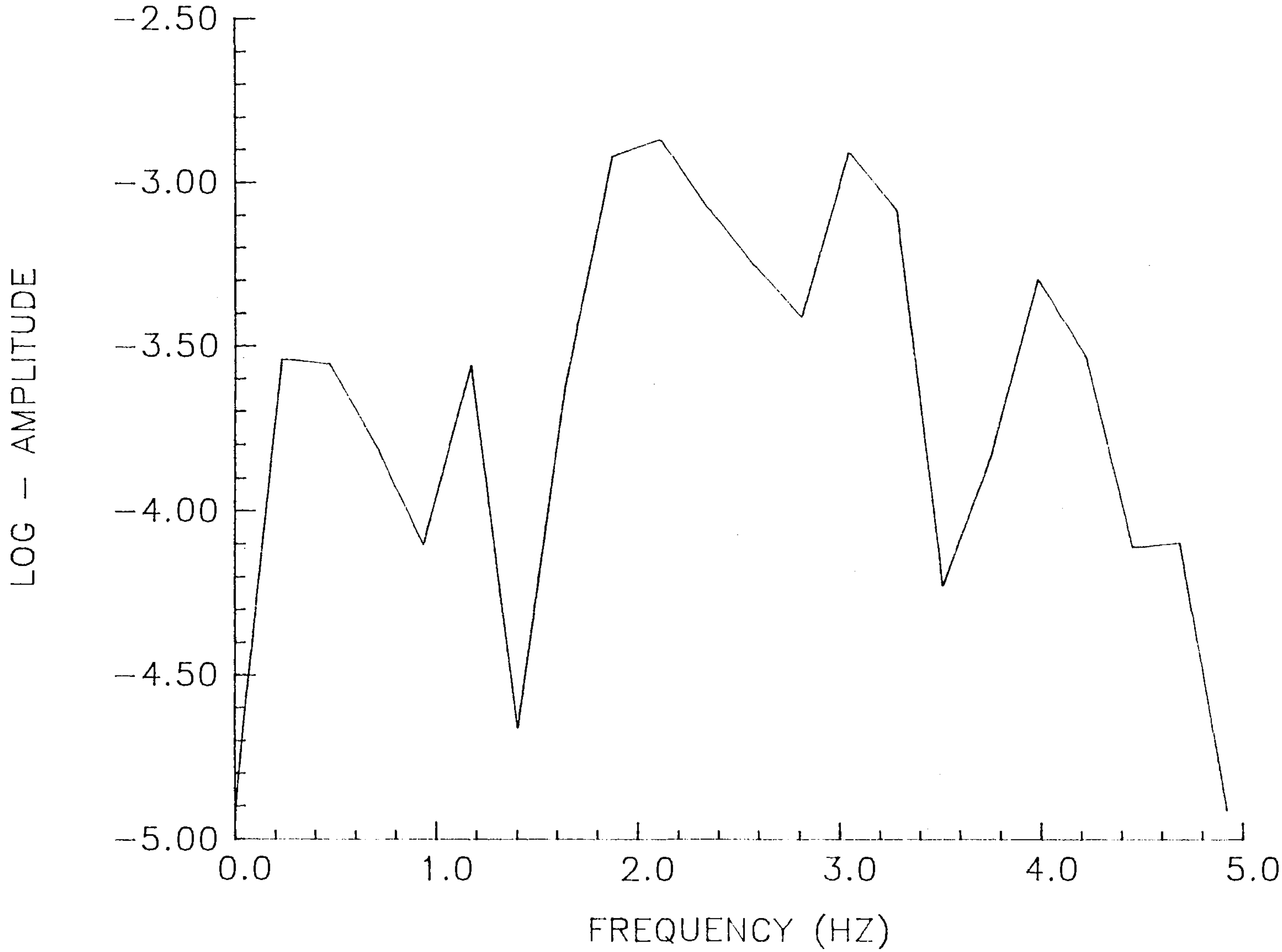

Figure 8. Power Spectrum of the Command Feedrate Signals

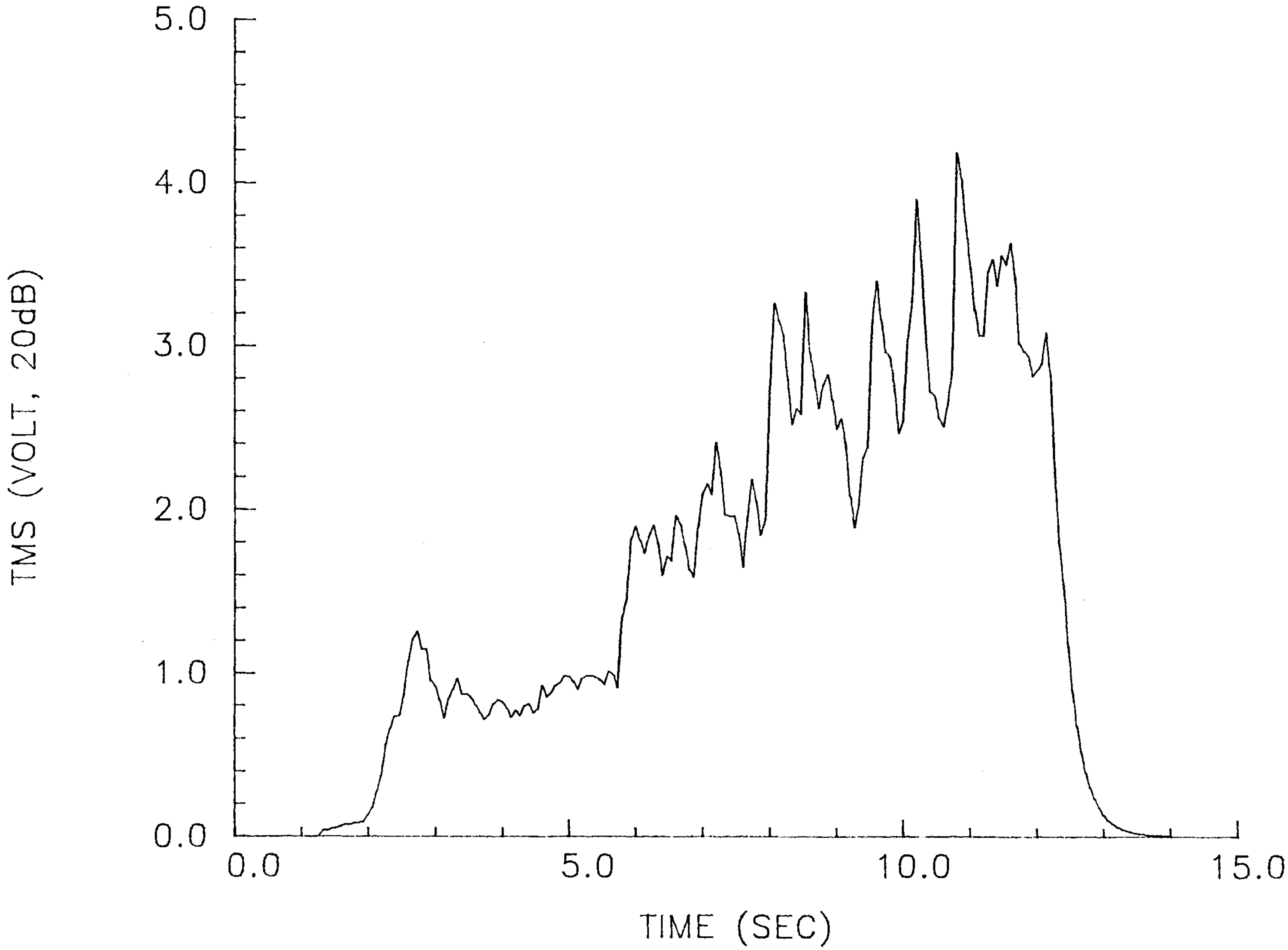

Figure 9. Typical AE TMS Signals Due to a Step Input

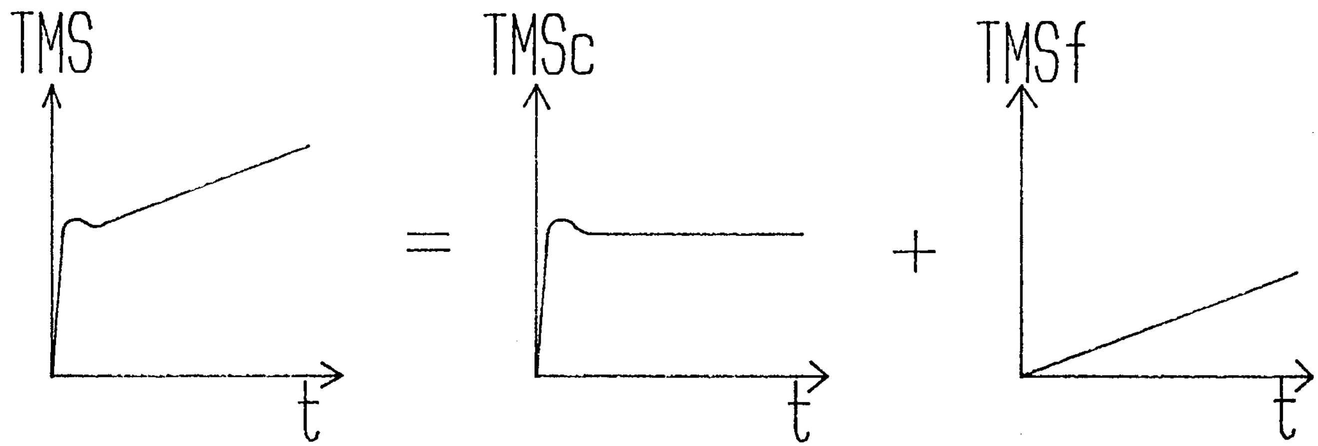

Figure 10. AE TMS as the Combination of Two Main Sources: TMSc and TMSf

The value of TMSc and the slope of TMSf was found to be dependent on cutting conditions from the result of experiments.

3.5.1 Analysis of TMSc

It was found that TMSc is sensitive to the change of spindle speed. The values of TMSc obtained in different spindle speeds with averages for each drilling condition are given in Table III. The TMSc data in Table III are shown plotted on log-log paper against spindle speed in figure 11.

It can be seen that the TMSc is a function of the change of spindle speed, and the exponent of p is approximately equal to 2.17 in equation (2.23), i.e.,

$$TMSc \propto W^{2.17} \qquad (3.6)$$

It has been reported that acoustic emission is not sensititive to the change of feed (ipr) in the turning process [26][27]. The experimental data shown in Table III are also not easily compared with each other because of their similarities. However, the data shown above are obtained by setting the constant feedrate command step input for each test, and the stochastic nature of the drilling process causes the values of TMSc not to be easily distinguished.

To investigate the difference of TMSc due to the change of feedrate, a series of drilling tests were made by sending step change from lower to higher feedrate to compare the

TABLE III

VALUES OF TMSc OF THE DRILLING TESTS

Feedrate (Fr),ipm	Spindle Speed (W),rev/min	TMSc,volt
2	400	8.41×10^{-8}
2	600	4.9×10^{-7}
2	800	6.05×10^{-7}
2	1000	8.1×10^{-7}
2	1200	1.64×10^{-6}
3	400	1.23×10^{-7}
3	600	3.84×10^{-7}
3	800	6.4×10^{-7}
3	1000	1.12×10^{-6}
3	1200	1.85×10^{-6}
4	400	1.76×10^{-7}
4	600	4.23×10^{-7}
4	800	5.33×10^{-7}
4	1000	8.1×10^{-7}
4	1200	1.46×10^{-6}
5	400	1.6×10^{-7}
5	600	3.03×10^{-7}
5	800	4.9×10^{-7}
5	1000	9.51×10^{-7}
5	1200	1.56×10^{-6}

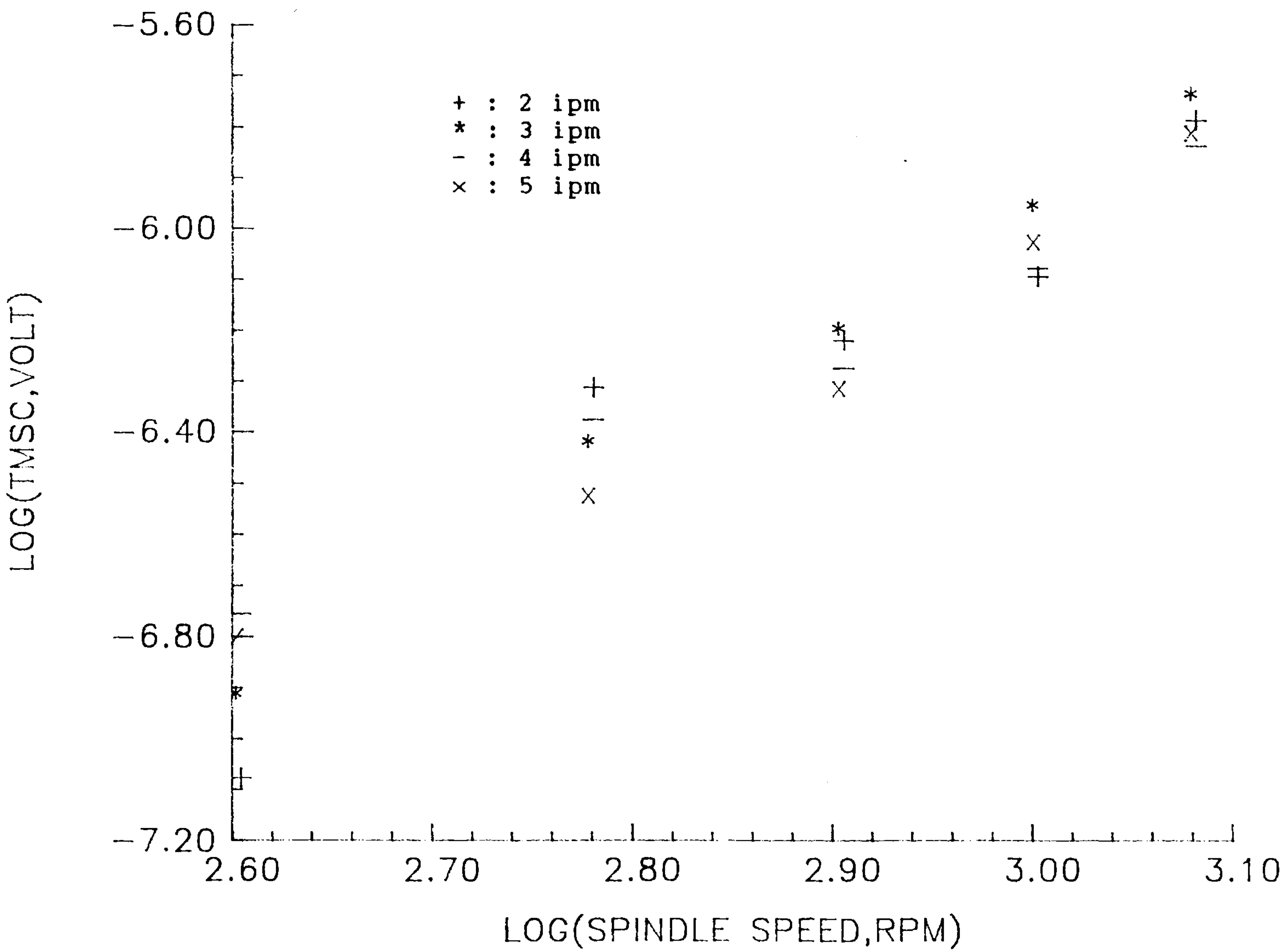

Figure 11. Plot of Log(TMSc) against Log(Spindle Speed)

value of TMSc for each feedrate with the same cutting condition. This cutting condition is the same except that feedrate are different.

The typical experimental data of TMS due to the step change of feedrate command is shown in figure 12. To analyze the TMSc due to the change of feedrate. Since the magnitude A of TMSc when feedrate is Fra and the increased magnitude B of TMSf between Fra and Frc, as shown in figure 13, are known, we can roughly measure the magnitude of TMSc when the feedrate is Frc.

Since the absolute value of TMSc, A, is known at a lower feedrate, we can easily obtain the absolute value of TMSc due to higher feedrate, C - B. The results of calculations with the spindle speed of cutting condition at 800 rpm are shown in Table IV.

The TMSc data of Table IV are shown plotted against the feedrate in figure 14. Since the spindle speed is 800rpm, the equation (2.23) yields

$$TMSc = K' \; Fr^{q} \qquad (3.7)$$

where

$$K' = Kc \; W^{2.17} \; ;$$

taking the logarithm of both sides of equation (2.27):

$$\log TMSc = q \log Fr + \log K' \qquad (3.8)$$

Since q is of interest and the TMSc data of Table IV is plotted on log-log paper anainst the feedrate, it will be found that the slope of regression line fitting the

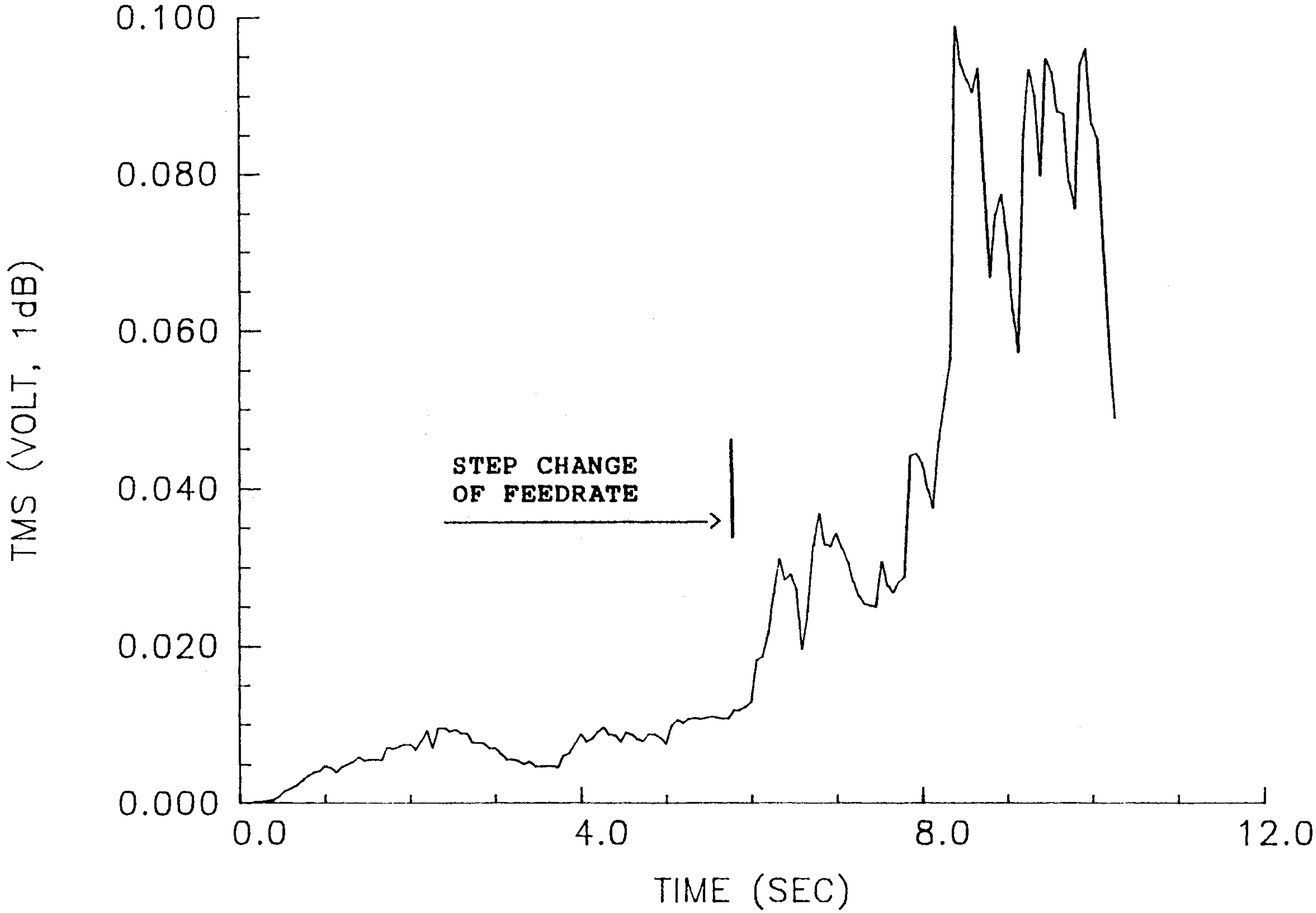

Figure 12. Typical Experimental Response of TMS Due to the Step Change of the Feedrate

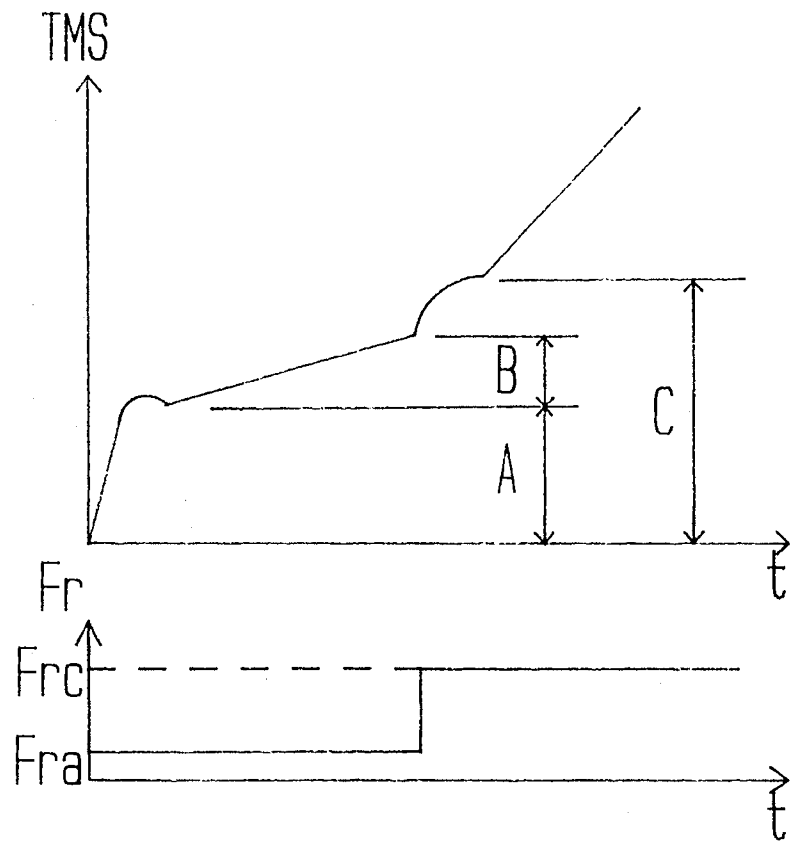

Figure 13. Analysis of the Magnitude of TMS Due to the Step Change of the Feedrate from Fra to Frc

TABLE IV

VALUES OF TMSc DUE TO STEP CHANGE OF FEEDRATE

Feedrate (Fr), ipm	Spindle Speed (W), rev/min	TMSc, volt
1	800	3.9×10^{-7}
2	800	6.43×10^{-7}
3	800	1.15×10^{-6}
4	800	1.56×10^{-6}
5	800	1.82×10^{-6}

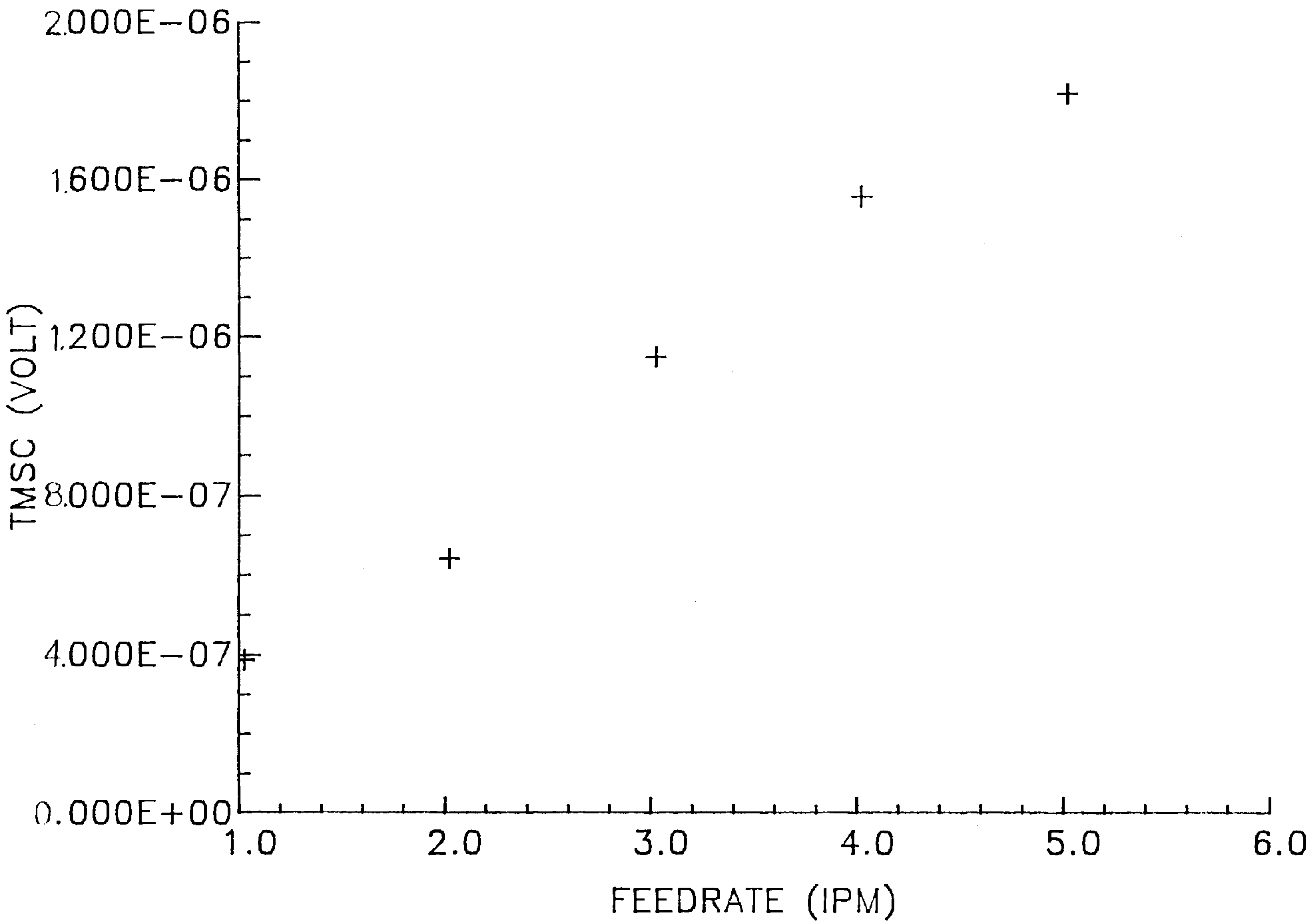

Figure 14. AE TMSc vs. Feedrate (Spindle Speed 800 rpm)

experimental points is very close to 1 as shown in figure 15. The equation (2.23) can be well approximated by an emperical equation of the form

$$TMSc = Kc\ W^{2.17}\ Fr \qquad (3.9)$$

By substituting the data of Table IV into equation (3.10), the value of Kc is approximated to be 1.854×10^{-13} (volt/rpm*ipm).

3.5.2 Analysis of TMSf

In figure 9, it can be seen that TMSf increases during drilling. TMSf is related to the spindle speed and the depth of the drilled hole.

To analyze TMSf generated during drilling, we can substract the value of TMSc with TMS to obtain TMSf as shown in figure 9. Since there is no frictional acoustic emission in the very beginning of the drilling process, we can be sure that the TMSf increases from zero to a value dependent on the cutting condition. The curve can be approximated as a triangle on TMSf v.s. time plot.

To investigate the influence of the depth of the drilled hole to the frictional acoustic emission, a series of works are made by evaluating TMSf/H (or TMSf/(Fr T)), the data is shown in Table V.

It can be seen that the values of TMSf/H are nearly constant for the change of feedrate. It can be concluded that TMSf generated during drilling is related to depth of

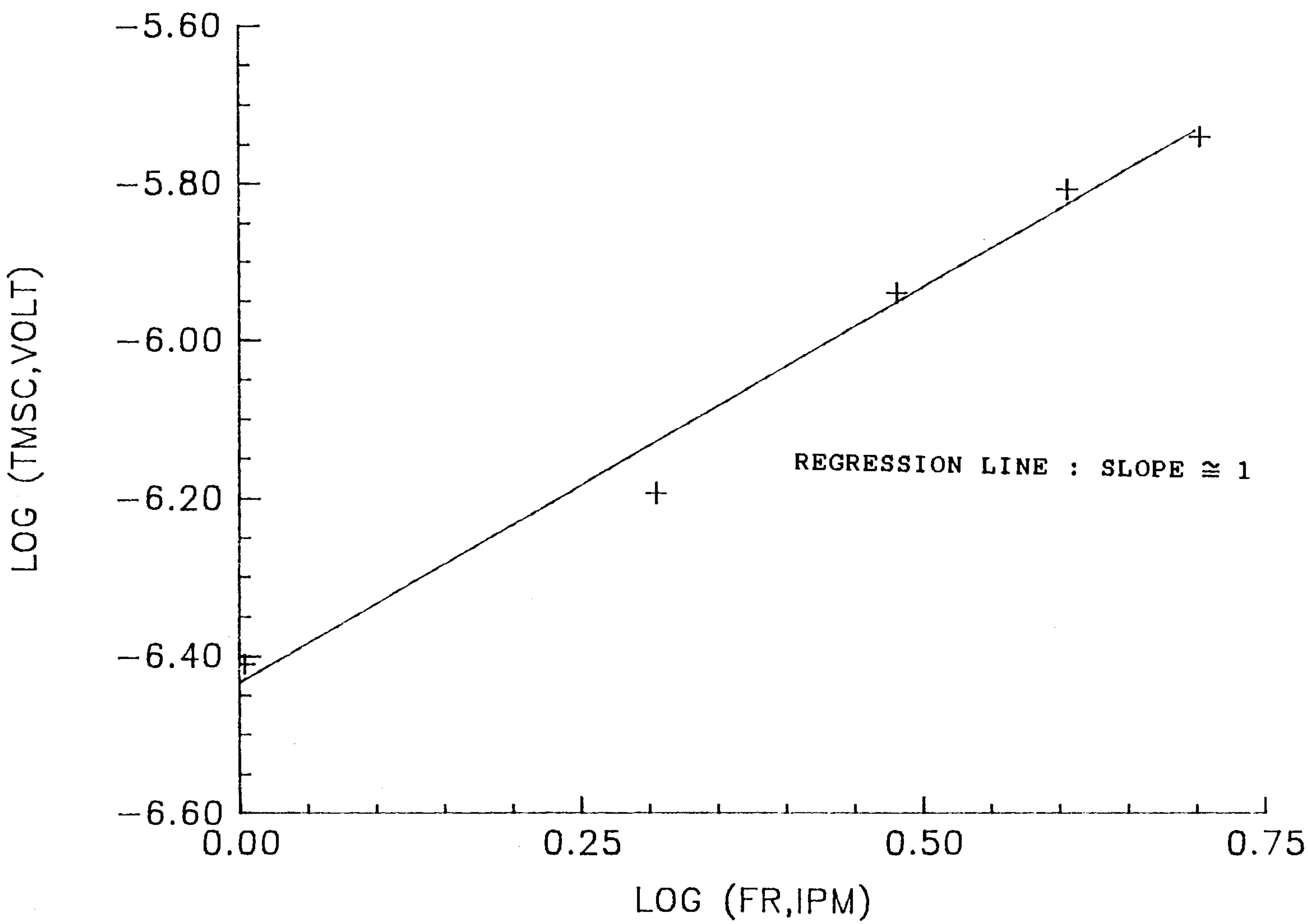

Figure 15. Plot of Log(TMSc) Against Log(Feedrate)

TABLE V

VALUES OF TMSf/H WITH CUTTING CONDITION
SPINDLE SPEED 800 rpm

Feedrate (Fr), ipm	TMSf/H, volt/inch
0.8	6.4×10^{-6}
1	8.6×10^{-6}
1.5	1.3×10^{-5}
2	1.1×10^{-5}
3	1.1×10^{-5}
4	8×10^{-6}
5	9.6×10^{-6}

the drilled hole rather than the feedrate. The reason why the TMSf is a function of the depth of the drilled hole during drilling is because the contact area of friction between the chips and the wall of drilled hole is increased, thus the frictional work rate is also increased.

It was found during drilling that TMSf is also sensitive to the change of spindle speed. For the same depth of the drilled holes, the values of TMSf generated are dependent on the magnitude of the spindle speed. In other words, the slope of the triangle as shown in figure 9 is a function of spindle speed. The values of TMSf obtained in the individual tests with averages for the same depth of the drilled hole are given in Table VI.

In figure 16, the TMSf data are shown plotted on log-log paper against W for the data of Table VI. The relation between TMSf and W is found to be

$$TMSf \propto W^{1.57} \tag{3.10}$$

It can be verified that equation (2.28) is in good agreement with the experimental data. i.e.

$$TMSf = Kf\ W^{1.57}\ H \tag{3.11}$$

By substituting the data of Table IV into equation (3.11). The mean value of Kf is 3.23×10^{-10} volt/rpm inch.

3.5.3 Identification of CNC Servo System

In order to develop a model for the cutting process

TABLE VI

VALUES OF TMSf WITH CUTTING CONDITION IN THE SAME DEPTH OF 0.3 INCH

Feedrate (Fr),ipm	Spindle Speed(W),rpm	TMSf,volt
2	400	8.4×10^{-7}
2	600	2.75×10^{-6}
2	800	3.39×10^{-6}
2	1000	3.8×10^{-6}
2	1200	5.65×10^{-6}
3	400	8.78×10^{-7}
3	600	3.03×10^{-6}
3	800	4.3×10^{-6}
3	1000	4.95×10^{-6}
3	1200	5.75×10^{-6}

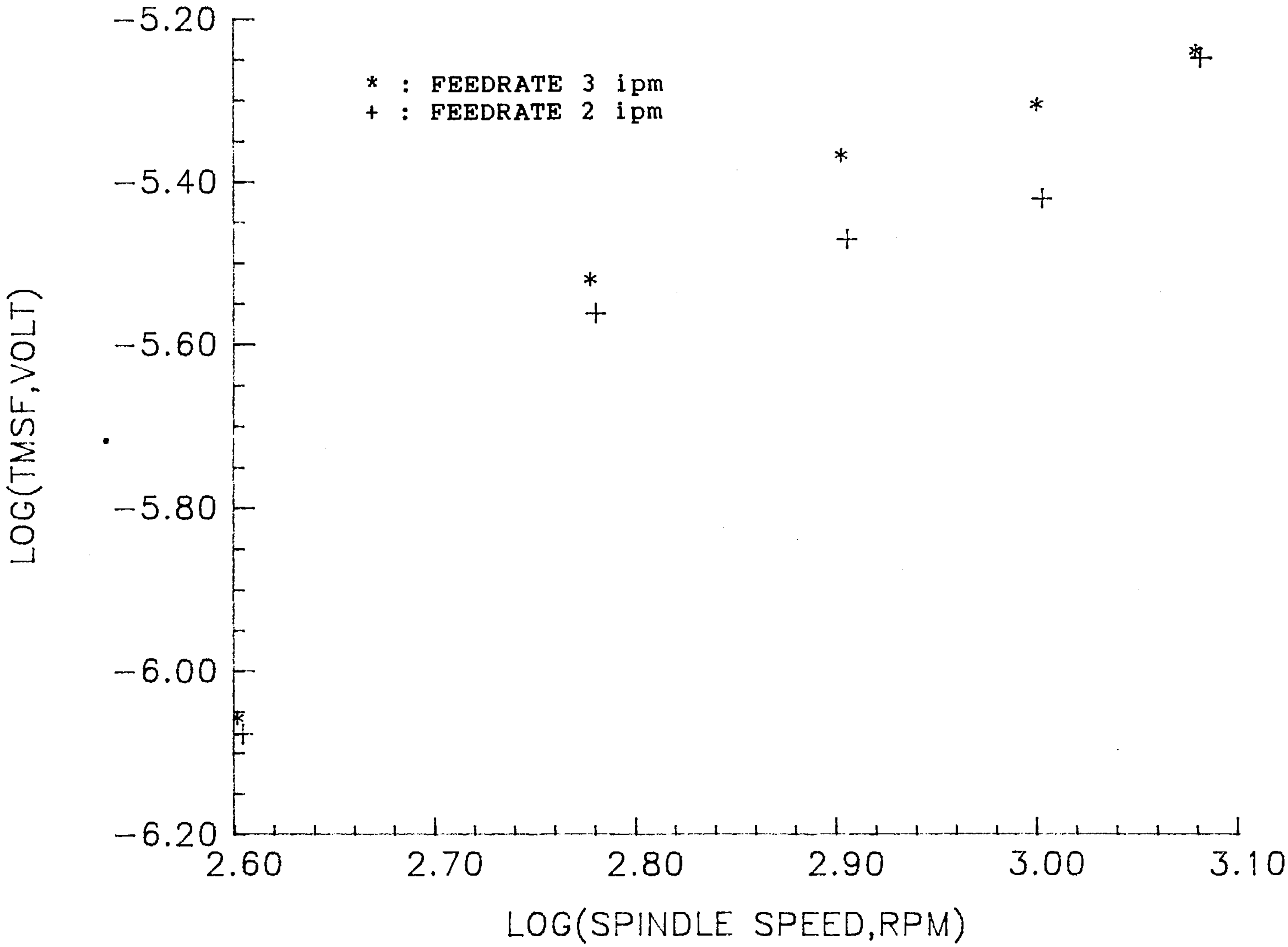

Figure 16. Plot of Log(TMSf) against Log(Spindle Speed)

with the feedrate command as input and the TMS as output, a series of open loop tests was conducted to determine the CNC servo structure model.

As mentioned in Section 2, the CNC servo system is a closed loop with a tachometer feedback system. The steady state error will be zero for constant thrust force disturbance. It is interesting to notice the dynamics of the CNC system are not strongly dependent on the cutting condition.

To consider the dynamics of CNC system, we have to measure the input of command feedrate signal from the override circuit and the output of actual feedrate signal from the LVT mounted in the CNC milling machine. Step response testing will usefully and relatively easily give a first idea of the general form of the trasnsfer function, and can also give some indication of how the linear system is. There are two kinds of tests with and without drilling workpiece conducted in the experiments.

Figure 17 shows a typical input and output signals obtained for a step change of feedrate from 2 to 5 ipm with drilling workpiece.

Figure 18 shows a typical input and output signals obtained for a step change of feedrate from 0.5 to 10 ipm without drilling workpiece.

The tests indicated that the dynamics from the feedrate command to the actual feedrate did not have strong dependence on cutting condition. Since the rise time was

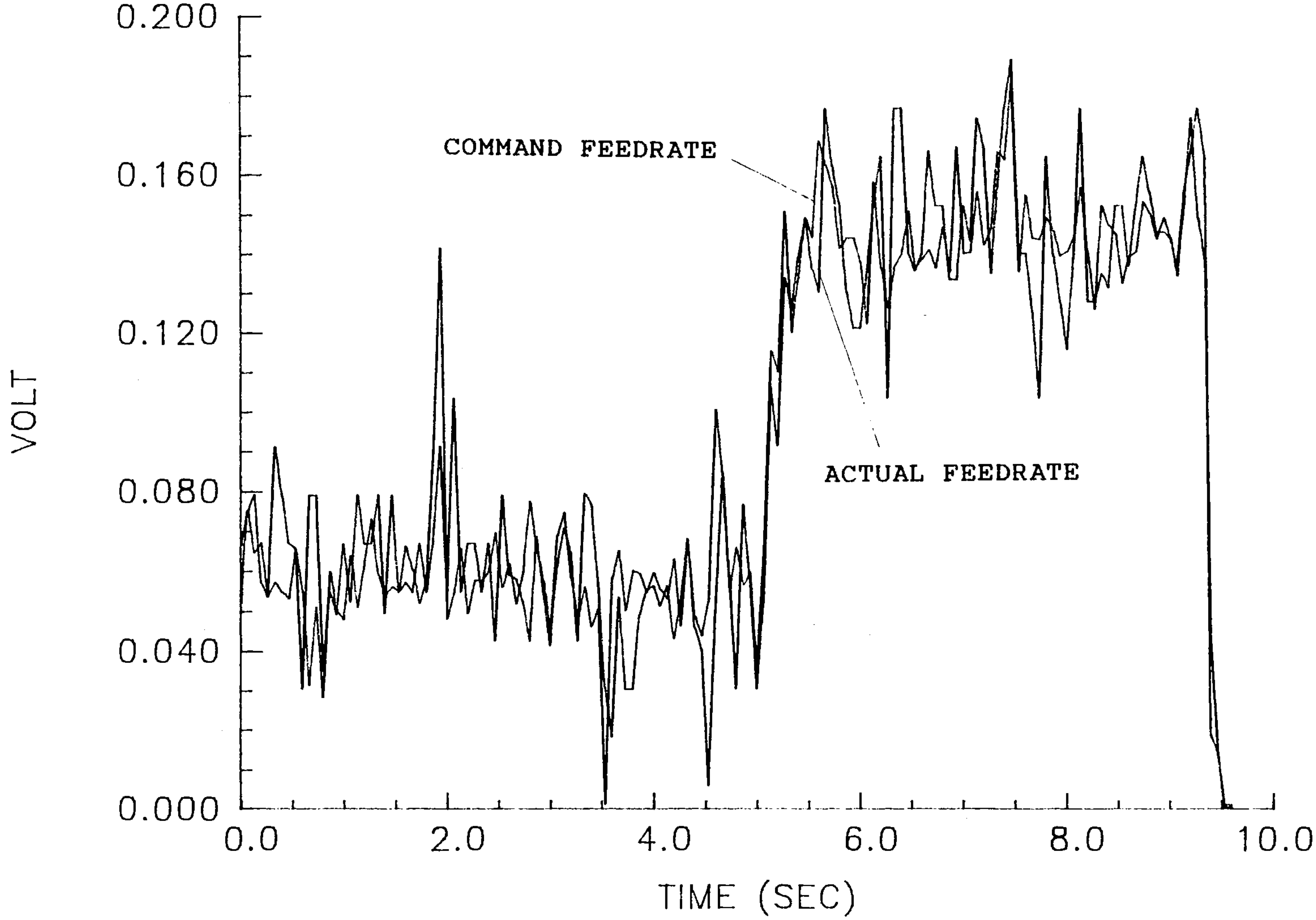

Figure 17. Typical Response of Actual Feedrate Due to the Step Change of The Command Feedrate from 2 to 5 ipm with Drilling Workpiece

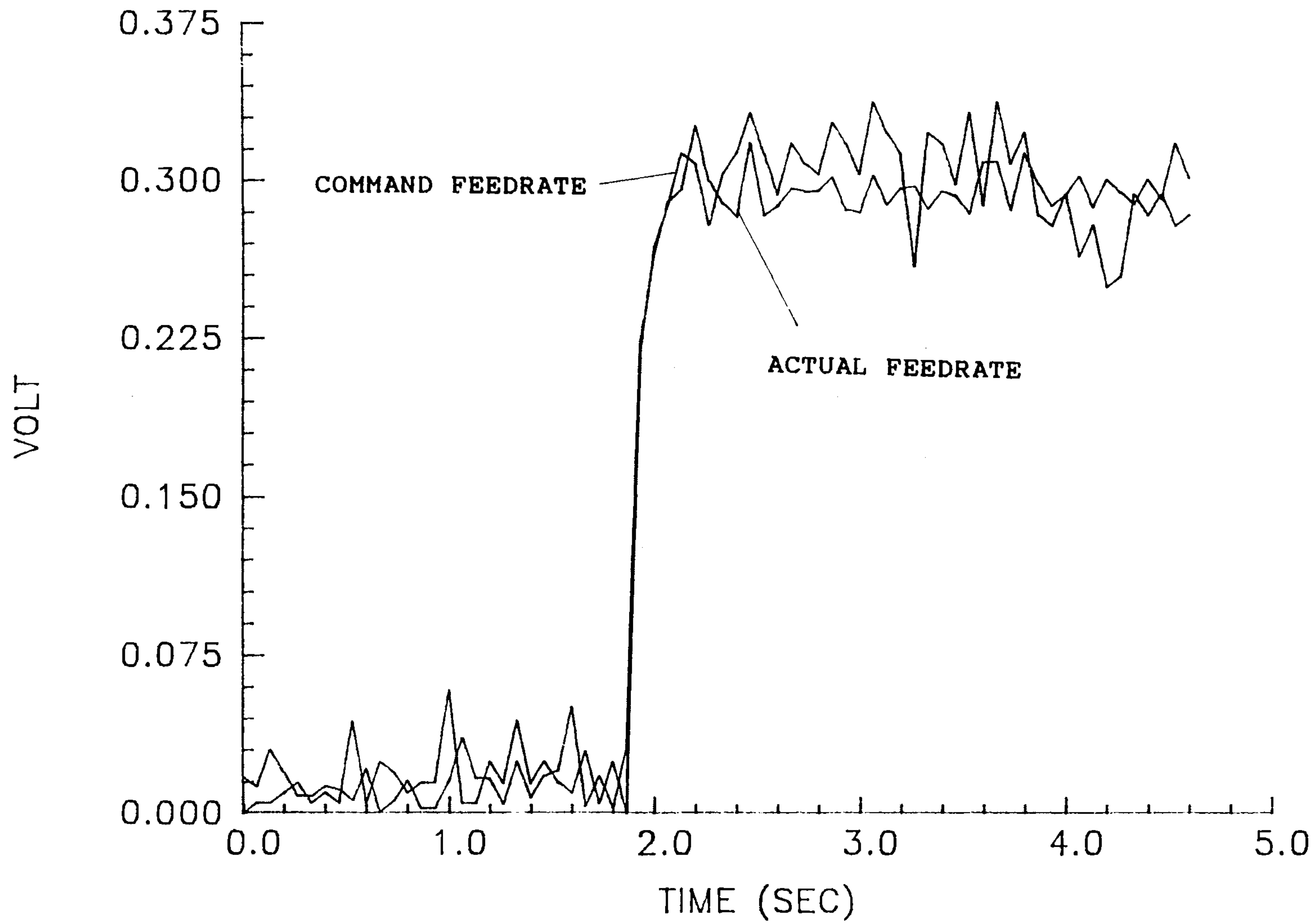

Figure 18. Typical Response of Actual Feedrate Due to the Step Change of the Command Feedrate from 0.5 to 10 ipm without Drilling Workpiece

fairly close for those two kinds of tests, it was observed to be roughly 100ms. However, rise time is only a part of the elements needed to describe a second order dynamic model, since the CNC servo system is characterized by the presence of inertia, stiffness and viscous damping.

Based on a rough estimate of required second order CNC servo system, we can identify the parameters of the transfer function from command to actual feedrate without drilling. This eliminates the limitation of set-up required to achieve the richness of parameter estimation as we mentioned before.

In order to indentify the dynamics of tool carriage and driver, the command feedrate signals were sent from override circuit by ajusting the handwheel on the controller as randomly as possible. For a 30 Hz sampling rate, the typical command feedrate and actual feedrate are shown in figures 19 and 20. Based on the least square identification by setting forgetting factor $\lambda = 1$, the identified parameters are shown in figure 21.

Since the convert gain of CNC servo system is found to be 33.3 ipm/volt, the dynamics from command feedrate to actual feedrate is approximately given by:

$$\frac{Fr(z)}{Uc(z)} = 33.3 \frac{1.03\, z - 0.55}{z^2 - 0.24\, z - 0.28} \qquad (3.12)$$

where

$Uc(z)$ = command feedrate (volt); and

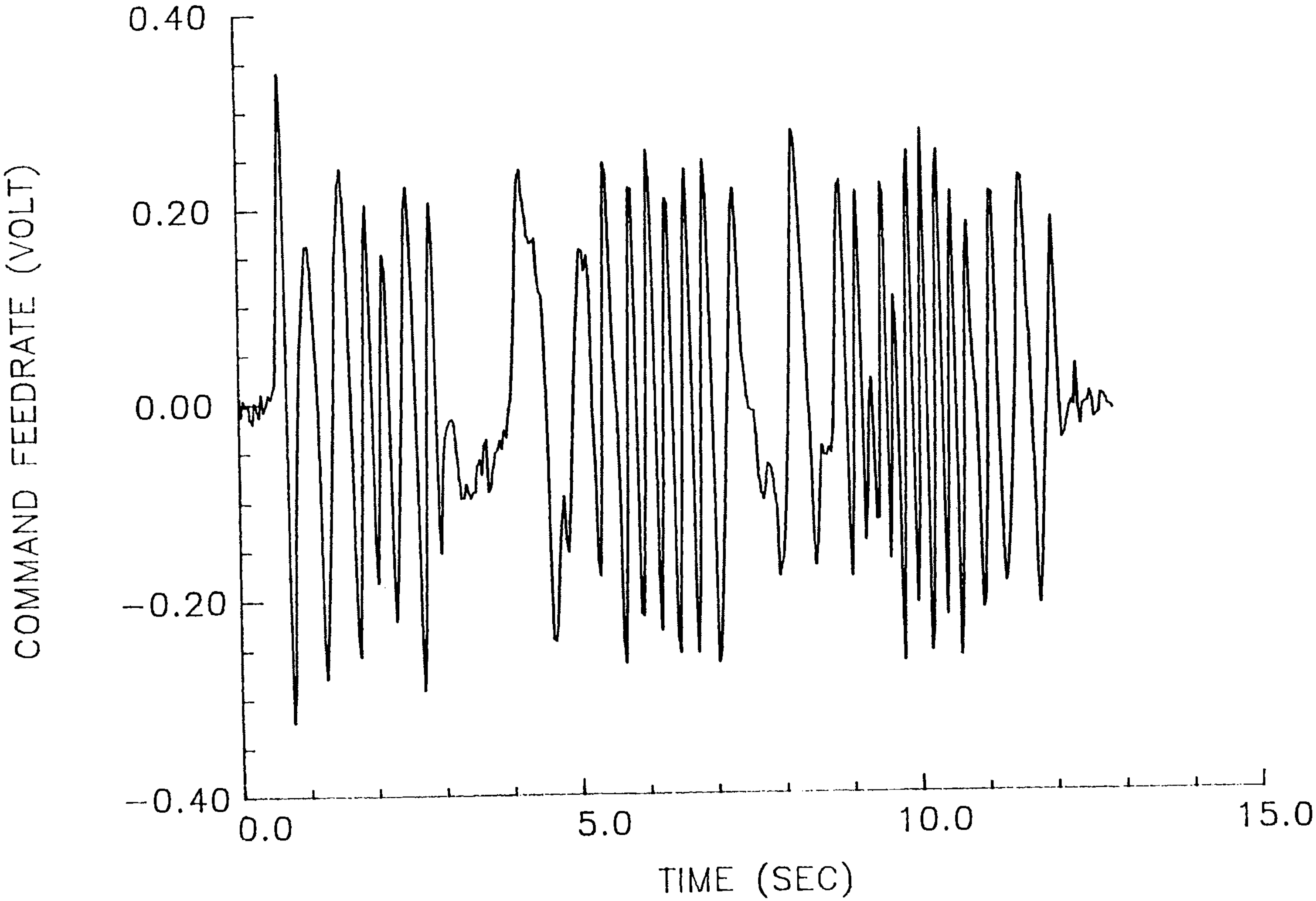

Figure 19. Test of Command Feedrate

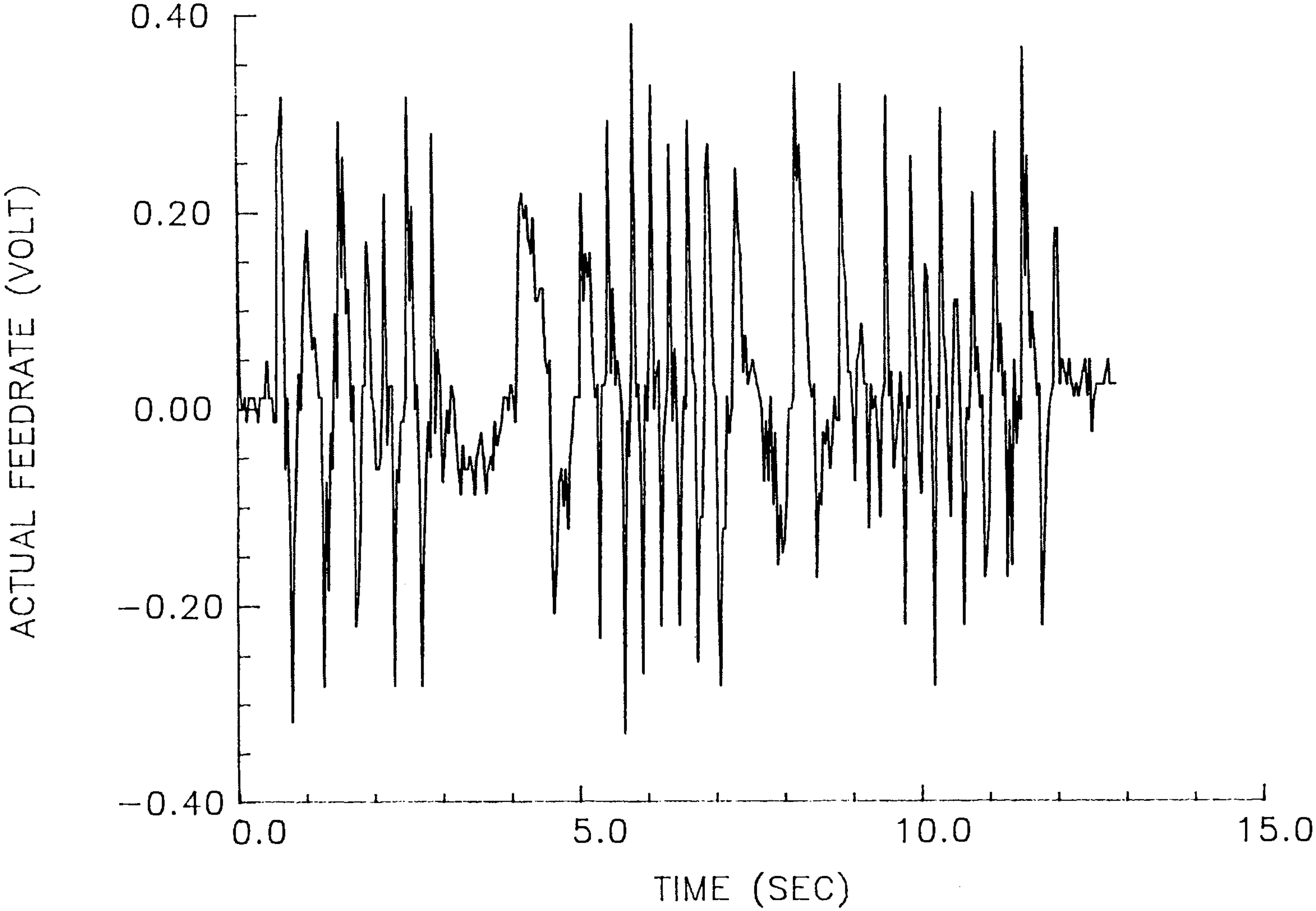

Figure 20. Test of Actual Feedrate

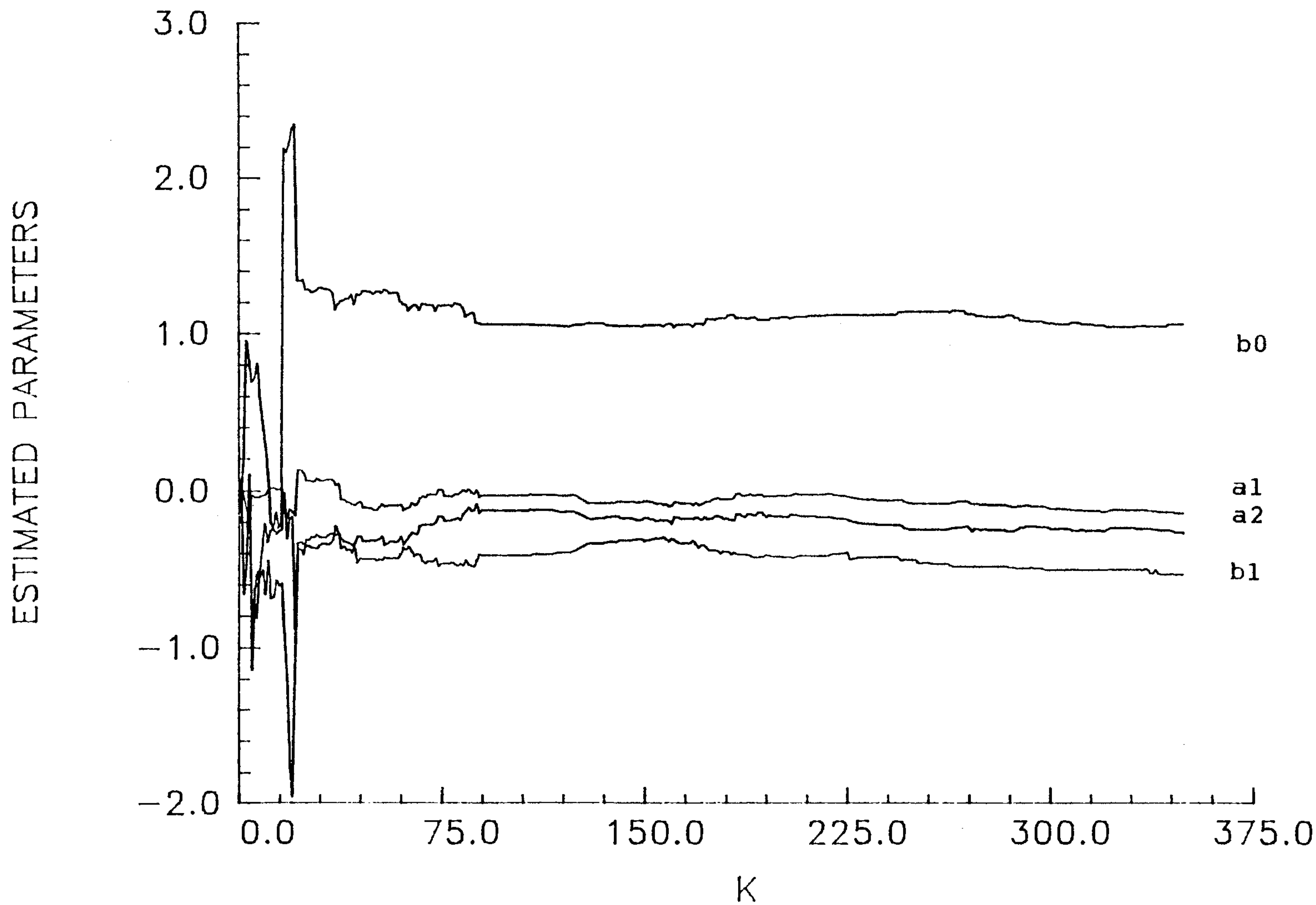

Figure 21. Test of Parameters Estimation at Sampling 30 Hz

Fr(z) = actual feedrate (ipm).

3.6 Metal Cutting Dynamics (Gp(z))

3.6.1 Dynamics of TMSc

As mentioned before, we are dealing with acoustic emission TMS in the sense of an average. In this section we derive the discrete time transfer function Gp(z) between the actual feedrate (input) and the averaged TMS (output).

In equation (3.5), the TMS generated during drilling has been verified to have two sources. For the first part, the TMSc is related to the feedrate and the spindle speed. Several papers have advocated the applicability of a first order model relating cutting force in the turning process [12][17][18][19][22] based on the following equation

$$\tau \dot{F_c} + F_c = K_v f \qquad (3.13)$$

where F_c is product of the actual cutting force, the sensor gain and the A/D convert gain; f is the feed; Kv is the process gain and depends on the depth of cut, the spindle speed, properties of the tool and workpiece, and the feed itself; and τ is the process time constant. By taking Laplace transform on both sides, the turning process model is given by

$$Gp(s) = \frac{\text{cutting force}}{\text{feed}} = \frac{Fc(s)}{f(s)} = \frac{Kv}{(\tau s + 1)} \qquad (3.14)$$

the time constant τ is proposed to be related to the period of spindle speed. Since incremental force increases roughly linearly with undeformed chip thickness, the force increase linearly over the duration of first revolution. The time constant is given on the basis of the time taken for the incremental value [23], i.e.,

$$\tau = 0.64\ \text{Trev} \qquad (3.15)$$

where Trev is the duration of one revolution.

Acoustic emission refers to the elastic stress waves generated as a result of the rapid release of strain energy within a material due to a rearrangement of its internal structure. AE based on monitoring has proven that the acoustic emission generated from machining process depends on the material properties of the workpiece, stress, strain rate and volume involved in the process. Similarly, the drilling cutting process model can also be given by

$$Gp(s) = \frac{\text{cutting TMS}}{\text{feedrate}} = \frac{\text{TMS}(s)}{\text{Fr}(s)}$$

$$= \frac{Kg}{(tc\ s + 1)} \qquad (3.16)$$

where

Kg = gain of plant transfer function; and

tc = time constant;

The gain Kg and time-constant are time-invariant for constant cutting conditions. The time constant of the cutting process is primarily related to the period of spindle revolution. Since the magnitude of acoustic emmision signal increases roughly linearly with undeformed chip thickness, the acoustic emission will also increase linearly over the duration of one revolution. Hence the dynamic response can be approximated by first order dynamics, on the basis of the time taken for the incremental acoustic emission to reach $(1-e^{-1})$ of its final incremental value, i.e..

$$tc = 0.64\ Trev \tag{3.17}$$

In discrete time domain, the transfer function can be approximated by

$$TMSc(k) = e^{\left(-\frac{T}{tc}\right)}\ TMSc(k-1) + Kg\left(1 - e^{\left(-\frac{T}{tc}\right)}\right) Fr(k-1) \tag{3.18}$$

where

T = sampling period.

By taking z-transform, the equation (3.18) becomes

$$Gc(z) = \frac{TMSc(z)}{Fr(z)} = Kg\,\frac{(1 - Bc)}{(z - Bc)} \tag{3.19}$$

where

$$Bc = e^{\left(-\frac{T}{tc}\right)}.$$

<u>3.6.2 Dynamics of TMSf</u>

For the second component of TMS in equation (3.11), $TMSf = Kf\ W^{1.57}\ H$, it can be derived as

$$\int_0^t d(TMSf(t)) = Kf\ W^{1.57} \int_0^t Fr(t)\ dt \tag{3.20}$$

then in discrete time domain,

$$TMSf(KT) - TMSf((K-1)T) = Kf\ W^{1.57} \int_{(K-1)T}^{KT} Fr(t)\, dt \qquad (3.21)$$

by using Forward Retangular Approximation (FRA),

$$TMSf(KT) = TMSf((K-1)T) + Kf\ W^{1.57}\ T\ Fr((K-1)T) \qquad (3.22)$$

where

T = sampling period;

so the transfer function can be simply expressed as:

$$Gf(z) = \frac{TMSf(z)}{Fr(z)} = \frac{Kf\ W^{1.57}\ T}{z - 1} \qquad (3.23)$$

From equation (2.24), (3.19), and (3.23), the plant transfer function is therefore given by

$$Gp(z) = Gc(z) + Gf(z)$$

$$= Kg \frac{1 - Bc}{z - Bc} + Kf \frac{W^{1.57}\ T}{z - 1} \qquad (3.24)$$

note that Kg is equal to Kc $W^{2.17}$ from equation (3.9).

3.7 Filtering modular dynamics (Gam(z))

During machining, a significant amount of the acoustic emission siganl is due to chip breaking and the impact of the chip on both the workpiece and the cutting tool. Acoustic emission signals due to these effects are typically large amplitude burst signals compared to the acoustic emission generated during normal cutting. Since we do not attempt to control the oscillatory components, we have to reject the fluctuating portion of the measured TMS.

For this purpose, the fast signals of the acoustic emission generated due to chip breaking and the impact of the chip on both the workpiece and the cutting tool can be filtered out using the module set at TMS slow response. In such a case, the RMS slow response acts as a low-pass filter and would have a relatively low band width. Therefore, the TMS slow response would also dominate the whole machining process; thus the controlling action becomes very slow because of its large time constant dominant pole. Hence the modular dynamics can not be ignored.

For a step change in input amplitude, the output will require three times the response time constant to come to within 95% of the ultimate value. The dynamics can be approximated as a first order transfer function in continuous time domain, ie..

$$Gam(s) = \frac{TMS(s)}{TMSi(s)} = \frac{1}{\tau m\ s + 1} \qquad (3.25)$$

where

TMSi = input signal of module;

s = Laplace transform operator; and

τm = time constant of RMS/TMS Module.

The transfer function can be converted into $Gam(z)$ in discrete time domain.

$$Gam(z) = \frac{1 - e^{\left(-\frac{T}{\tau m}\right)}}{z - e^{\left(-\frac{T}{\tau m}\right)}} \quad (3.26)$$

where

T = sampling period.

CHAPTER IV

MODELING OF AE SENSING DYNAMICS

4.1 Experimental Verification

In order to develop a model for the cutting process with the feedrate command as input and the TMS as output, a series of open loop tests were conducted to determine the model structure of drilling process. The experiments were based on the cutting condition, spindle speed 800 rpm and sampling rate 15 hz. The slow response 240ms was chosen for RMS/TMS module. The results of open loop simulation are in good agreement with experimental result.

4.1.1 Transfer function of Gc(z)

As mentioned in chapter 3, the acoustic emission increases linearly over the duration of one spindle revolution to reach its new value. Hence for a spindle speed of 800 rpm, we have

$$Trev = \frac{60}{800} = 0.075 \text{ sec/rev} \qquad (4.1)$$

Therefore, $tc = 0.64 \times Trev = 0.048$ sec. Substituting sampling time T, 0.0666 sec, and tc into equation (3.19), we have

$$Gc(z) = \frac{TMSc(z)}{Fr(z)} = \frac{Kc\ W^{2.17}\ 0.75}{z - 0.25} \qquad (4.2)$$

where

$Kc = 1.854\times10^{-13}$;

equation (4.2) can also be given as:

$$Gc(z) = \frac{2.78\times10^{-8}}{z - 0.5} \qquad (4.3)$$

4.1.2 Transfer function of Gf(z)

For the cutting condition of the spindle speed set at 800 rpm, $Kf=3.23\times10^{-10}$ volt/rpm inch. Substituting T = 0.0666/60 min and Kf into equation (3.23), we have

$$Gf(z) = \frac{TMSf(z)}{Fr(z)} = \frac{1.295\times10^{-8}}{z - 1} \qquad (4.4)$$

4.1.3 Dynamics of Filtering Module

The slow response was set for the experiments, i.e., τ_s = 240ms. Substituting τ_s into equation (3.26) and evaluating, then

$$Gam(z) = \frac{1 - e^{\left(-\frac{66.6}{240}\right)}}{z - e^{\left(-\frac{66.6}{240}\right)}} = \frac{0.24}{z - 0.76} \qquad (4.5)$$

Note that the time constant set for module may not be in the form for the drilling process because the chip breaking that occurs in drilling can cause random fluctuations in the acoustic emission signal.

4.1.4 Gain of Conditioner and Module

Due to limitation of diagnostic circuit in the CNC milling machine, the measurement allows the computer to detect the volatage from 0 to 0.5 volt from the override circuit milling machine. The gains,1 dB, 5 dB and 10 dB were selected for the signal conditioner, and 0 dB for RMS/TMS module for these experiments. Then the voltage of signals from RMS/TMS module and override circuit can be collected.

If the voltage V(t) of input signal for RMS/TMS module is amplified by gain Kam, i.e. Kam V(t), and substituted into equation (2.6), then the output of signal energy of TMS is Kam expressed as:

$$TMS = Kam^2 \frac{1}{\Delta T} \int_0^{\Delta T} V(t)^2 \, dt \qquad (4.6)$$

4.1.5 Random Noise

During machining, AE signals due to chip-breaking are typically large amplitude burst signals compared to the AE signals generated during normal cutting. Each significant burst event represents the breaking of a chip.

The energy required to form the chip that determines the amplitude and noisiness of continuous acoustic emission. The burst amplitude of chip breaking is dependent on the cross sectional area of the chip and the hardness of the material [35]. Because of the stochastic nature of the machining process the chip size cannot be uniformly controlled thus some scatter in chip-breaking frequency occurs. The chip-breaking frequency is estimated as a function of feed [31]. For turning SAE 1018 steel with a carbide insert tool, the conclusion of this study [31] shows that there is an excellent correlation of measured event count rate with the chip-breaking frequency as shown in Table VII and figure 22. The event count per sec indicates the frequency of chip-breaking. i.e.

$$\dot{N} = Bhz \tag{4.7}$$

where

$\dot{N}$ = event count rate; and

Bhz = chip-breaking frequency;

the chip-breaking frequency data in figure 22 has been plotted on log-log paper against the feed and it was found that the slope of regression line fitting the experiment is very close to 1.6 as shown in figure 23. Therefore the chip-breaking frequency as a function of feed can be estimated as:

$$Bhz = Kb\, f^{1.6} \tag{4.8}$$

TABLE VII

FEEDS AND CORRESPONDING ESTIMATED CHIP-BREAKING FREQUENCY [31]

Feed (f), (inch/rev)	Estimated Chip-Breaking Frequency (HZ)
0.005	5.4
0.0075	23.4
0.010	35.1
0.012	51.6
0.015	48.8
0.020	52.6

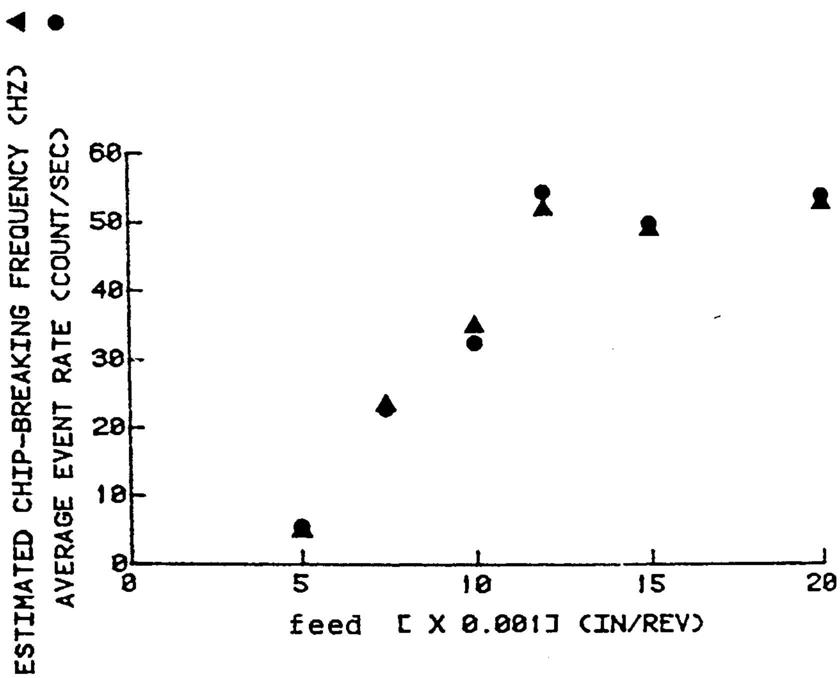

Figure 22. Average Event Rate and Estimated Chip-Breaking Frequency vs. Feed [31]

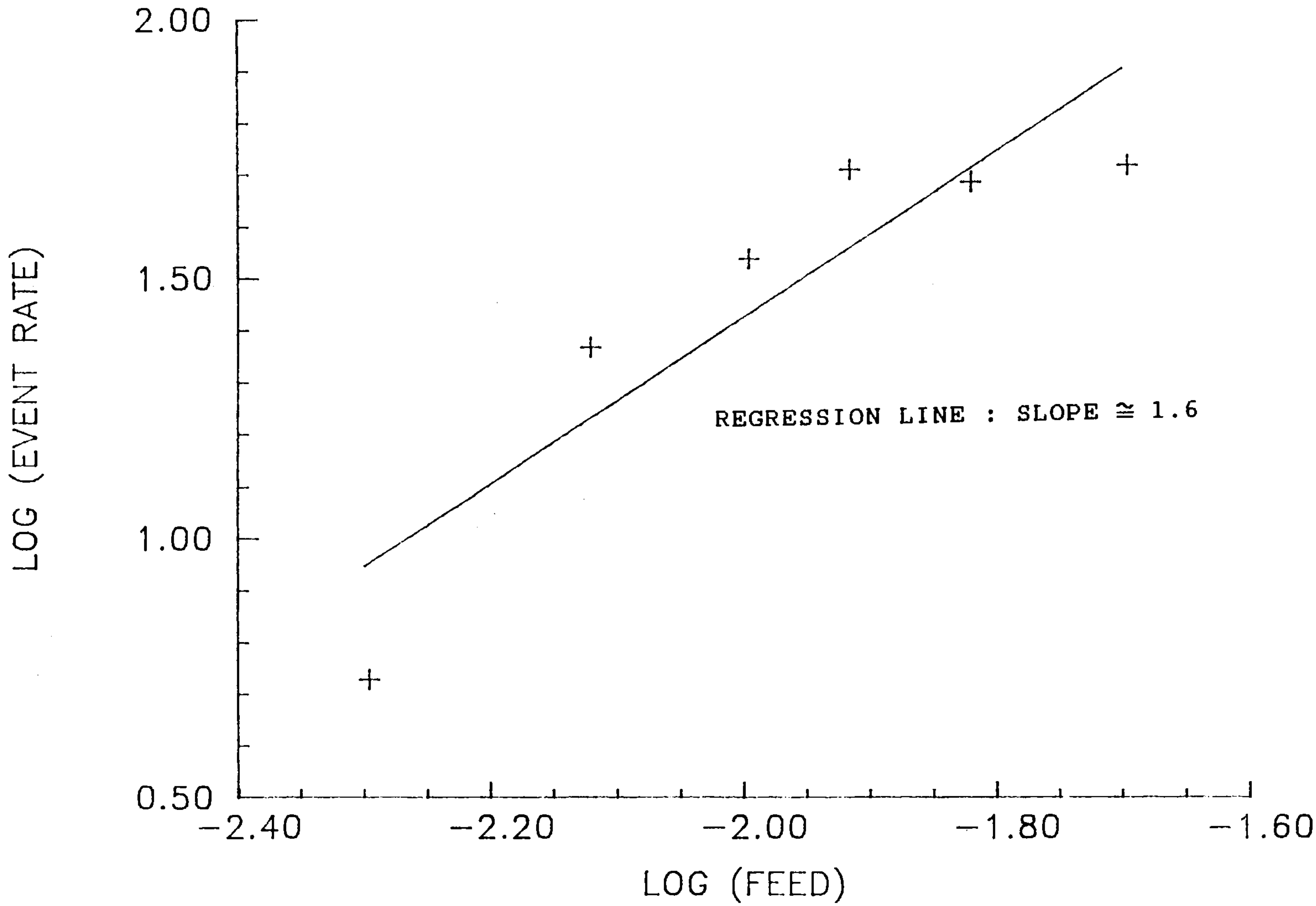

Figure 23. Plot of Log(Chip-Breaking Frequency) vs. Log(Feed)

where

f = instantaneoous feed (in/rev)(Fr/W); and

Kb = constant dependent on material;

it has been shown that the energy rate of acoustic emisson is correlated to the event count rate [30],

$$\dot{E} = Ce\ \dot{N} \qquad (4.9)$$

where

$\dot{E}$ = the rate of energy dissipation; and

Ce = proportionality constant;

from equations (4.7), (4.8), and (4.9), the energy rate of chip-breaking can be given as

$$TMSb = \dot{E} = Ce\ \dot{N} = Ce\ Bhz = Ce\ Kb\ f^{1.6}$$

$$= Ce\ Kb\ (Fr/W)^{1.6} = Kn\ Fr^{1.6} \qquad (4.10)$$

where

TMSb = energy rate of chip-breaking; and

$Kn = Ce\ Kb\ W^{-1.6}$;

Kn is observed and approximated to be 1×10^{-9} volt/(ipm) from the previous experiments in this research.

By ignoring the time constant and using (4.7), the transfer function between the TMSb and Fr can be written as:

$$Gn(z) = \frac{TMSb(z)}{Fr(z)} = Kn\ Fr^{0.6} \qquad (4.11)$$

Since the chip-breaking process is of a stochastic nature, therefore this process is accompanied with random noise. To investigate the effect of the output noise, zero mean Gausian random noise W(k) with a standard deviation 0.3 is mutiplied with the transfer function in equation (4.11).

4.1.6 Model Summary

Summarizing equations (4.2), (4.3), (4.4), (4.5) and (4.11), the discrete time model of the drilling system becomes as shown in figure 24,

$$\frac{TMS(z)}{Uc(z)} = Kh \frac{(1.03z-0.55)(z-0.966)}{(z^2-0.24z-0.28)(z-0.76)(z-0.25)(z-1)} \tag{4.12}$$

Where

$$Kh = 2.88\times10^{-2};$$

note that the noise transfer function is not considered in the whole plant transfer function in (4.12) since its magnitude is not controllable. All the certain aspects in metal cutting are represented by a gain Kh and the model is deterministic. Model validation is based on the open loop response. The AE sensor output signal was predicted by simulation and compared with experimental data.

4.2 Experimental Result and Discussion

Model validation is based on the open loop response. The AE sensor output signal was predicted by simulation and

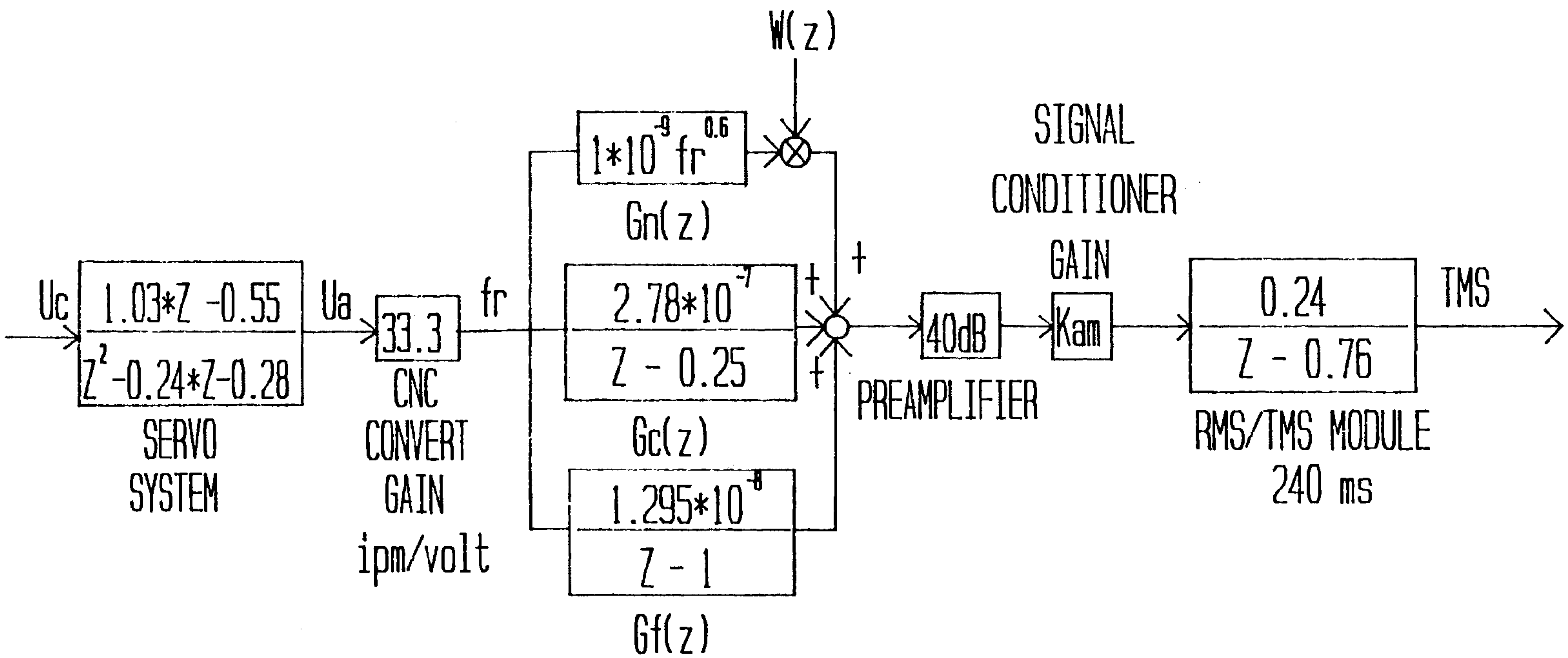

Figure 24. Discrete Time Model for the Drilling Process

compared with experimental data. The overall gain of the model was adjusted by matching the predicted and experimental data at steady state.

For a step input of command feedrate, the TMS generated during drilling increases as a ramp output. In figure 25, Uc= 0.9 volt. The simulation is shown in figure 26.

For a step change of command feedrate, the acoustic emission sensor senses the change of strain rate of workpiece and the AE TMS will increase abrubtly. The simulation is shown in figure 27. It can be compared with the experimental result in figure 12.

In figures 28, 29, there are four step changes of command feedrate for the experiments and simulation. The data are very close to each other during the transient as well as steady state TMS. In figures 30, 31, there are six step changes of command feedrate for the experiments and simulation.

The development model will be utilized for designing PID controllers in Chapter 5. When utilized in the design of PID controllers, the model is simulated for the effects of cutting conditions upon the system's closed loop performance and stability.

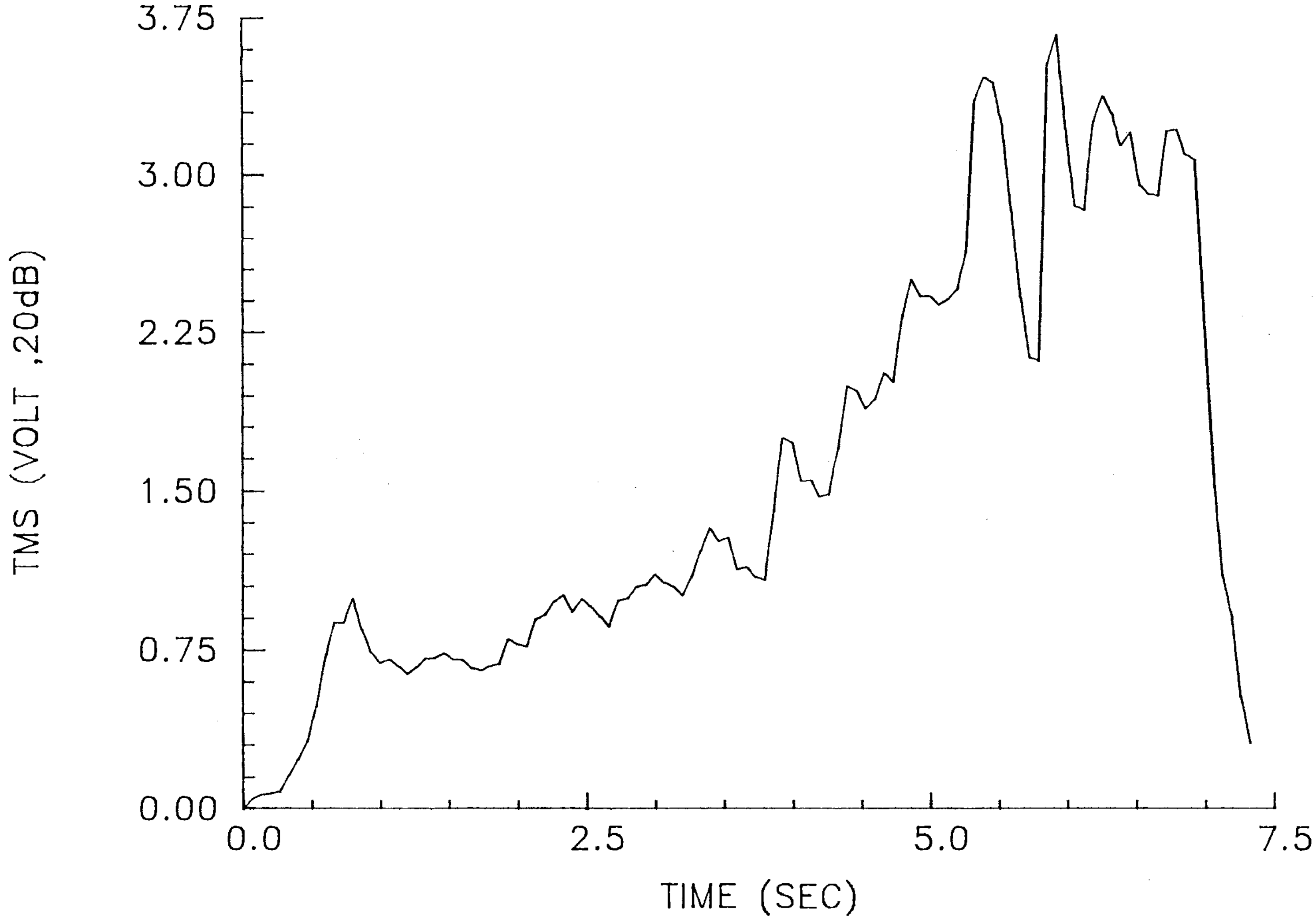

Figure 25. Experimental AE TMS output Due to the Step Input of Command Feedrate 0.3 volts

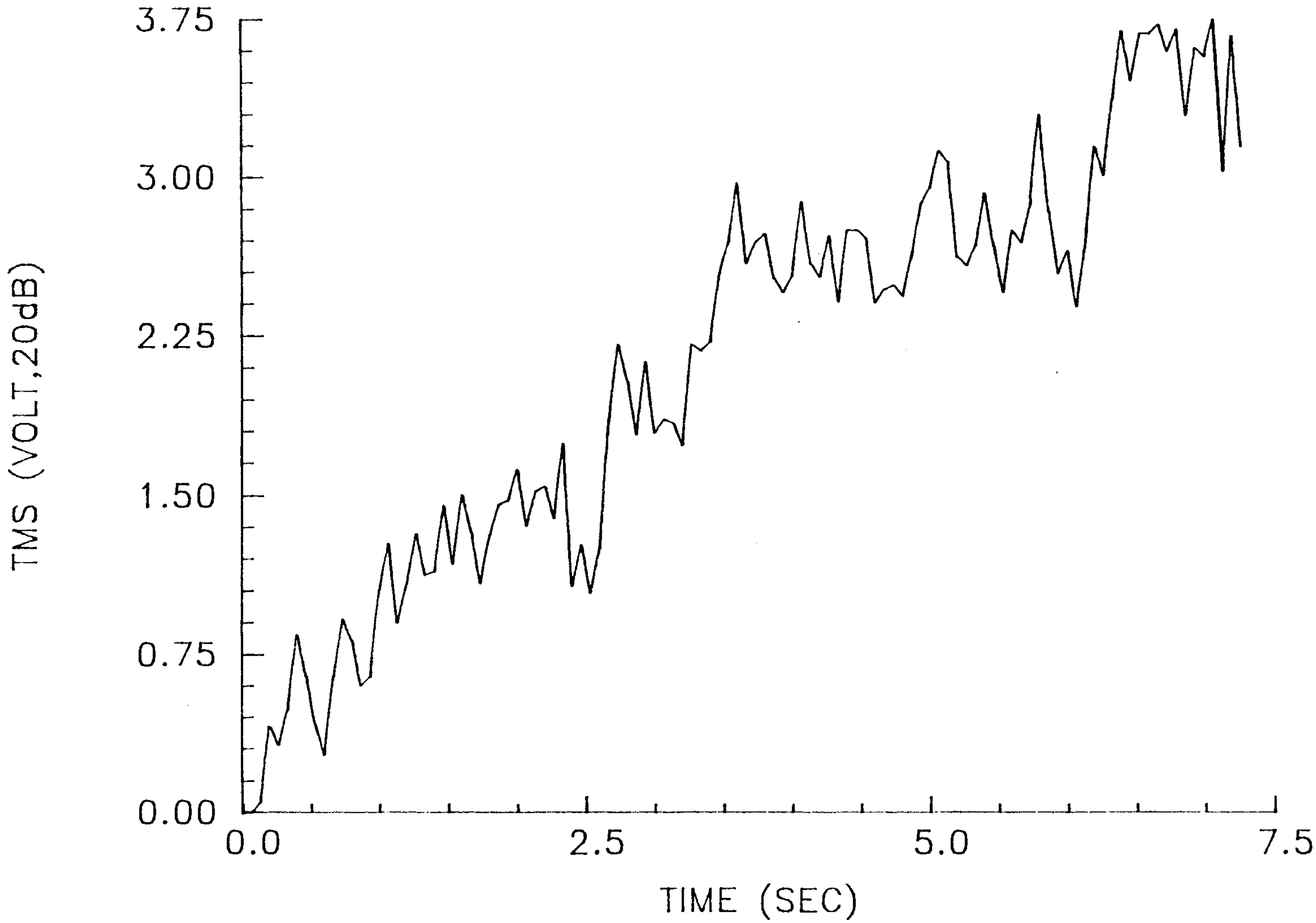

Figure 26. Simulated AE TMS output Due to the Step Input of Command Feedrate 0.3 volts

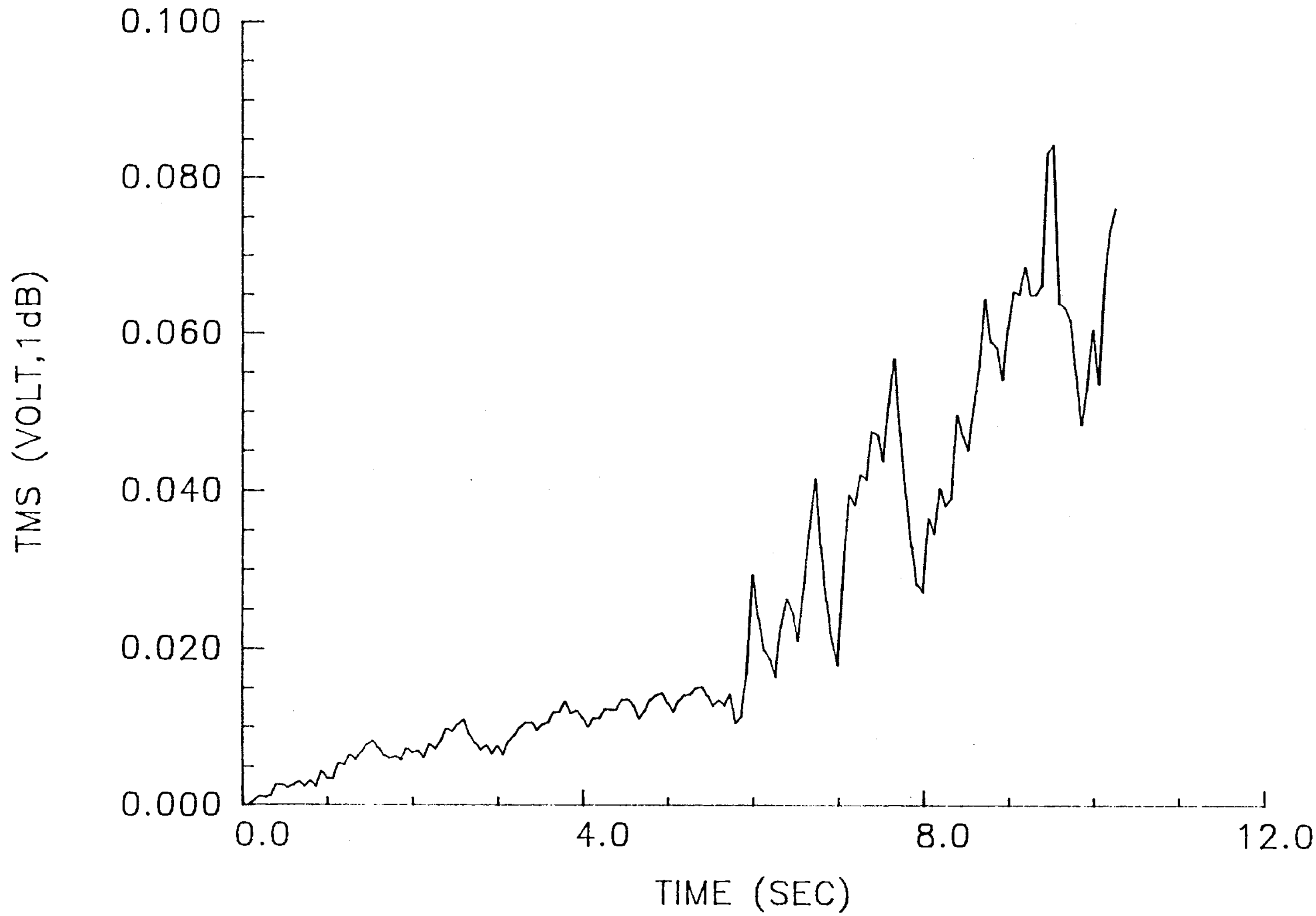

Figure 27. Simulated AE TMS Output Due to the Step Change of Command Feedrate from 0.1 to 0.5 volts

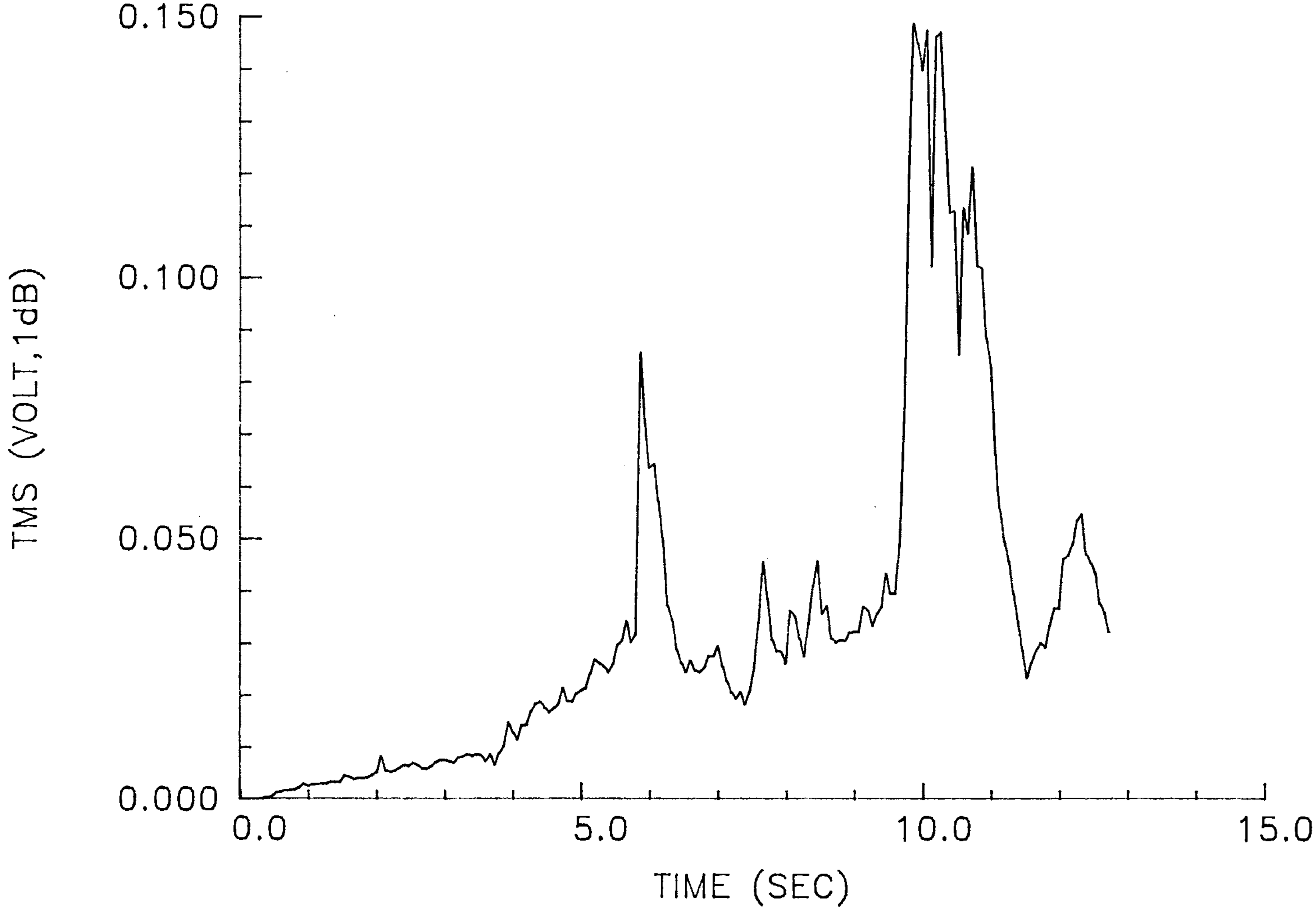

Figure 28. Experimental AE TMS Output Due to Four Step Changes of Command Feedrate between 0.1 and 0.5 volts

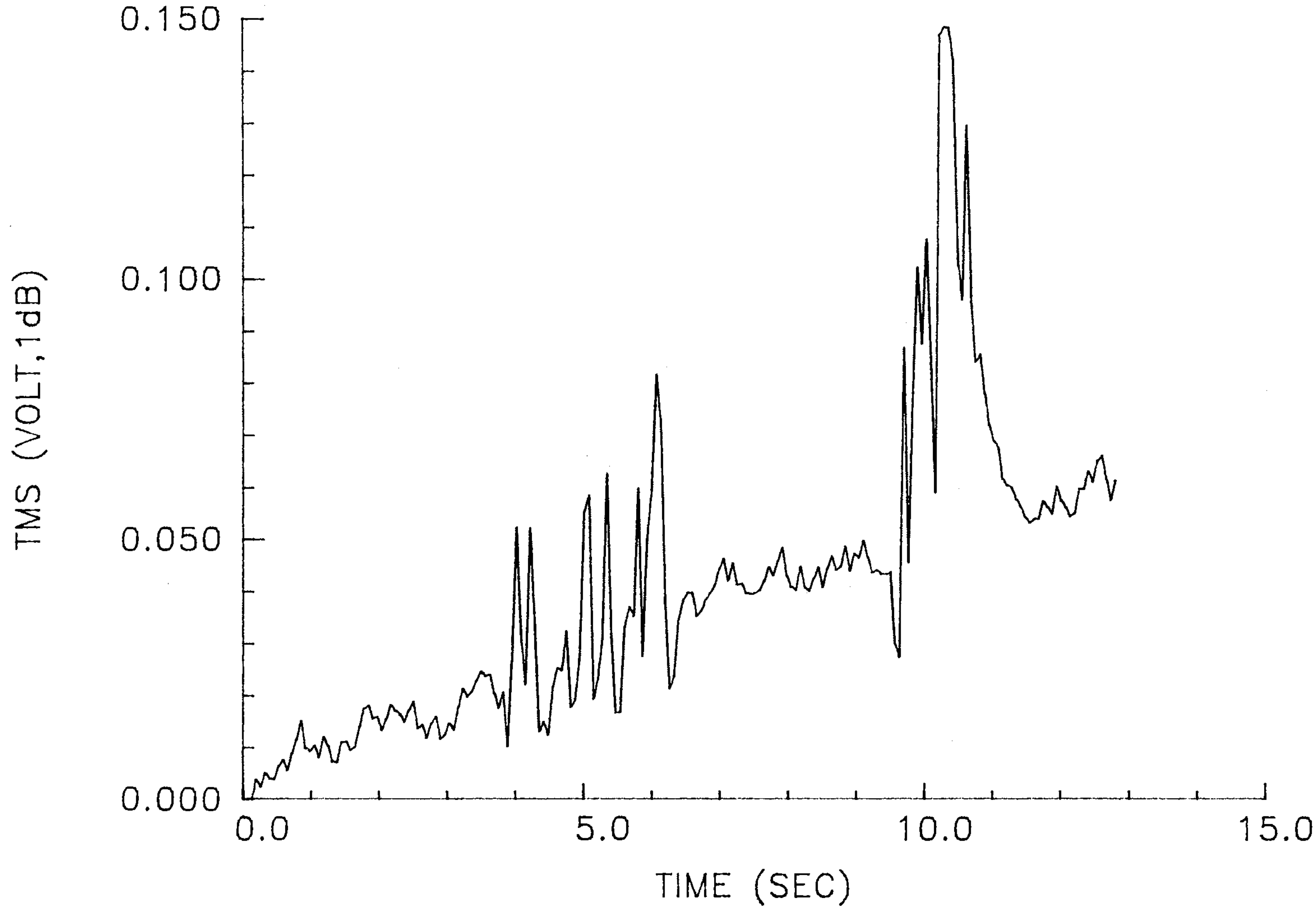

Figure 29. Simulated AE TMS Output Due to Four step Changes of Command Feedrate between 0.1 and 0.5 volts

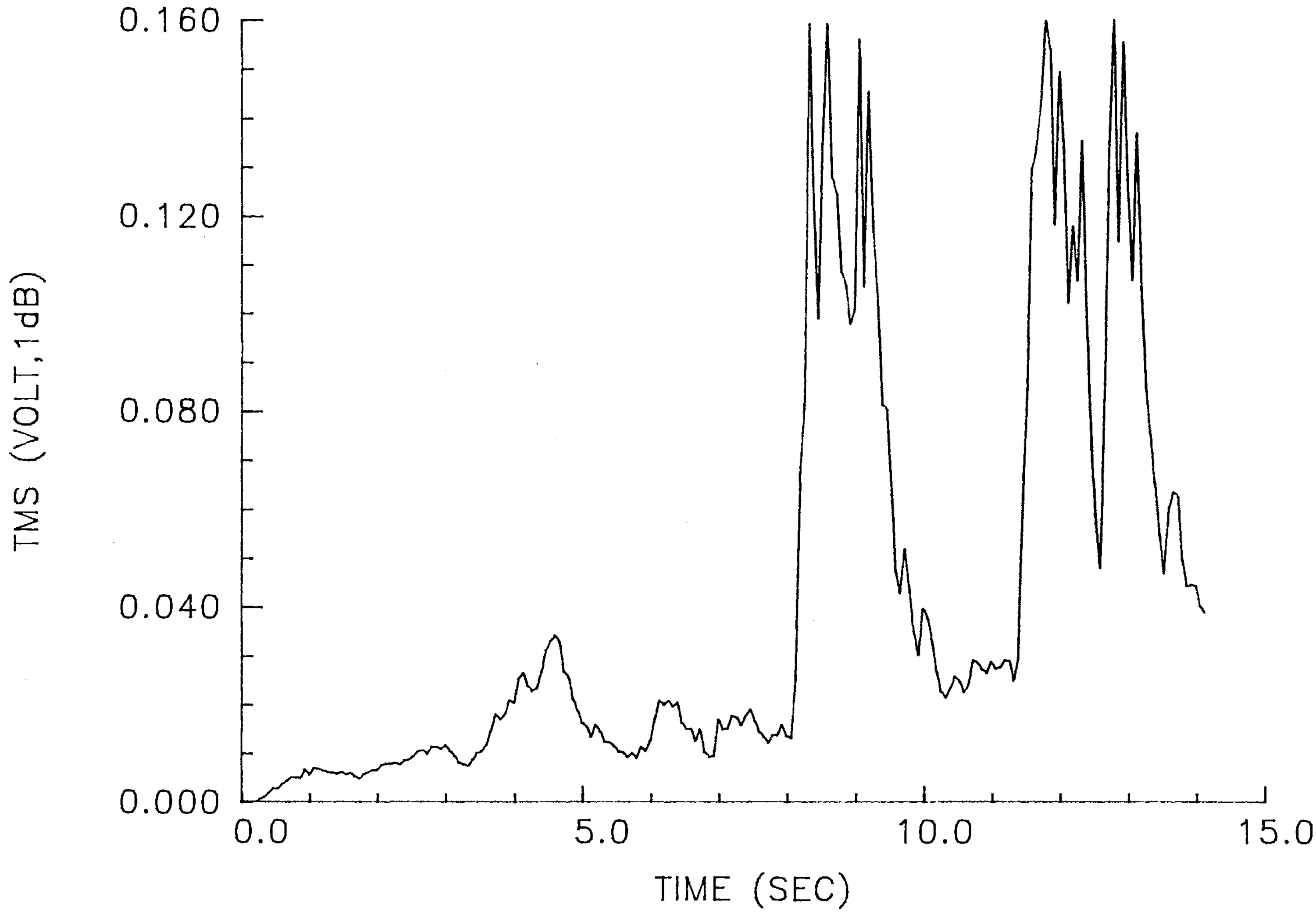

Figure 30. Experimental AE TMS output Due to Six Step Changes of Command Feedrate between 0.1 and 0.5 volts

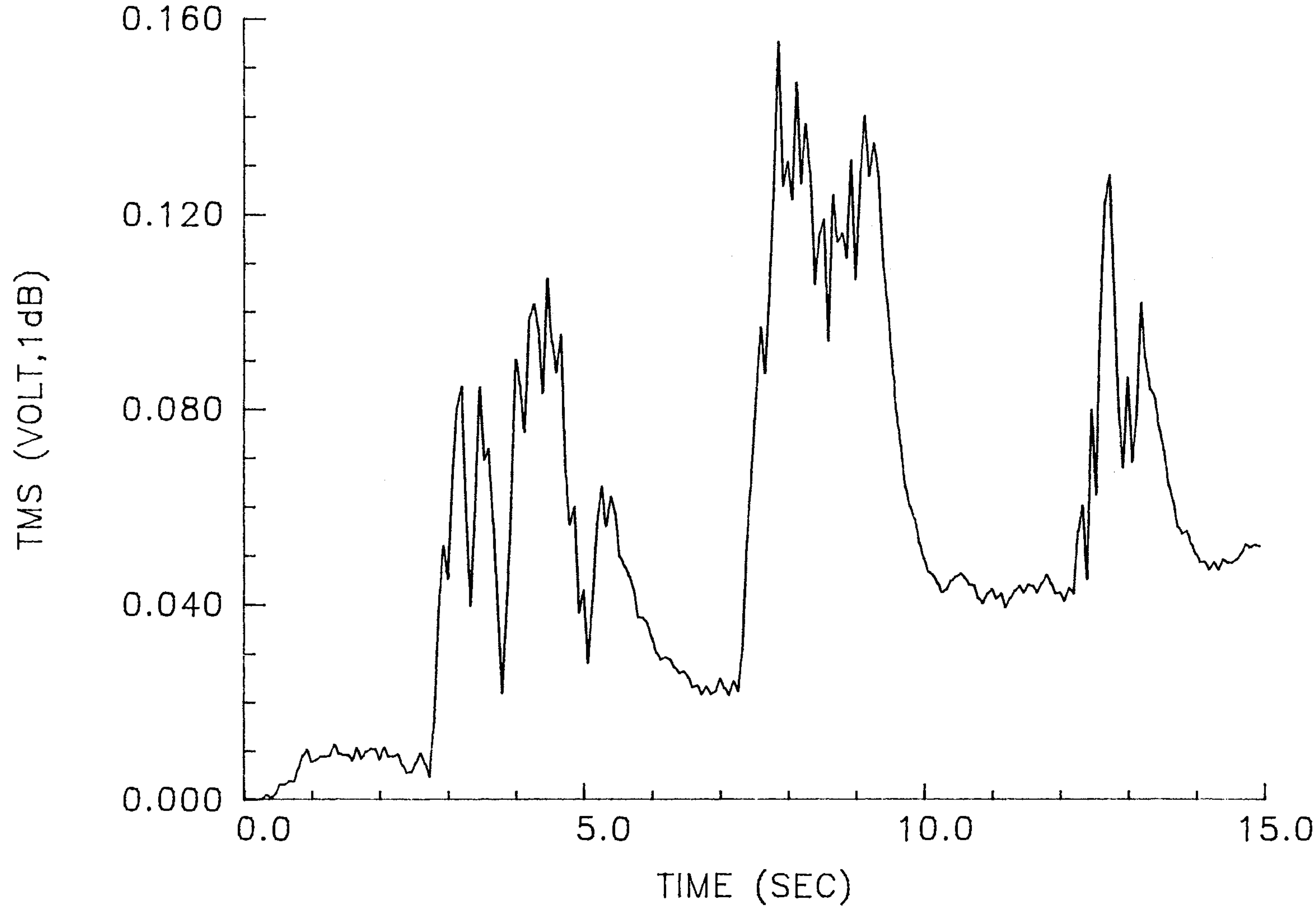

Figure 31. Simulated AE TMS output Due to Six Step Changes of Command Feedrate between 0.1 and 0.5 volts

CHAPTER V

APPLICATIONS TO SYSTEM CONTROL

5.1 Controller Structure

PID controller is one of the most widely used controllers in the design of control system [33], where PID stands for Proportional-Integral-Derivative control. Figure 32 shows the block diagram of a continuous-data PID controller acting on an error signal e(t) with a constant Kp; the integral control multiplies the integral of e(t) by Ki, and the derivative control generates a signal which is proportional to the time derivative of the error signal. The function of the integral control is to provide the action to reduce the steady-state error, whereas the derivative control provides an anticipatory action to reduce the overshoots in the response.

In digital control, the proportional control is still implemented by a proportional constant Kp. There are many ways to implement integration and derivatives digitally [33][42][43]. By approximating the integral term by the trapezoidal summation and the derivative term by a two-point (backward)difference term form, the PID controller is obtained as shown in figure 33.

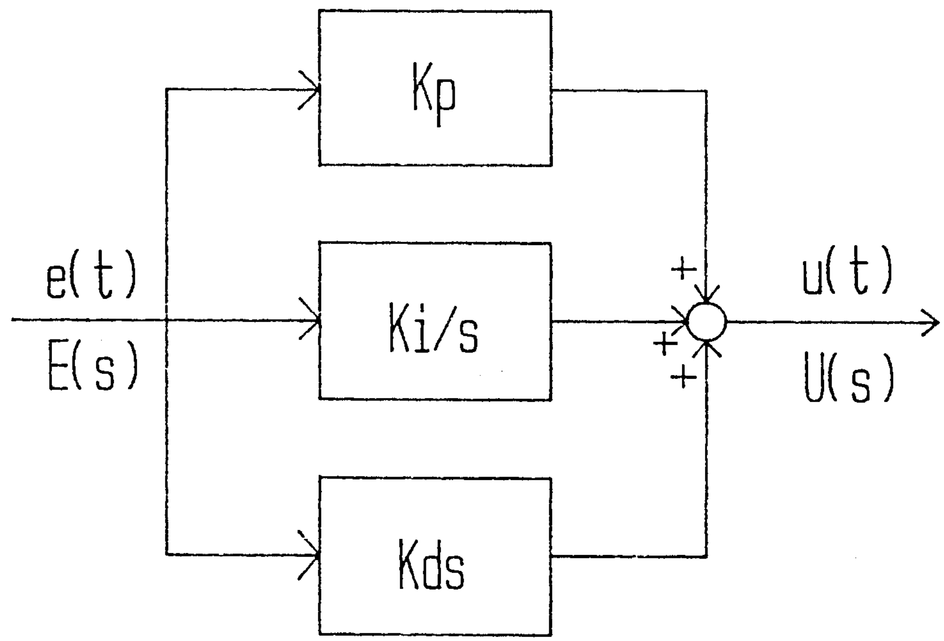

Figure 32. A Continuous-Data PID Controller

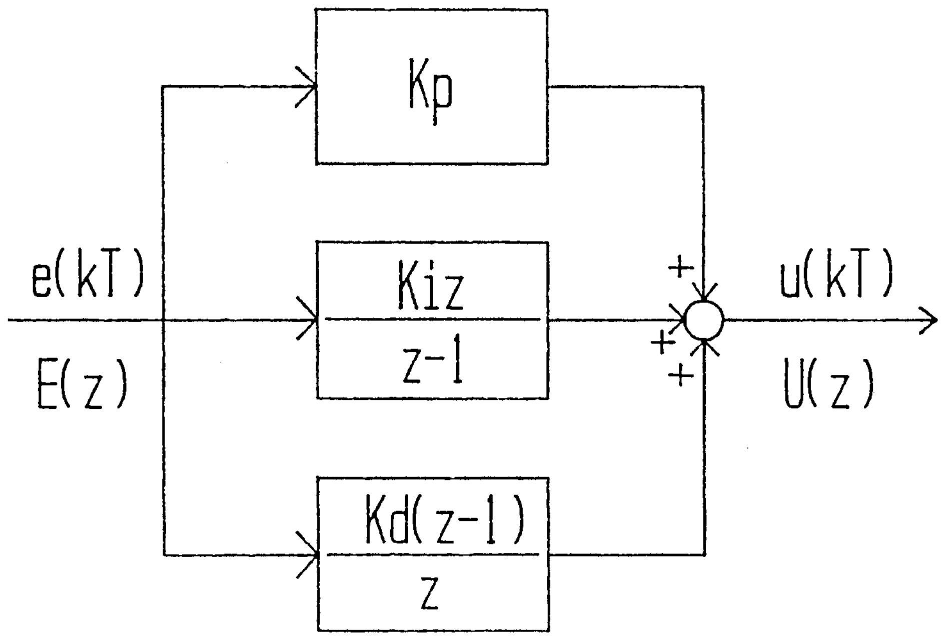

Figure 33. A Digital PID Controller

The overall TMS control loop can be represented as shown in figure 34, where $Gc(z)$ denotes the PID controller, whose transfer function can be expressed as:

$$Go(z) = Kp + Ki \frac{z}{z - 1} + Kd \frac{z - 1}{z} \qquad (5.1)$$

where

Kp = proportional gain;

Ki = integral gain; and

Kd = derivative gain;

the PID controller in equation (5.1) can also be expressed as:

$$Go(z) = Ko \frac{(z^2 + D0\, z + D1)}{z^2 - z} \qquad (5.2)$$

where

$Ko = Kp + Ki + Kd$;

$D0 = \frac{-2\, Kd - Kp}{Kc}$; and

$D1 = \frac{Kd}{Kc}$;

the process of control algorithm design is often to select the parameters of the controller to give the close-loop system poles at desired locations on the z-plane. With a known plant and specified compensator, the effect of varying a given parameter of the closed-loop roots may be examined

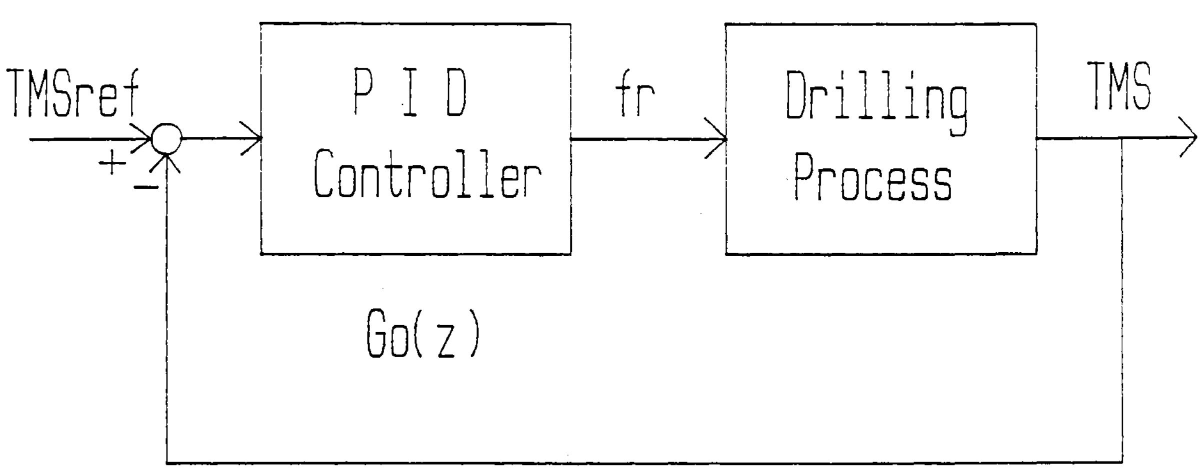

Figure 34. A TMS Feedback Control of Drilling System with PID Controller

by the conventional root-locus plots.

In this section, the application of the root-locus method will be demonstrated for the design of PID controller with constant damping ratio 0.707 such that there would not be an excessive over-shoot response.

In the s plane we are commonly interested in fixing the parameter ζ so as to control overshoot and settling time of the close-loop control system. Lines of ζ in the s plane are shown in figure 35. The angle is related to the damping ratio by

$$\zeta = \cos \beta \tag{5.3}$$

The damping ratio ζ of a close-loop pole can be analytically determined from the location of the close loop pole in the z-plane. If the damping ratio of a close-loop pole is ζ, then in the s plane the close-loop pole can be given by

$$S = - \zeta \omega_n \pm j \omega_n (1 - \zeta^2)^{1/2} \tag{5.4}$$

where

ω_n = undamped natural frequency;

since $z = e^{Ts}$, the corresponding radial location of the poles in the z plane is given to be

$$R = \exp [- \zeta \omega_n T] \tag{5.5}$$

and the angular location is given to be

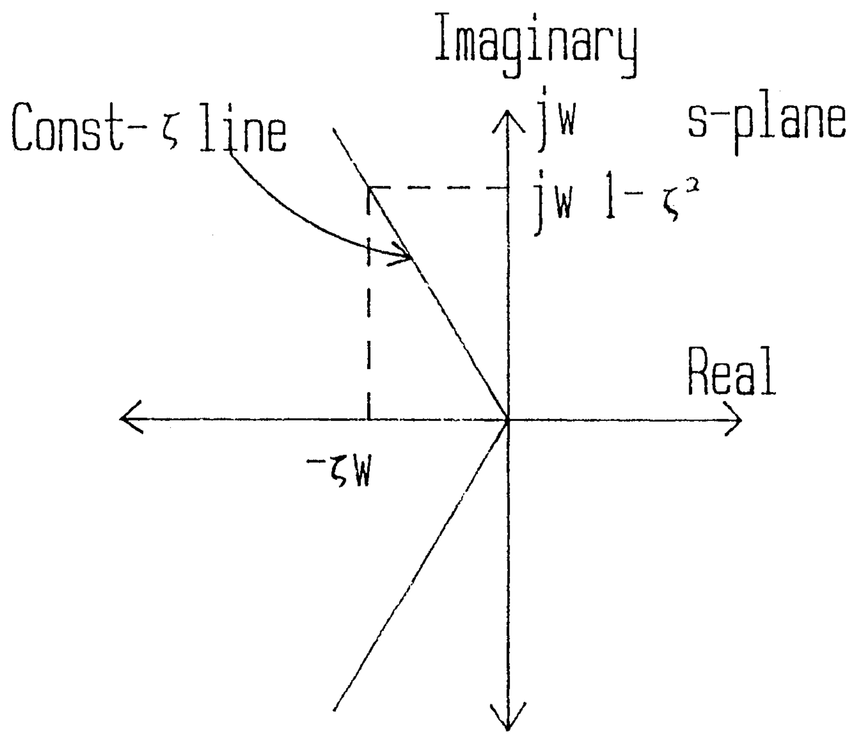

Figure 35. Diagram Showing the Constant ζ loci in the S Plane

$$\Theta = \omega_n T (1 - \zeta^2)^{1/2} \tag{5.6}$$

If we solve equation (5.5) for $\omega_n T$ and substitute it into equation (5.6), then the radial pole location is a function of the angular location and the parameter ζ

$$R = \exp\left(\frac{-\zeta \Theta}{(1 - \zeta^2)^{1/2}} \right) \tag{5.7}$$

This is the equation of a logarithmic spiral, These loci for various values are illustrated in figure 36.

In this drilling process, the characteristic equation has the following form:

$$1 + F(z) = 0 \tag{5.8}$$

where

$$F(z) = K\, Gc(z)\, Gp(z)\, Gam(z);$$

note that $F(z)$ is the open-loop pulse transfer function. The characteristic equation given by equation (5.8) can be written as

$$F(z) = -1 \tag{5.9}$$

since $F(z)$ is a complex quantity, equation (5.9) can be split into two equations by equating first the angles and then the magnitudes of the two sides to obtain

ANGLE CONDITION:

$$\angle F(z) = \pm 180^\circ (2K+1) \quad K = 0, 1, 2, \tag{5.10}$$

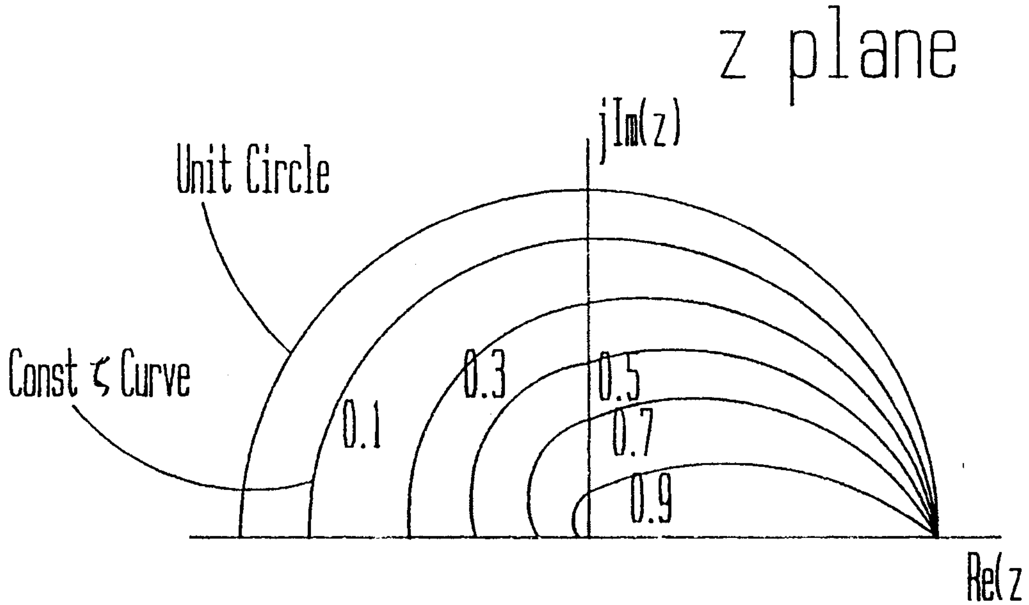

Figure 36. Diagram Showing the Constant ζ loci in the Z Plane

MAGNITUDE CONDITION:

$$|F(z)| = 1 \qquad (5.11)$$

The values of z which fulfill both the angle and the magnitude condition are the roots of the characteristic equation, or the close-loop poles.

Since the intersection point P of the root-locus and constant damping ratio $\zeta = 0.707$ is to be the location for the dominant close-loop pole in the upper half of z-plane as shown in figure 37, the sum of the angle contributions at point P must be $\pm 180°(2K+1)$, i.e..

$$\Sigma \Theta_{zk} - \Sigma \Theta_{PK} = \pm 180°(2K+1) \quad K = 0, 1, 2 \qquad (5.12)$$

Where

Θ_{zk} = the corresponding phase angle of zeros; and

Θ_{pk} = the corresponding phase angle of poles;

since sampling time T is known, it is easy to find the undamped natural ratio, and the coordinate at point P.

If one can select the two zeros of controller so that they cancel the undesired two poles of the process, then substitute the point P into magnitude condition, the value of Kc will be known.

By knowing three conditions for the PID controller, coodinates of two zeros, and the value of Ko, then three original unknown Kp, Ki, Kd can be decided, and the specification of performance for the drilling process will be achieved.

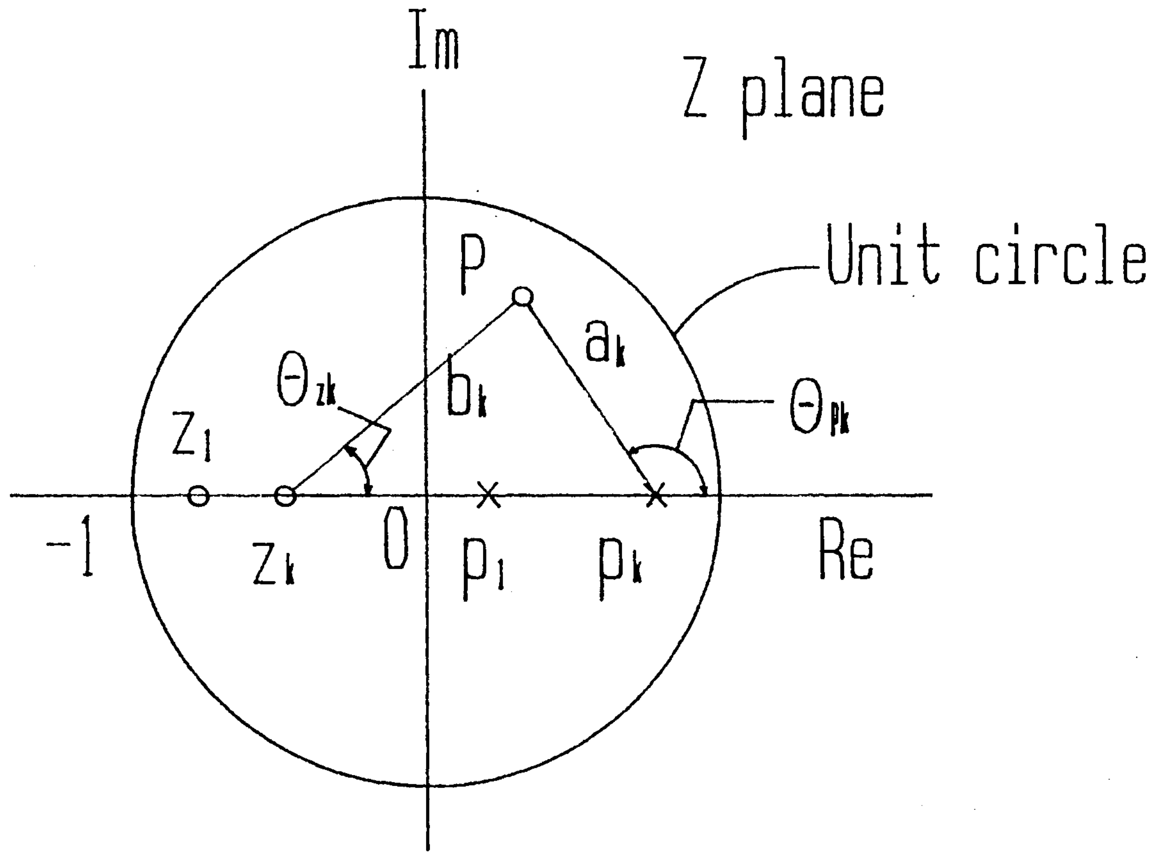

Figure 37. Open-Loop Pole-Zero Distribution

5.2 Simulation of PID Control

In this section, a simple method is described for the design of PID controller. The process is of type 1: i.e., an integrator is included in the drilling process. Therefore an integral action should be included in the feedback controller to ensure a zero offset error for a ramp desired TMS reference input. Figure 38 shows the block diagram of the TMS feedback control loop. The model from the previous section is utilized in the simulation.

The root locus plot for varying open loop gain can be immediately constructed for the open loop transfer function as soon as the zeros and the constant of the PID are selected.

Based on the pole-zero cancellation principle, the two zeros of the PID controller should cancel the two poles of the controlled process at z = 0.6626 and z = 0.76. From equation (5.2),

$$\frac{-2Kd - Kp}{Kp + Ki + Kd} = -1.4226 \qquad (5.13)$$

and,

$$\frac{Kd}{Kp + Ki + Kd} = 0.504 \qquad (5.14)$$

The open loop transfer function becomes

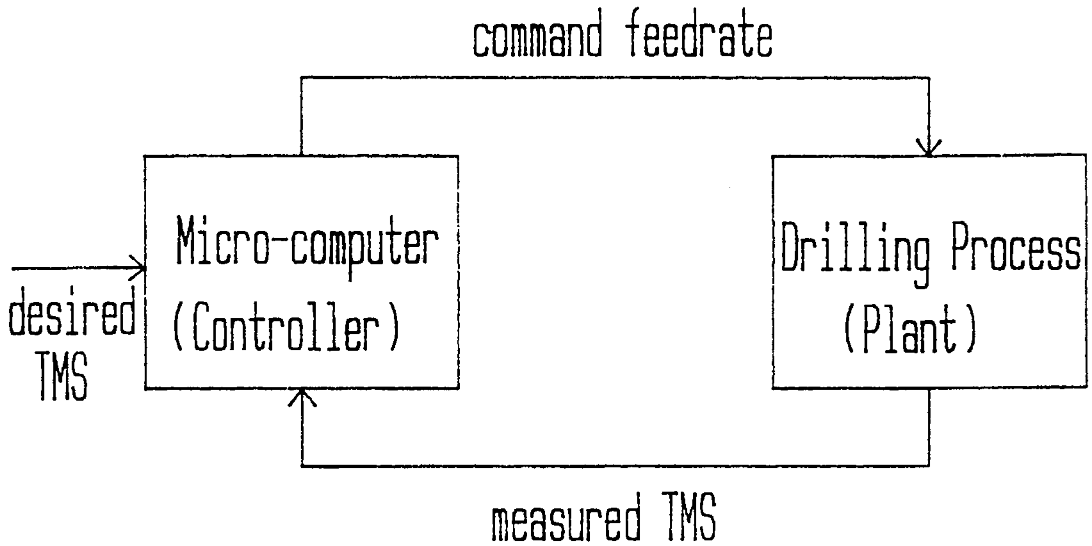

Figure 38. Digital Control of the TMS Feedback Control of the Drilling Process

$$Go(z)\ Gp(z)\ Gam(z) =$$

$$2.88\times10^{-2}\times(Kp+Ki+Kd)\times\frac{(z-0.534)(z-0.966)}{z(z-1)(z+0.4226)(z-0.5)(z-1)} \quad (5.15)$$

The open loop transfer function can also be expressed as:

$$G_{open}(z) = K_{open}\frac{(z - 0.534)\ (z-0.966)}{z(z-1)(z+0.4226)(z-0.5)(z-1)} \quad (5.16)$$

Where

$$K_{open} = 2.88\times10^{-2}\ (Kp+Ki+Kc).$$

Since damping ratio ζ = 0.707 line is desired for the close loop control, then we need to find the intersection of root locus and ζ = 0.707 line to find Wn for the close loop pole.

Substituting sampling time T=0.0666, and ζ=0.707 into equations (5.5) and (5.6), then the close loop pole is

$$\begin{aligned} z &= \exp(0.0471(-Wn+jWn)) \\ &= Re + j\ Im \end{aligned} \quad (5.17)$$

Where

$$Re = \exp(-0.0471Wn)\ \cos(0.0471Wn), \text{ and}$$

$$Im = \exp(-0.0471Wn)\ \sin(0.0471Wn).$$

From equation (5.16), the intersection point root locus and constant damping ratio is to be the location for the dominant closed-loop pole in the upper half of z plane and the sum of the angle contributions at the point P must be

±180°.

$$\Theta_{z1} - \Theta_{p1} - \Theta_{p2} - \Theta_{p3} - \Theta_{p4} = \tan^{-1}\frac{Im}{Re-0.966} +$$

$$\tan^{-1}\frac{Im}{Re - 0.534} - 2\times\tan^{-1}\frac{Im}{Re - 1} - \tan^{-1}\frac{Im}{Re - 0.25} -$$

$$\tan^{-1}\frac{Im}{Re} - \tan^{-1}\frac{Im}{Re + 0.4226} = 3.141\ (180°) \qquad (5.18)$$

It was found that the value of Re and Im are 0.3126, 0.3223, by solving equations (5.17) and (5.18), i.e., the coordinate at point P of the close loop is 0.3126 ± j 0.323 as shown in figure 39.

The open loop gain can be determined from the magnitude condition in equation (5.11), then

$$K_{open} \left| \frac{(z-0.54)(z-0.966)}{z(z-1)(z-0.25)(z+0.4226)(z-1)} \right| = 1 \qquad (5.19)$$

Substituting close loop pole into equation (5.19), it is found that K_{open} = 0.233.

Since the objective of PID control is to keep desired TMS ramp output in order to keep feedrate constant. In the simulation, Kam is selected to be gain 1dB, and the feedrate is assumed to be kept at 3.33 ipm, and substituted into K_{open}, then

$$Kp+Ki+Kd = 8.09 \qquad (5.20)$$

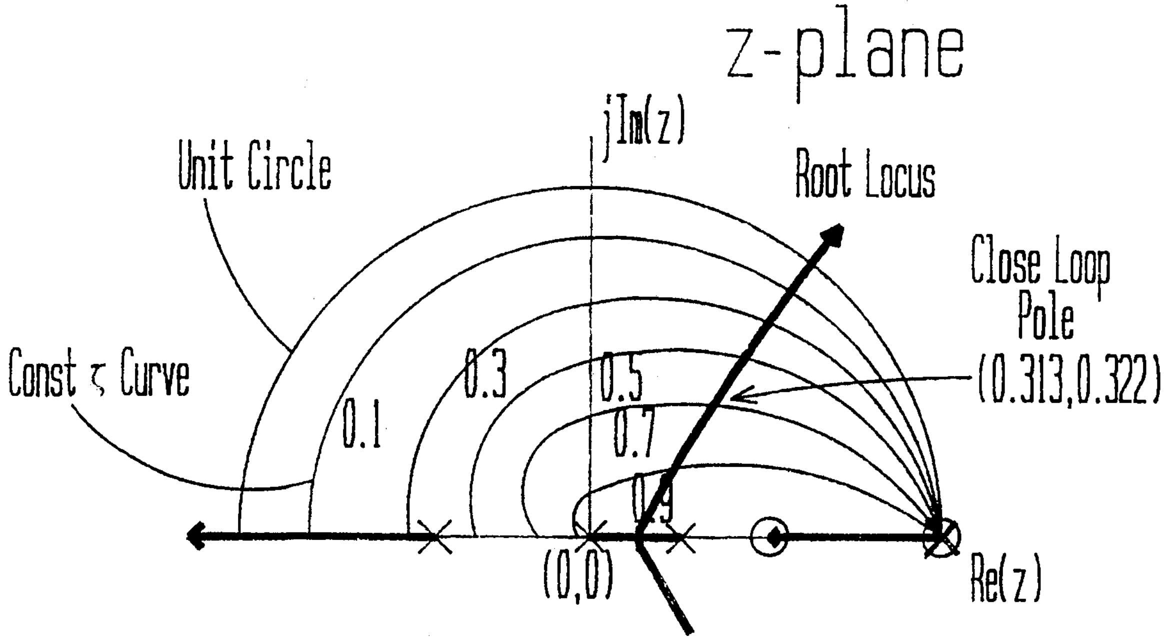

× : open loop pole
o : open loop zero

Figure 39. Root Locus Plot for the Compensated System with PID Controller

From equations (5.13),(5.14) and (5.20), the values of Kp, Ki and Kd are found to be 3.346, 0.667 and 4.007 respectively.

For the controller, which has zeros as above, the values of Kp, Ki and Kd were selected to be 3.346, 0.667 and 4.007 respectively. The TMS feedback control system becomes as shown in figure 40 corresponding to the nominal case. Simulation results indicate that the PID controller does work very well and the output response of TMS follow the desired TMSref as shown in figure 41.

Since the drilling process transfer function is of type 1, there is a steady state error for the output response of TMS if the controller is only proportional controller. The response cannot follow the desired TMSref as shown in figure 42.

Simulations also show that the PI controller works well if the gain of Kd is selected to be zero as shown in figure 43. However, the amplitude of fluctuating portion PI control is still a little larger than that of PID control. This is simply because of the function of derivative control of PID controller to reduce the overshoot.

The improper choices for the gains of PID controller would also lead to undesired output response of TMS. In figure 44, if the amplifier gain Kam were selected as a low value 0.0112, the response is not satisfactory.

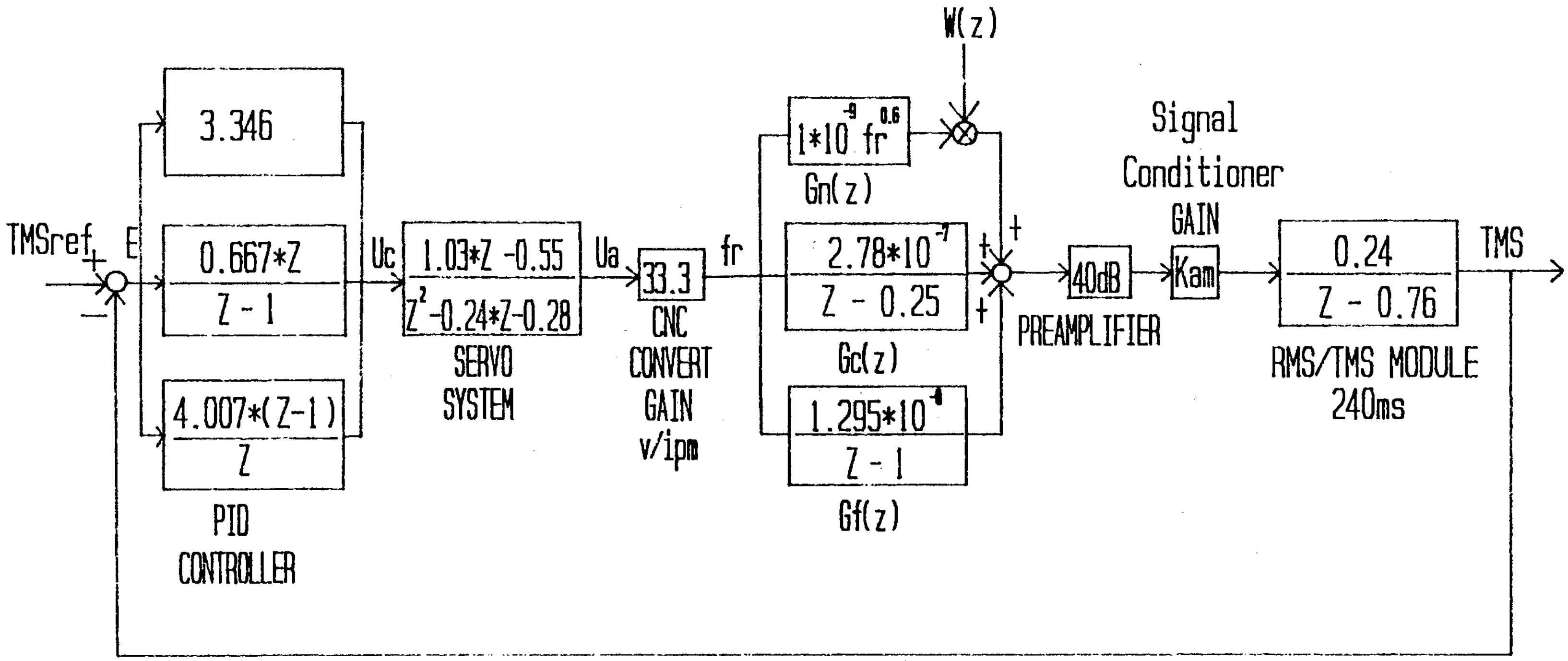

Figure 40. Block Diagram of a Feedback Control System with PID Controller

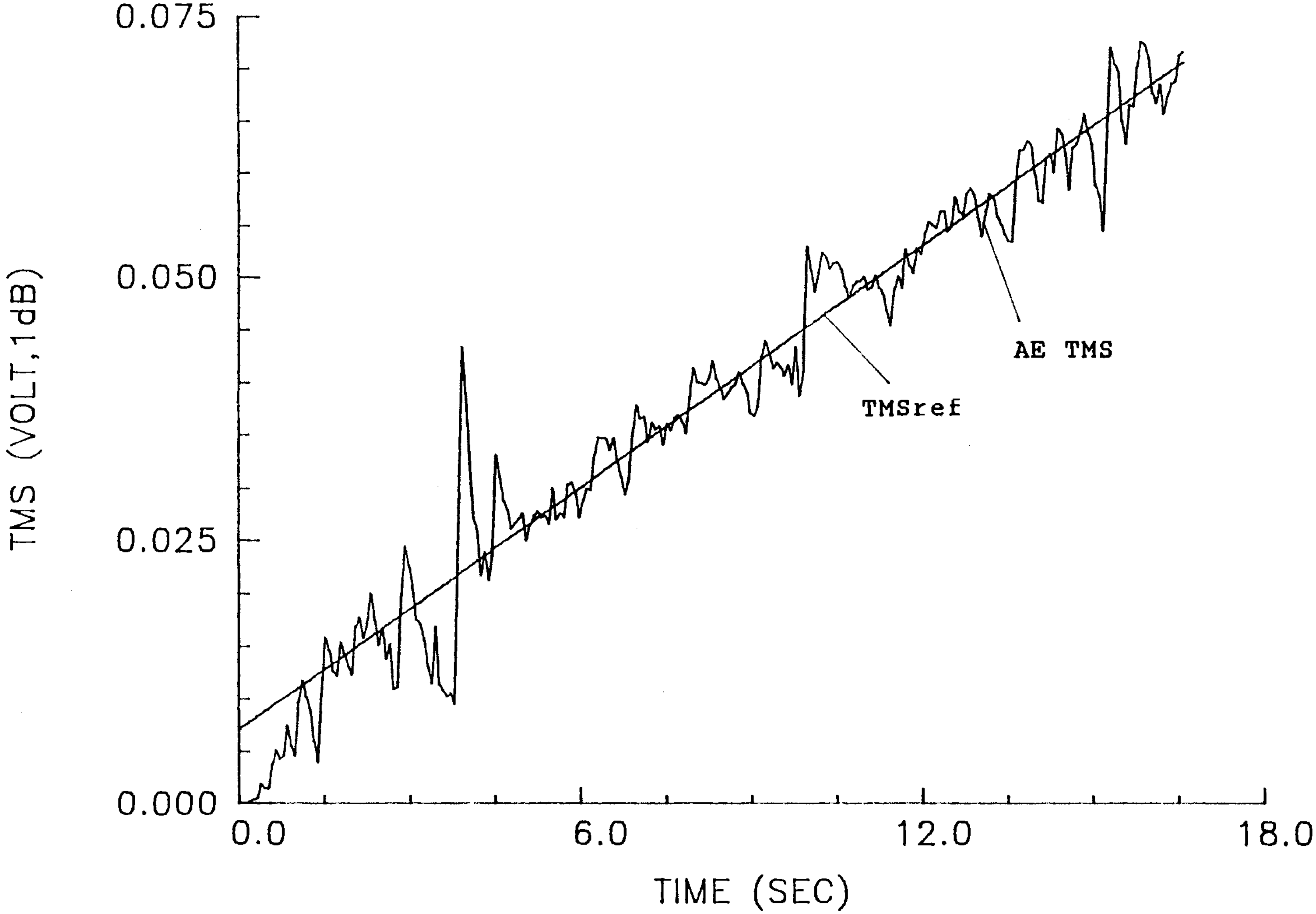

Figure 41. Simulated PID Control with Kp = 3.346, Ki = 0.667 and Kd = 4.007

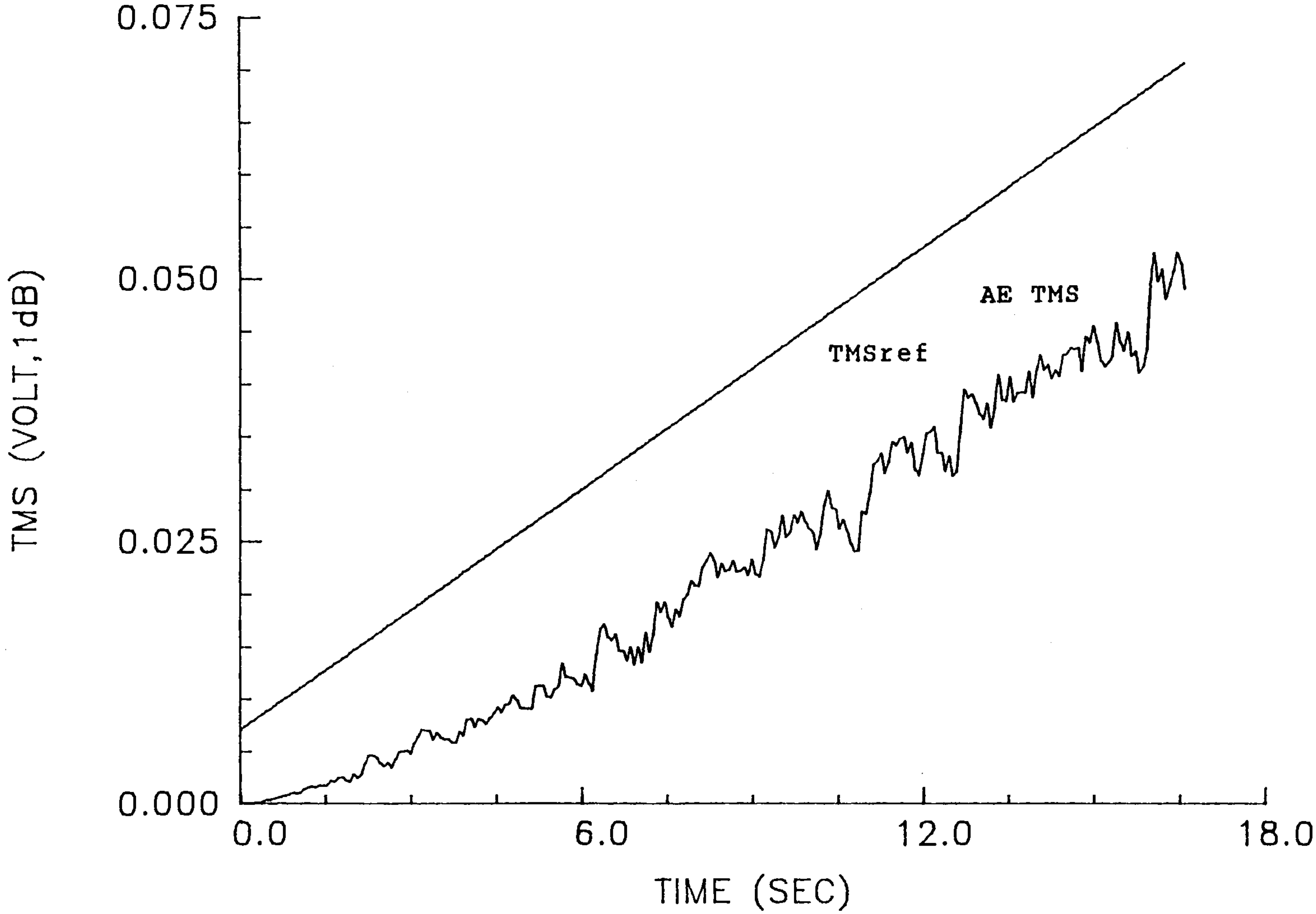

Figure 42. Simulated P Control with Kp = 3.346

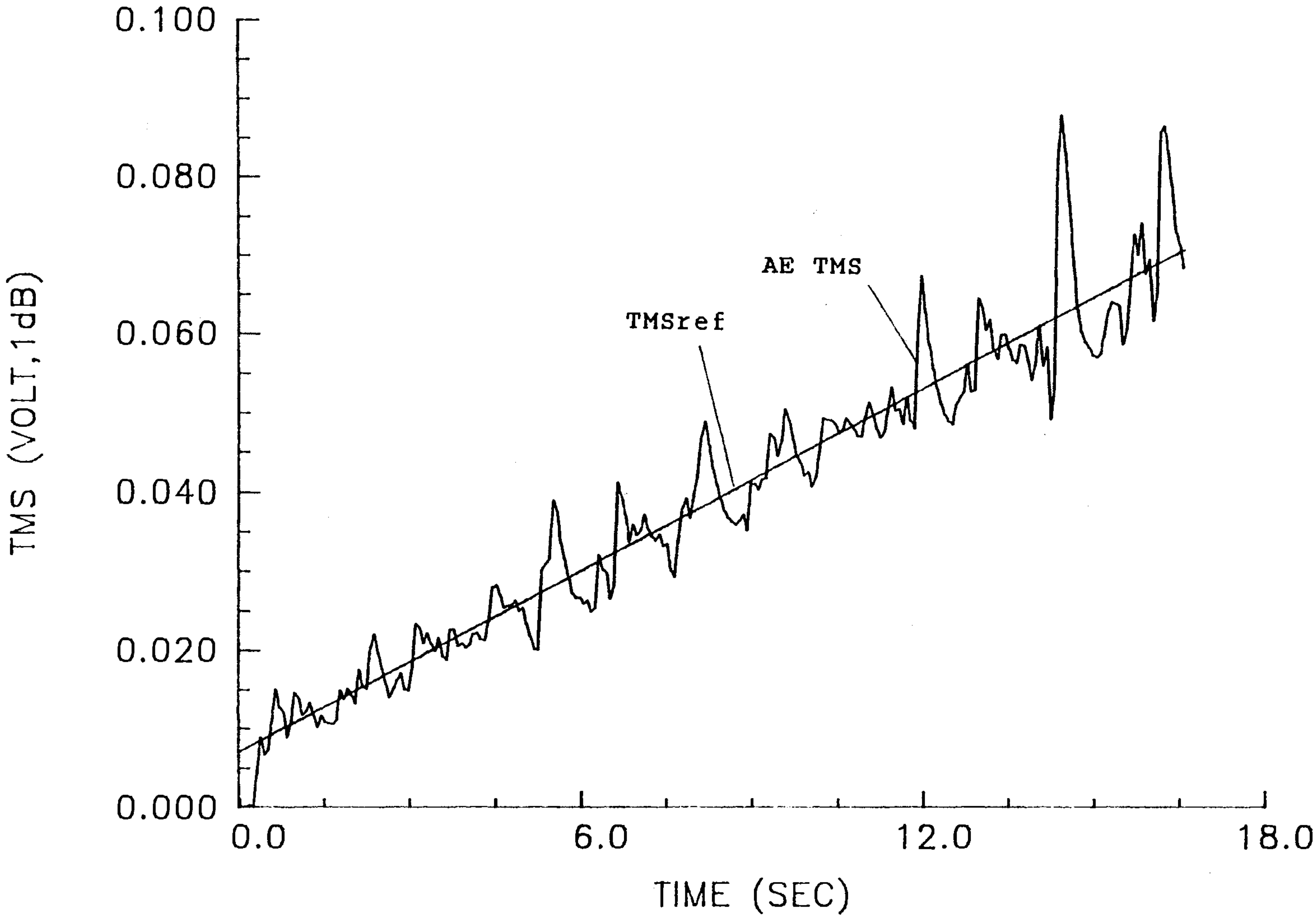

Figure 43. Simualted PI Control with Kp = 3.346 and Ki = 0.667

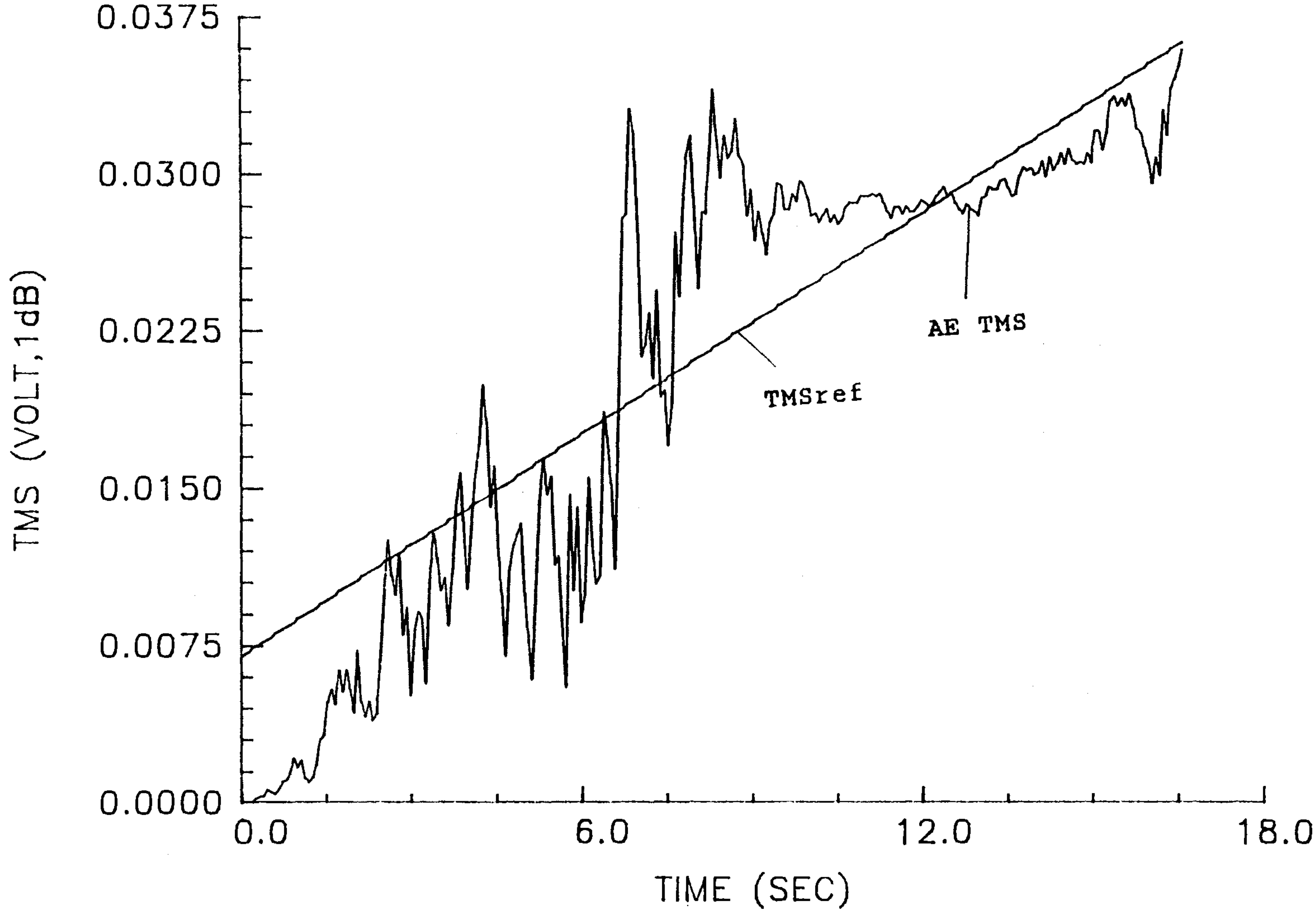

Figure 44. Simulated PID Control for Low Value of Kam = 0.0112

CHAPTER VI

CONCLUSIONS AND RECOMMENDATIONS

6.1 Summary and Conclusion

In this thesis, a theoretical relationship has been drawn between the modeling of the drilling process and acoustic emisson signals generated. The application of PID control techniques are also utilized to maintain the TMS (work rate) at a desired output during drilling under variation of cutting conditions. The drilling process considers the cutting processes occurring in the cutting edges of the tool and along chip-workpiece interface as distinct sources of AE. This work includes development of static equation and dynamics modeling of the drilling process, application of PID control algorithm, root locus analysis, simulations, and experimentation. This section summarizes the results obtained in each chapter and leads us to final conclusions.

In chapter 2, the characteristics of the drilling process was introduced based on the structure of the drill tool and the mechanics of cutting process. The derivation of the drilling process was based on the relationship between the feedrate, spindle speed, and the TMS generated during drilling.

In chapter 3, a static equation of the drilling process was derived based on the tool-workpiece interaction of a series of experiments. A dynamics modeling of drilling process was developed by sensing AE generated during drilling. The modeling of the drilling process includes the dynamics of cutting TMS between the tool and workpiece and frictional TMS between the chips and workpiece. This work justifies the assumption that the TMS generated in the drilling process can be represented by feedrate and spindle speed.

In chapter 4, the result of experimental work during drilling was in good agreement with the simulations. This work justifies that the modeling of the drilling process using AE can be represented by distinct sources.

In chapter 5, conventional PID control based on the root locus design was discussed. The simulation work showed that the conventional PID control is effective for the drilling process. The control objective of the drilling process was to keep the TMS constant by controlling the feedrate. To achieve the objective, a desired closed loop pole was located in the intersection of root locus and constant damping ratio $\xi = 0.707$ line.

Through the study, it was provided that the AE sensor can be applied for the control of the drilling process. Also, it shows in the simulation that the PID control techniques can be successfully applied to the TMS feedback control of the drilling process.

Finally it should be pointed out that the PID control is simply the simulation as an example applied in the drilling process since it is convenient and powerful.

6.2 Recommendation for future work

This study has been undertaken to show how AE sensor could be utilized to the control of the drilling process. Several suggestions for future work are outlined in this section as follows:

1) The drilling process was modeled for the material SAE 1018 only. Other materials should be also investigated and compared.
2) The drilling process was modeled only for a single layer for this research. An extension for multi-material sandwich structures should be developed for many cases in industry.
3) Real time PID control for the drilling process should be carried out and compared with the simulation for the future work.
4) Adaptive control system or robust controllers should be investigated and may be developed for the multi-material drilling system.
5) The tool used for drilling in this research was only a specification. The other specifications of drill bit

should also be applied for investigation.

6) The variance in amplitude of the signal from the sensor must be minimized. The amplitude of the sensor signal decreases as the distance from the drilling location increases. A solution is to place the sensor as far from the drilling location as is practical to minimize the variation of coupling path to each hole. Insertion of the AE sensor in the drilling tool is also one possible method for future work.

7) This work can be extended to other types of machine tool systems such as turning, milling, grinding, etc.

REFERENCES

[1] Oxford, C. J. Jr., "On the Drilling of Metals-I. Basic Mechanics of the Drilling Process." ASME Journal of Engineering for Industry, Vol. 77, 1955, pp. 103-114.

[2] Shaw, M. C., and Oxford, C. J. Jr. "On the Drilling of Metals-II. Basic Mechanics of the Drilling Process" ASME Journal of Engineering for Industry, Vol. 79, 1957, pp. 139-148.

[3] Williams, R. J., "A Study of the Drilling Process." ASME Journal of Engineering for Industry, Vol.96, 1974, pp. 1207-1215.

[4] Beer, Larry D. "Power Consumption - A measure of Tool Performance." Technical paper MR79-398. Dearborn, MI : Society of Manufacturing Engineering, 1979.

[5] Wu, S. M., Saxena, U. K., and Devries, M.F., "Temperature Distributions in Drilling." ASME Journal of Engineering for Industry, Vol. 90, 1968, pp. 231-238.

[6] D. A. Stephenson, and S. M. Wu, "Computer Models for the Mechanics of Three-dimensional Cutting Processes-Part I: Theory and Numerical Method." ASME Journal of Engineering for Industry, Vol. 110, February 1988, pp. 32-37.

[7] D. A. Stephenson, and S. M. Wu, "Computer Models for the mechanics of Three-Dimensional Cutting Processes-Part II: Results for Oblique End Turning and Drilling." ASME Journal of Engineering for Industry, Vol. 110, February 1988, pp. 38-43.

[8] Neda S. Fabris, and Robin K. Podder, "Optimization of drill life. Part I: Influence of Cutting Condition on Tool Wear." SME proc. NAMRC, 1982, pp. 337-341.

[9] Charles J. Conrad, and N. Harris McClamroch, "The Drilling Problem : A stochastic Modeling and Control Example in Manufacturing." IEEE Trans

on Automatic Control, Vol AC-32, No.11, November 1987.

[10] A. Thangaraj, and P. K. Wright, "Computer-Assisted Prediction of Drill-failure Using In-process Measurements of Thrust Force", ASME Journal of Engineering for Industry, Vol. 110, August 1988, pp. 297-300.

[11] P. G. Li and S. M. Wu, "Monitoring Drilling Wear States by Fussy Pattern Recognition Technique." ASME journal of Engineering for Industry, Vol. 110, August 1988, pp. 297-300.

[12] A. Galip Ulsoy, Yoram Koren, and Fred Rasmussen, "Principal Developments in the Adaptive Control of Machine Tools." ASME Journal of Dynamic System, Measurements, And Control, Vol. No. 2, June 1983, pp. 107-112.

[13] Mathias, R. A., Boock, W., and Welch, A., "Adaptive Control : Monitoring and Control of Metal-Cutting Processes." Proceedings of the Machine Tool Task Force Conference Vol. 4, sect. 7.13, Oct 1980.

[14] Los Angeles, "Computer-Controlled Drill Designed to Meet Unique B-2 Fabrication Needs." Aviation Week & Space Technology, April 17, 1989, pp. 51-52.

[15] L. K. Lauderbaugh, A. G. Ulsoy, "Dynamic Modeling for Control of the Milling Process", ASME Journal of Engineering for Industry, Vol. 110, November 1988, pp. 367-375.

[16] G. M. Zhang, and S. G. Kapoor, "Dynamic Modeling and Analysis of the Boring Machining System." ASME Journal of Engineering for Industry Vol. 109, August 1987, pp. 219-226.

[17] O. Masory, "Real-Time Estimation of Cutting Process Parameters in Turing." ASME Journal of Engineering for Industry, Vol. 106, August 1984, pp.218-221.

[18] Bor-Sen Chen, and Yih-Fang Chang, "Constant Turning Force Adaptive Controller Design." Journal of Engineering for Industry, Vol. 111, May 1989, pp. 125-132.

[19] Spiewak, S., and Szafarczyk, M., "Algorithms of Operation and Structures of ACC Controller for Rough Turning." Annals of the C.I.R.P., Vol. 27, No.1, 1978, pp. 413-418.

[20] Patrick Burgam, "Today's Adaptive Control Systems." Manufacturing Engineering, August 1983, pp. 50-52.

[21] Pak, H. A., and Daneshmend, L. K., "Microprocessor Control of Multi-Axes Continuous-Path Motion." Microprocessors and Microsystems, Vol. 6, No. 10, Dec. 1982, pp.519-527, Butterworths, London.

[22] M. Tomizuka, and S. Zhang, "Modeling and Convectional/Adaptive PI Control of a Lath Cutting Processes." ASME Journal of Engineering for Industry, Vol. 110, December 1988, pp. 350-354.

[23] L. K. Danesshmend, and H. A. Pak, "Model Reference Adaptive Control of Feed Force in Turning." ASME Journal of Dynamic Systems, Measurement, and Control, Vol. 108, September 1986, pp. 215-222.

[24] Tomizuka, M., Oh, J. H., and Dornfeld, D. A., "Model Reference Adaptive Control of the Milling Process." Control of Manufacturing Process and Robotic System, Edited by D. E. Hardt and W. J. Boak, ASME, New York, 1983.

[25] D. A. Dornfeld, "The Role of Acoustic Emission Monitoring and Analysis of Manufacturing Processes." Manufacturing Engineering Transactions, 13th, NAMRC, SME, 1985, pp. 69-74.

[26] M. S. Lang, and Y. Naerheim, "Application of Acoustic Emission Monitoring in Machining", Manufacturing Engineering Transactions, 13th NAMRC, SME, 1985, pp. 310-313.

[27] Y. Naerheim and A. Arora, "In-Process Monitoring in Machining Using Acoustic Emission." Rev. of Process in Quantitative NDE, 1983, pp. 753-762.

[28] Asibu, E. K., and D. A. Dornfeld, "Quantitative Relationship for Acoustic Emission from Orthogonal Metal Cutting." Transactions ASME, Series B, Vol. 103, 1981, pp. 330-340.

[29] Pan. C. and D. Dornfeld. "Modeling the Diamond Turning Process with Acoustic Emission for Monitoring Application." Proceedings of the Fourteenth NAMRC. Dearborn. MI: Society of Manufacturing Engineerings, Vol. 1, 1986. pp. 257-265.

[30] R. Teti, and D. Dornfeld. "Modeling and Experimental

Analysis of Acoustic Emission from Metal Cutting." ASME Journal of Engineering for Industry, Vol. 111, August 1989, pp. 229-237.

[31] Dornfeld, D. and M. Lan. "Chip Form Detection Using Acoustic Emission." Proceedings of the Eleventh NAMRC. Dearborn. MI. Society of Manufacturing Engineerings, May 1983, pp. 386-389.

[32] George Chryssolouris, and Michael Domroese. "Some Aspects of Acoustic Emission Modeling for Machining Control." Transactions of the NAMRC. SME, May 1989, pp. 228-234.

[33] Katsuhiko Ogata, Discrete-Time Control Systems. Prentice-Hill, N. J., 1987.

[34] Serope Kalpakjian, Manufacturing Process for Engineering Materials. Addision-Wesley, 1984.

[35] Paul Mclntire and Ronnie K. Miller, Nondestructive Testing Handbook Acoustic Emission Testing. Vol. 5, 2nd Edition, American Society for Nondestructive Testing, 1987.

[36] Galloway, D, F, "Some Experiments on the influence of Various Factors on Drill Performance." Transactions ASME, vol. 79, 1957, pp. 191-231.

[37] Ernst. H. and Merchant, M. E., "Chip Formation, Friction, and High Quality Machined Surfaces." Surface Treatment of Metals, Trans. ASME. Vol. 29, 1941, pp. 299-378.

[38] Lan, M. S. and Dornfeld, D. A., "Acoustic Emission and Machining-Process Analysis and Control." Advanced Manufacturing Process, 1, (1), 1986, pp. 1-21.

[39] Hamstad, M. A., and Mukherjee, R.G., "Acoustic Emission v.s. Strain and Strain Rate: Measurement and A Dislocation Theory Model for a Dispersion-Strengthened Aluminum Alloy." Lawrence Livermore Laboratory, Report No. UCRL-76077, Oct. 1974.

[40] Inasaki, I., and Yonetsu, S., "In-Process Detection of Cutting Tool Damage by Acoustic Emission Measurement." proc. 22nd MTDR Conf., 1981, pp. 261-268.

[41] Landau, I. D., "A Survey of Model Reference Adaptive Techniques Theory and Application." Automatica, Vol. 10, 1974, pp. 353-379.

[42] J. Schwarzenbach, and K. F. Gill, System Modeling and Control. Edward Arnold, 1984.

[43] Julius T. Tou, Digital and Sampled-Data Control Systems. McGraw-Hill, 1959.

[44] G. C., Goodwin, and K. S. Sin, Adaptive Filtering Prediction and Control. Prentice-Hall, New Jersey, 1984.

[45] Operator's Manual of Bridgeport Machines, Bridgeport, Connecticut.

[46] Operator's Manual of Dunegan Model 302A & Model 202A BIN, California.

[47] Catalog of AST/SERVO System for LVT Model P/N 895001-2D.

[48] MetraByte Catalog of Data Acquisition & Control.

VITA

YUNSHUN CHIOU

Candidate for the Degree of

Master of Science

Thesis: DYNAMIC MODELING FOR CONTROL OF THE DRILLING PROCESS USING ACOUSTIC EMISSION

Major Field: Mechanical Engineering

Biographical:

Personal data: Born in Taiwan, R.O.C., June 19, 1960, the son of Mr. and Mrs. Chehming Chiou.

Education: Graduated from Chungcheng High School, Taipei, Taiwan, R.O.C., in July 1978; Recieved Bachelor of Science Degree from National Central University, Chung-Li, Taiwan, R.O.C. in July, 1983; completed requirements for the Master of Science degree at Oklahoma State University in December, 1989.

Professional Experience: Mechanical Engineer centering around the design, construction, operation and maintenance of plant facilities and equipment, Chunghwa Picture Tubes, Ltd. Taiwan, R.O.C. July, 1983, to September, 1987; Research Assistant, Integrated Manufacturing System, Oklahoma, Septemper, 1988, to August, 1989.